

ANALYSIS AND OPTIMIZATION OF CYLINDRICAL STRUCTURES
MANUFACTURED BY AUTOMATED FIBER PLACEMENT TECHNIQUE

A THESIS SUBMITTED TO
THE GRADUATE SCHOOL OF NATURAL AND APPLIED SCIENCES
OF
MIDDLE EAST TECHNICAL UNIVERSITY

BY

SEDAT GÜLDÜ

IN PARTIAL FULFILLMENT OF THE REQUIREMENTS
FOR
THE DEGREE OF MASTER OF SCIENCE
IN
AEROSPACE ENGINEERING

JANUARY 2014

Approval of the thesis:

**ANALYSIS AND OPTIMIZATION OF CYLINDRICAL STRUCTURES
MANUFACTURED BY AUTOMATED FIBER PLACEMENT TECHNIQUE**

Submitted by **SEDAT GÜLDÜ** in partial fulfillment of the requirements for the degree of **Master of Science in Aerospace Engineering Department, Middle East Technical University** by,

Prof. Dr. Canan Özgen _____
Dean, Graduate School of **Natural and Applied Sciences**

Prof. Dr. Ozan Tekinalp _____
Head of Department, **Aerospace Engineering**

Prof. Dr. Altan Kayran _____
Supervisor, **Aerospace Engineering Dept., METU**

Examining Committee Members

Prof. Dr. Levend Parnas _____
Aerospace Engineering Dept., METU

Prof. Dr. Altan Kayran _____
Aerospace Engineering Dept., METU

Assoc. Prof. Dr. Demirkan Çöker _____
Aerospace Engineering Dept., METU

Assoc. Prof. Dr. Melin Şahin _____
Aerospace Engineering Dept., METU

Gökhan Tursun _____
Chief Engineer of Composite Structures, TAI

Date: _____
29.01.2014

I hereby declare that all information in this document has been obtained and presented in accordance with academic rules and ethical conduct. I also declare that, as required by these rules and conduct, I have fully cited and referenced all material and results that are not original to this work.

Name, Last name : Sedat Gld

Signature :

ABSTRACT

ANALYSIS AND OPTIMIZATION OF CYLINDRICAL STRUCTURES MANUFACTURED BY AUTOMATED FIBER PLACEMENT TECHNIQUE

Güldü, Sedat

M.S., Department of Aerospace Engineering

Supervisor: Prof. Dr. Altan Kayran

January 2014, 115 Pages

Automated Fiber Placement (AFP) is a highly automated manufacturing process which has made it possible to manufacture composite parts utilizing curved tow paths resulting in variable stiffness composite structures. During the manufacturing of the composite structures with the automated fiber placement machines, fiber orientation angle can be changed according to the specific design needs. Therefore, variable fiber orientation can be sought in an optimization framework for favorable structural response. The purpose of this thesis is to show how the structural behavior of the cylindrical shell can be improved through the use of fiber placement technology in the manufacturing of the layers of the cylindrical shell of revolution. For this purpose, a methodology is developed for generating the finite element model of tow-placed variable-stiffness laminated composite cylindrical shells. The developed method allows the calculation of the ply thicknesses including the gaps and overlaps which occur as a result of the manufacturing of the plies of the cylindrical shell using curvilinear fiber paths. Fiber orientation angle of each element is determined by making use of the reference fiber path which is defined by two parameters. Along the reference fiber path, fiber orientation angle changes linearly in a specified direction. Finite element model creation and analyses are carried out using the finite element program MSC.NASTRAN®. For the

optimization of the reference fiber path, Particle Swarm Optimization (PSO) code is developed in Matlab environment. PSO is a robust optimization technique based on the movement and intelligence of swarms. Optimization of the parameters of the reference fiber path is performed for axially and circumferentially variable stiffness cylinders including the strength and manufacturing constraints. Optimization results are also compared with results of the baseline constant stiffness cylinders. The objective of the optimization is taken as the maximization of the buckling factor of the cylindrical shell subjected to different load cases. Results show that higher buckling load factors can be obtained for variable stiffness cylinders compared to the constant stiffness laminated cylinders.

Keywords: Automated Fiber Placement, Optimization of Composite Cylindrical Shells, Particle Swarm Optimization, Variable Stiffness Composite Structures, Fiber Path Optimization

ÖZ

OTOMATİK FİBER SERME TEKNİĞİ İLE ÜRETİLEN SİLİNDİRİK YAPILARIN ANALİZİ VE OPTİMİZASYONU

Güldü, Sedat

Yüksek Lisans, Havacılık ve Uzay Mühendisliği Bölümü

Tez Yöneticisi: Prof. Dr. Altan Kayran

Ocak 2014, 115 sayfa

Otomatik Fiber Serme yüksek seviyede otomatikleştirilmiş bir üretim yöntemidir, fiberlerin eğrisel yollar izlemesine olanak sağlayarak değişken sertlikli kompozit yapıları ortaya çıkarmıştır. Kompozit yapıların otomatik fiber serme ile üretimi sırasında fiber yönelim açıları özel tasarım gereksinimlerine göre değiştirilebilir. Bu yüzden değişken yönelim açıları optimizasyon yapılarak daha iyi yapısal tepkiler almak için tercih edilebilir. Bu tezin amacı silindirik yapıların otomatik fiber serme ile değişken açılı olarak üretilmesi durumunda yapısal davranışın iyileşebileceğinin gösterilmesidir. Bu amaç için fiber yerleştirilmiş değişken sertlikteki kompozit silindirin sonlu elemanlar modelini oluşturacak bir yöntem geliştirilmiştir. Bu geliştirilen yöntem, eğrisel fiberlerin silindir yüzeyine yerleştirilmesi sırasında fiberler arasındaki oluşabilecek boşluk ve üst üste binmeleri hesaba katarak, her bir eleman için katman kalınlıklarını ve yönelim açılarını hesaplamaktadır. Fiber yönelim açıları iki değişken ile tanımlanan referans fiber yolu kullanılarak hesaplanmaktadır. Fiber yönelim açıları referans yolu boyunca doğrusal olarak belirtilen yönde değişmektedir. Sonlu elemanlar modeli ve yapısal analizler için sonlu elemanlar programı MSC.NASTRAN® kullanılmıştır. Referans fiber yolunun optimizasyonu için, Parçacık Sürüsü Optimizasyonu (PSO) kodu Matlab ortamında

geliştirilmiştir. PSO sürülerin hareketini ve zekasını temel alan güçlü bir optimizasyon metodudur. Eksenel ve dairesel yönde değişken sertlikli silindirler için referans fiber yolunun parametrelerinin optimizasyonu dayanıklılık ve üretim kısıtlamalara göre gerçekleştirilmiştir. Sabit sertlikli temel silindirler ile optimizasyon sonuçları karşılaştırılmıştır. Optimizasyonun amacı silindirik yapıların burulma yük faktörlerini değişik yükler altında maksimuma çıkarmaktır. Elde edilen sonuçlar değişken sertlikli silindirlerin sabit sertlikteki silindirlerle karşılaştırıldığında daha yüksek burulma yük faktörü elde edilebileceğini göstermiştir.

Anahtar Kelimeler: Otomatik Fiber Serme, Kompozit Silindir Yapıların Optimizasyonu, Parçacık Sürüsü Optimizasyonu, Değişken Katılıklı Kompozit Yapılar, Fiber Yolu Optimizasyonu

ACKNOWLEDGMENTS

I want to express my deepest appreciation to Prof. Dr. Altan KAYRAN for his supervision, guidance, and valuable support during the course of this research.

I would also like to thank to our chief engineer of composite structures, Gökhan TURSUN, for encouragement to me for this research. And of course to my company, TAI.

Finally, I am heartily thankful to my parents for their complimentary support and insightfulness throughout my years of study.

Ankara, 16 December 2013

Sedat Güldü

TABLE OF CONTENTS

| | |
|--|-------------|
| ABSTRACT..... | v |
| ÖZ..... | vii |
| ACKNOWLEDGMENTS | ix |
| TABLE OF CONTENTS | x |
| LIST OF TABLES | xiii |
| LIST OF FIGURES | xv |
| CHAPTERS | |
| 1. INTRODUCTION..... | 1 |
| 1.1. Introduction..... | 1 |
| 1.2. Motivation of the Study | 3 |
| 1.3. Scope..... | 4 |
| 2. LITERATURE SURVEY | 5 |
| 3. AUTOMATED FIBER PLACEMENT..... | 17 |
| 3.1. Introduction..... | 17 |
| 3.2. Minimum Turning Radius..... | 21 |
| 3.3. Gaps and Overlaps | 22 |
| 3.4. Minimum Cut Length..... | 25 |
| 3.5. Coverage Parameter | 26 |
| 4. PARTICLE SWARM OPTIMIZATION AND CONSTRAINED OPTIMIZATION | 27 |
| 4.1. Introduction..... | 27 |
| 4.2. PSO Algorithm..... | 28 |
| 4.3. The Constrained Problem..... | 31 |
| 4.4. The Verification of PSO Code..... | 33 |
| 4.4.1. The Test Problem 1 | 34 |
| 4.4.2. The Test Problem 2 | 35 |

| | |
|--|------------|
| 5. FINITE ELEMENT MODELLING AND OPTIMIZATION OF VARIABLE STIFFNESS COMPOSITE CYLINDER STRUCTURES | 37 |
| 5.1. Introduction..... | 37 |
| 5.2. Determination of Optimum Fiber Paths of Variable Stiffness Composite Cylinder Structures | 38 |
| 5.2.1. Nomenclature of Variable Stiffness Lamina..... | 38 |
| 5.2.2. Variation of fiber orientation angle in the axial direction for the cylindrical shell..... | 40 |
| 5.2.3. Variation of fiber orientation angle in the circumferential direction for the cylindrical shell..... | 40 |
| 5.2.4. Shifted fiber path..... | 41 |
| 5.2.5. Cylinder Shell Geometry | 44 |
| 5.2.6. Material Properties..... | 45 |
| 5.2.7. Finite Element Solver..... | 46 |
| 5.2.8. Failure Criteria..... | 46 |
| 5.2.9. The Buckling Load Factor | 47 |
| 5.2.10. Creation of Variable Stiffness Finite Element Model..... | 48 |
| 5.2.10.1. Finite Element Modeling of a Reference Path | 48 |
| 5.2.10.2. Nastran input file..... | 51 |
| 5.3. Optimization Procedure by Coupling the Nastran Finite Element Solver and Particle Swarm Optimizer in MATLAB | 51 |
| 6. RESULTS OF FINITE ELEMENT ANALYSIS AND OPTIMIZATION..... | 59 |
| 6.1. Introduction..... | 59 |
| 6.2. Problem Definition and Optimization Procedure..... | 60 |
| 6.3. Design of the Laminated Shell Wall | 62 |
| 6.4. Finite Element Model Verification Case Study | 64 |
| 6.5. Results of Bending Load Case..... | 68 |
| 6.5.1. Design Sensitivity Analysis | 77 |
| 6.6. Results of Torsional Load Case | 78 |
| 6.7. Results of the Combined Load Case..... | 84 |
| 6.8. Results of Axial Load Case..... | 90 |
| 7. CONCLUSION..... | 97 |
| REFERENCES..... | 103 |
| APPENDICES | |
| Appendix A : Nastran Input File | 107 |

| | |
|---|-----|
| Appendix B : Golden Section Method | 111 |
| Appendix C : Example for the Optimization Variable Stiffness Cylinder | 112 |

LIST OF TABLES

TABLES

| | |
|--|----|
| Table 1 Variation of minimum turning radius with tow width [23] | 22 |
| Table 2 The PSO and penalty multiplier | 33 |
| Table 3 Comparison of optimization results for the test problem 1 | 35 |
| Table 4 Comparison of optimization results for the test problem 2 | 36 |
| Table 5 Material Properties of AS4/855-2, Graphite Epoxy [38] | 45 |
| Table 6 Description of Buckling Load Factor values | 47 |
| Table 7 An example of Main Matlab code input parameters | 53 |
| Table 8 The PSO code parameters | 54 |
| Table 9 Buckling load factor results of constant stiffness laminated shell designs under bending loading | 69 |
| Table 10 Optimization results of laminated cylinders composed of non-traditional fiber orientation angles under bending loading | 69 |
| Table 11 Optimization results of variable stiffness cylinders with axially varying fiber orientation angle under bending loading | 71 |
| Table 12 Optimization results of variable stiffness cylinders with circumferentially varying fiber orientation angle under bending loading | 71 |
| Table 13 The best optimization results under bending load | 76 |
| Table 14 The comparison of the optimization result under bending loading for different discretization value | 77 |
| Table 15 Buckling load factor results of constant stiffness laminated shell designs under torsional loading | 78 |
| Table 16 Optimization results of cylinders composed of non-traditional fiber orientation angles under torsional loading | 79 |
| Table 17 Optimization results of variable stiffness cylinders with axially varying fiber orientation angle under torsional loading | 80 |
| Table 18 Optimization results of variable stiffness cylinders with circumferentially varying fiber orientation angle under torsional loading | 80 |
| Table 19 The best optimization results under torsional load | 83 |
| Table 20 Buckling load factor results of constant stiffness laminated shell designs under combined loading | 84 |
| Table 21 Optimization results of cylinders composed of non-traditional fiber orientation angles under torsional loading | 85 |
| Table 22 Optimization results of variable stiffness cylinders with axially varying fiber orientation angle under combined loading | 86 |

| | |
|---|----|
| Table 23 Optimization results of variable stiffness cylinders with circumferentially varying fiber orientation angle under combined loading | 87 |
| Table 24 The best optimization results under combined load..... | 89 |
| Table 25 Buckling load factor results of constant stiffness laminated shell designs under axial loading | 90 |
| Table 26 Optimization results of cylinders composed of non-traditional fiber orientation angles under axial loading | 91 |
| Table 27 Optimization results of variable stiffness cylinders with axially varying fiber orientation angle under axial loading | 92 |
| Table 28 Optimization results of variable stiffness cylinders with circumferentially varying fiber orientation angle under axial loading | 93 |
| Table 29 The best optimization results under axial load..... | 95 |

LIST OF FIGURES

FIGURES

| | |
|--|----|
| Figure 1 Steered fibers laid down by an advanced fiber placement machine [4] | 2 |
| Figure 2 Comparison of Constant Stiffness Laminate and Variable Stiffness Laminate..... | 6 |
| Figure 3 18 element quarter panel with a central hole [12] | 7 |
| Figure 4 Tensile test comparison [19]..... | 7 |
| Figure 5 Fiber orientation varying with position [10]..... | 8 |
| Figure 6 The parameters T_0 , T_1 , d and \emptyset determining the linear angle variation [10] | 9 |
| Figure 7 $\langle 0/45 \rangle$ fiber path and orientation [15]..... | 10 |
| Figure 8 Shifted and parallel fiber method, reference path $90 \langle 30/75 \rangle$ [15] | 10 |
| Figure 9 The composite panels [1]..... | 11 |
| Figure 10 Cylinder model [4]..... | 15 |
| Figure 11 An automated fiber placement machine [22]..... | 17 |
| Figure 12 Schematic view of a fiber deposition head used for AFP machine [20] ... | 18 |
| Figure 13 An actual fiber placement machine's head while laying down [8] | 19 |
| Figure 14 The manufactured fuselage section and nose cone of Boeing 787 Dreamliner by AFP [37]..... | 19 |
| Figure 15 A350 XWB fuselage section manufacturing | 20 |
| Figure 16 Manufacturing of composite tail boom by AFP, Automated Dynamics [22] | 20 |
| Figure 17 Minimum turning radius is required to prevent local fiber buckling due to excessive compressive forces [4] | 21 |
| Figure 18 (1) Straight tow (2) Curved tow and (3) Curved tow which violates the curvature constraint [4] | 22 |
| Figure 19 Local fiber buckling due to the violation of the curvature constraint..... | 22 |
| Figure 20 The illustration of overlaps and gaps [4] | 23 |
| Figure 21 Nominal tow width variation by angle for $\langle 0/45 \rangle$ curved tow | 23 |
| Figure 22 The shift distance effect in a lamina resulting in overlaps (a) and gaps (b) | 24 |
| Figure 23 Demonstration of minimum cut length constraint [4] | 25 |
| Figure 24 A lamina with 0 % coverage parameter..... | 26 |
| Figure 25 Concept of modification of a searching point by PSO | 28 |
| Figure 26 Particle Swarm Optimization Algorithm | 31 |
| Figure 27 Test Problem 1 | 34 |
| Figure 28 Test Problem 2..... | 35 |

| | |
|--|----|
| Figure 29 Fiber path parameters, T_0 and T_1 for the axially varying fiber orientation case..... | 38 |
| Figure 30 Reference path and shifted fiber paths along the axial direction..... | 42 |
| Figure 31 Variable stiffness cylinder with axially varying fiber orientation angle .. | 42 |
| Figure 32 Variable stiffness cylinder with circumferentially varying fiber orientation angle | 43 |
| Figure 33 Dimensions of the cylindrical shell | 44 |
| Figure 34 The mesh of the cylinder shell..... | 45 |
| Figure 35 Single $\langle 0/45 \rangle$ Axially Varying Reference Tow Path Discretized over the Cylinder..... | 49 |
| Figure 36 $\langle 0/45 \rangle$ Axially varying fiber tow through the panel..... | 50 |
| Figure 37 Thickness distribution of the $[\pm \langle 0/45 \rangle]_s$ laminate with axially varying fiber orientation angle | 50 |
| Figure 38 The fiber path optimization procedure flowchart | 57 |
| Figure 39 Applied loads and the edge displacement boundary conditions for the case study | 65 |
| Figure 40 Thickness distribution of $[\pm \langle 0/50 \rangle]$ plate design..... | 66 |
| Figure 41 Bending loads applied to the cylindrical structure..... | 68 |
| Figure 42 Maximum Von Mises stress distribution (MPa) of the CS-1 design under bending loading..... | 70 |
| Figure 43 Thickness distribution for the VA-1 design under bending loading..... | 73 |
| Figure 44 Maximum Von Mises stress distribution (MPa) of the VA-1 design under bending loading..... | 73 |
| Figure 45 Maximum Failure Index distribution of the VA-1 design under bending loading..... | 74 |
| Figure 46 First buckling mode of CS-1 design under bending load | 75 |
| Figure 47 First buckling mode of the VA-1 design under bending loading | 76 |
| Figure 48 Torsional loads applied on the cylindrical structure..... | 78 |
| Figure 49 First buckling mode of the CS-3 design under torsional loading | 79 |
| Figure 50 Thickness distribution of the VA-3 design under torsional loading..... | 81 |
| Figure 51 First buckling mode of the VA-3 design under torsional loading | 82 |
| Figure 52 Thickness distribution of the VC-3 design under torsional loading | 82 |
| Figure 53 First buckling mode of the VC-3 design under torsional loading | 83 |
| Figure 54 First buckling mode of the CS-3 design under combined loading | 85 |
| Figure 55 Thickness distribution of the VA-3 design under combined loading | 86 |
| Figure 56 First buckling mode of the VA-3 design under combined loading | 87 |
| Figure 57 Thickness distribution of the VC-3 design under combined loading | 88 |
| Figure 58 First buckling mode of the VC-3 design under combined loading..... | 88 |
| Figure 59 Axial loads applied to the cylindrical structure | 90 |
| Figure 60 First buckling mode of the CS-1 design under axial loading | 91 |
| Figure 61 Thickness distribution of the VA-3 design, $[\pm \langle 3/9 \rangle / \pm \langle 24/78 \rangle]_s$ | 92 |

| | | |
|-----------|---|----|
| Figure 62 | First buckling mode of the VA-3 design under axial loading | 93 |
| Figure 63 | Thickness distribution of the VC-3 design under axial loading | 94 |
| Figure 64 | First buckling mode of the VC-3 design under axial loading..... | 95 |

CHAPTER 1

INTRODUCTION

1.1. Introduction

Aerospace engineering applications demand high-performance materials that combine high stiffness, high strength and low weight while improving safety, durability, and performance of an airplane. Therefore, the composite materials are especially attractive for aviation and aerospace applications because of their remarkable strength and stiffness properties. Another advantage is that composite materials can be formed into more complex shapes compared to metallic materials. Therefore, the assembly time can be shortened and cost savings can be realized because the number of parts needed to make a given component, and the need for fasteners and joints are reduced. When the fasteners and joints are removed, weak points such as stress concentration and potential crack-initiation sites can be eliminated in a structural component.

Composite laminates that are currently used in the aerospace industry typically consist of layers with 0° , 90° , $+45^\circ$ and -45° fiber orientations. Each composite ply has specific material properties, thickness and orientation angles that remain constant throughout the entire ply. Also, the loading response that remains constant throughout each ply. However, it is desirable to consider ways to further tailor the design of composite materials so that the resulting structures will offer an advantage over current practices. Even though there are many techniques to optimize traditional composite laminates have been developed, the modern methods allow for more complex structures to be conceived. An important feature of fiber-reinforced

composites is that the material properties depend on the orientation of the material. With composite materials, high strength to weight ratio as well as the ability to lay-up the fibers along the desired orientation can be achieved, and composites laminates can be manufactured according to the needs of the end users. One concept that has been used in expanding the tailorability of the design of composite structures is the variable stiffness composite laminates. Variable-stiffness laminates are different than traditional straight-fiber composite laminates in terms of thickness or fiber orientation spatially throughout the laminate. The variable stiffness composites existed in theory for a long time, and with improvements achieved in advanced fiber placement machines, today variable stiffness composite laminates can be manufactured [1, 7, 3].

Hand laying methods would not provide the required precision for laying the fibers at the correct angles and preserving these angles during curing. Moreover, variability in quality resulting from the manual process has to be addressed. Automated fabrication processes are able to provide accuracy of lay-up and improved quality component production with a reduced production cycle time. Automated Fiber Placement (AFP) is a technology that combines the capability of filament winding and, the compaction and cut-restart capabilities of automated tape laying. [2, 10]

In Figure 1, steering of fibers by an AFP machine is seen. In a variable-stiffness composite, the stiffness can be altered to create more efficient load paths, resulting in weight savings that cannot be achieved using traditional laminates.



Figure 1 Steered fibers laid down by an advanced fiber placement machine [4]

1.2. Motivation of the Study

The work presented in this thesis aims to explore the effectiveness of variable stiffness concept as applied to cylindrical shell structure because variable-stiffness laminates has showed significant design improvements in a large number of theoretical and experimental studies in the past. A middle or front section of an airplane fuselage and helicopter tail boom can be simplified as a cylindrical structure, and to improve the structural performance of these primary structures, cylindrical shell geometry can be used to ease the definition of the fiber paths on the geometry. The variable stiffness concept offers a much wider range of tailorability than simply choosing the best stacking sequence for the given loading conditions. In a variable stiffness laminate stiffness and strength properties vary spatially to adapt to the existing stress field, thus structures can exhibit greater resistance to the local conditions which results in increased load-carrying capability of the structure. This research examines the design of curvilinear fiber paths defined by fiber orientation parameters, taking into account the manufacturing aspects of the tow placement machine.

Optimization of fiber path parameters to get best design for structural performance is difficult and computationally expensive. The number of optimization parameters and computational cost are directly related each other and three design parameters can be enough to define reference fiber path by using the developed method for curvilinear fiber path by Gürdal and Olmeda. [6] This approach is the most important part of the design, analysis and optimization of variable stiffness laminates. Firstly, the analysis tool is developed for variable stiffness laminates, because the available laminate analysis programs are for the constant stiffness laminates, and it is not possible to create finite element model of variable stiffness laminates by using available programs. The subroutines are generated for analysis of variable stiffness laminates. For the optimization method, “Particle Swarm Optimization” method which is an evolutionary optimization technique which is based on the movement and intelligence of swarms. One of significant contribution of the present thesis is the development of “Particle Swarm Optimization” code from scratch in Matlab environment.

1.3. Scope

This thesis is organized in seven chapters. Brief explanation of the chapters is as follows;

Chapter 1 includes the introduction and motivation of the study.

Chapter 2 gives the literature survey of variable-stiffness composite research. Definition of fiber path, creation of variable stiffness laminate using the reference path is explained by using literature. How the structural performance is affected and comparisons of the variable stiffness with the constant stiffness laminates are given. Analysis and optimization research of the variable stiffness laminates also included in the chapter.

Chapter 3 focuses on automated fiber placement process. The information about this process is explained in detail. The fiber placement machine's working principle is also showed. In addition, the manufacturing constraints about automated fiber placement are presented.

Chapter 4 details the optimization method, Particle Swarm Optimization (PSO). The penalty approach is also given to solve constrained optimization problem with PSO. The verification of PSO code and the penalty approach are also performed in this chapter.

Chapter 5 represents the coupling of finite element solver MSC.Nastran and the PSO code. How finite element model is created is explained in detail. The formulation of the optimization problem is also given in this chapter.

Chapter 6 gives the optimization results of different load cases. Based on the numerical results, the conclusion is drawn. The thickness distributions and von Mises stress distribution of the variable stiffness cylinder structures are also added to evaluate the results.

Chapter 7 comprises a conclusion for the whole study. This chapter also gives a summary on the contribution of the thesis and includes recommendations on future studies that can be appended to.

CHAPTER 2

LITERATURE SURVEY

In principle, there are three basic methods to manufacture variable stiffness laminates as dropping or adding of plies to the laminate, fiber volume fraction and variation of the fiber orientation angle through a ply. In each case, the resulting structure will have spatially varying properties. Variable stiffness structures refers to structures that have different mechanical properties at different locations in the structure. With the variable stiffness concept, it becomes possible to redistribute an applied loading such that fibers can be aligned the high stress directions resulting in structures with higher structural integrity. Figure 2 shows that the comparison between the constant stiffness composites and variable stiffness composites. The orientation angle, α of a single layer is constant for constant stiffness composites, but α varies in variable stiffness composites. The same argument is also valid for layer thickness t . Moreover, fiber spacing, s also changes and it does not remain constant for variable stiffness composites. An overview of the available literature on the variable stiffness composite structures, and optimization process of variables stiffness composites are given in this chapter.

One of the first theoretical researches on the effect of tailoring elastic properties of composite laminates was carried out by Muser and Hoff [9]. In their study, closed-form solution for the stress concentration for a plate with a hole under uniaxial tension was performed. The elastic properties were varying radially around the hole.

Their analysis showed that the fiber arrangement in the surrounding of the hole is very effective in reducing stress concentrations.

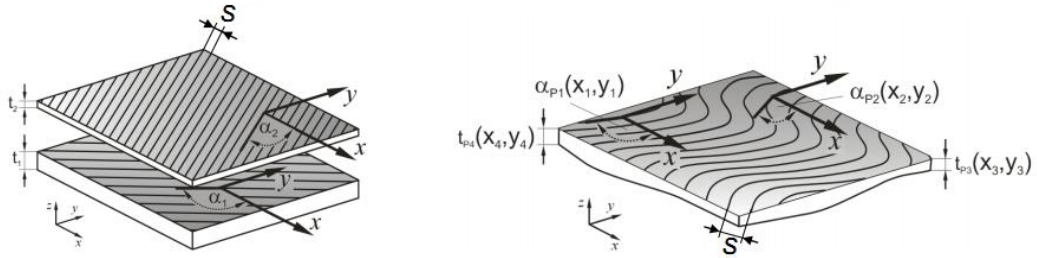


Figure 2 Comparison of Constant Stiffness Laminate and Variable Stiffness Laminate

The first milestone study on exploiting curvilinear fibers on the improvement of the tensile load carrying capacity of a plate with a central hole has been performed analytically by Hyer and Charette [11]. According to this study, a gain in structural efficiency can be achieved by aligning the fibers in some, or in all of the layers, in a laminate with the principal stress directions in those layers. Hyer and Charette presented the first studies about curvilinear fiber laminates and explained how the curvilinear fiber laminate is analyzed. In their study, a quarter plate was analyzed. The finite element model of the plate studied is shown in Figure 3. As shown in Figure 3 finite element model has 18 elements. In the composite laminate outer layers are composed of $\pm 45^\circ$ layers, and 12 curvilinear plies between $\pm 45^\circ$ straight fiber plies. Unique fiber orientation angles for each element were given separately. Results showed that the load carrying performance of composite laminates was increased significantly through the optimization of fiber orientation angle distribution around the hole.

Figure 4 shows the tensile test results [19]. In this study, it is shown that mass-specific failure load of an open-hole CFRP tensile disk could be increased up to 50%. The first laminate stacking sequence is $[45/0/-45]_s$ and the other design's stacking sequence is $[C_1/45/-45]$. C_1 designates the ply which is laid down around the hole. In the layer C_1 , fiber orientations were aligned with the principal stress directions. As a

result, a more effective load path around a hole was determined when compared to the straight-fiber counterpart.

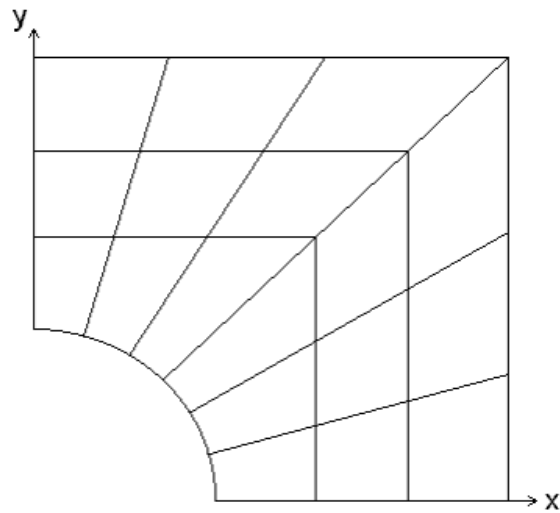


Figure 3 18 element quarter panel with a central hole [12]

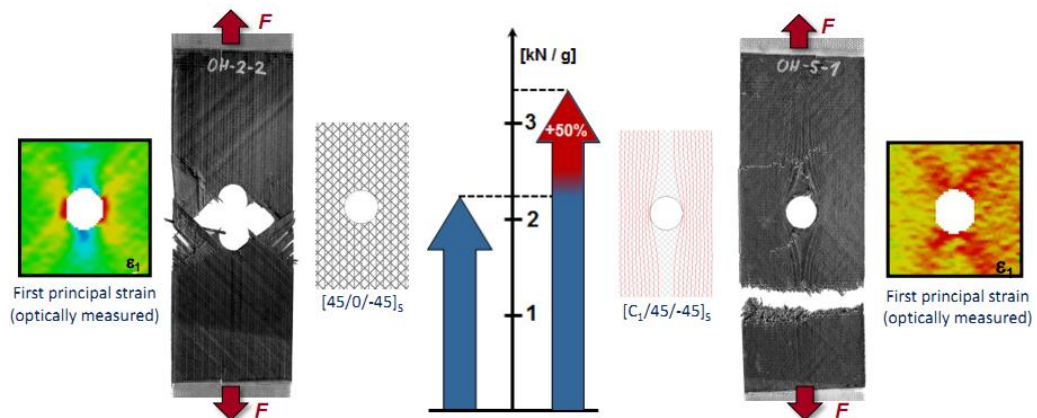


Figure 4 Tensile test comparison [19]

As a follow up of their previous work, Hyer and Lee focused on how could the buckling load of panels with a central hole can be improved [12]. The optimum fiber orientation angles were determined under the compression loads for a composite plate by using gradient search technique. Useful increases in buckling load were succeeded. The observation in all designs was that with the optimal orientation of the fibers, it was possible to distribute the load from the region close to the hole to the edges of the plate. The buckling load was increased by up to 2.96 times the buckling load of the baseline designs. It was also shown that by combining both straight and

curvilinear fiber plies within a laminate, resulting hybrid laminates produced the best buckling and failure results.

There are several approaches to formulate fiber paths. One technique is to vary the fiber path continuously as a function of position. One of the method to model tow paths was developed in the research carried out by Gürdal and Olmedo [6]. The work resulted in the formulation of variable stiffness laminate definition with minimum number of parameters for a rectangular plate. The proposed fiber orientation variation was generated from a base curve which defines the fiber orientation angle such that it varies linearly from one side of the panel to the other side. By varying the fiber orientation angle with position, the ply will have properties which also change with position. Figure 5 illustrates an example which shows how the fiber orientation angle varies with position.

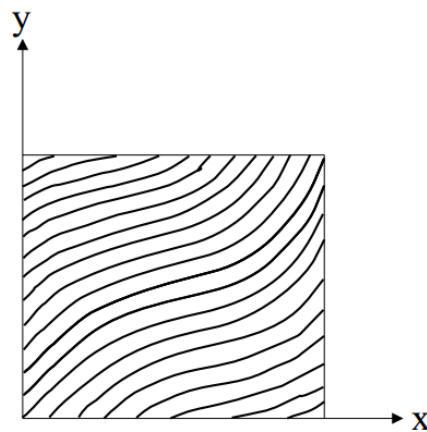


Figure 5 Fiber orientation varying with position [10]

The main advantage of the variable stiffness concept is that the stiffness and strength parameters, which both depend on the fiber orientation angle, can be altered spatially to tailor the structure to the expected loads and stresses. With the fiber placement machines, fiber tows can follow the curvilinear fiber paths [10]. Olmedo developed numerical techniques to calculate the stress distribution and buckling loads for variable stiffness plates [13]. After Olmedo, the analysis tool to study the possible improvements in performance of the curvilinear fibers over traditional composite laminates was introduced by Waldhart [10]. During his study, manufacturability of the prototype laminate was also taken into account, and manufacturing constraints

regarding the variation of the fiber orientation angle was imposed in the optimization process. Improvements in the buckling load of up to 80% over straight fiber configurations were found. The research showed that the variable stiffness plates could be analyzed effectively and marked improvement over traditional composite laminate designs.

The definition of fiber path was done by using small number of parameters: the fiber orientation angle at the center of the laminate T_0 , the fiber orientation angle at a characteristic distance d from the panel center T_1 , and the direction of variation angle ϕ [6]. These variables are shown in Figure 6.

By using the parameters T_0 and T_1 , a realistic curvilinear fiber path is described. The most basic function for the condition of the variation of the fiber orientation was linear variation in one direction only. Thus the fiber orientation angle for a reference path was defined as in Eqn. 2.1. [6]

$$\theta(x) = \begin{cases} \frac{2}{d}(T_0 - T_1)x + T_1 & \text{for } 0 \leq x \leq \frac{d}{2} \\ \frac{2}{d}(T_1 - T_0)x + 2T_0 - T_1 & \text{for } \frac{d}{2} \leq x \leq 0 \end{cases} \quad (2.1)$$

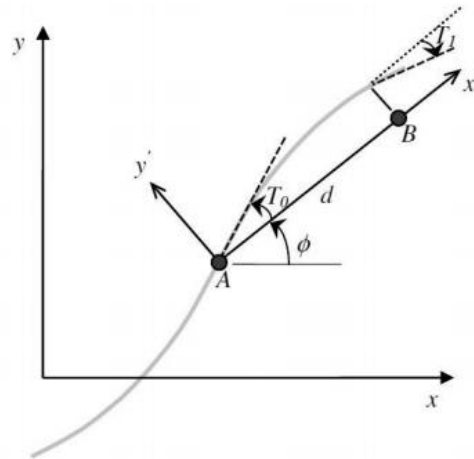


Figure 6 The parameters T_0 , T_1 , d and ϕ determining the linear angle variation [10]

The notation for the representation of a single layer in the stacking sequence of a variable stiffness laminate using linear variation of fiber orientation angle is shown as $\phi < T_0/T_1 >$. Figure 7 shows an $< 0/45 >$ layer which has zero direction of variation angle ϕ , T_0 value of 0^0 and T_1 value of 45^0 .

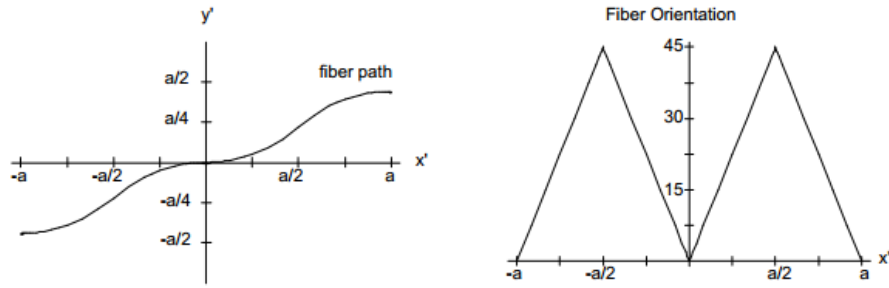
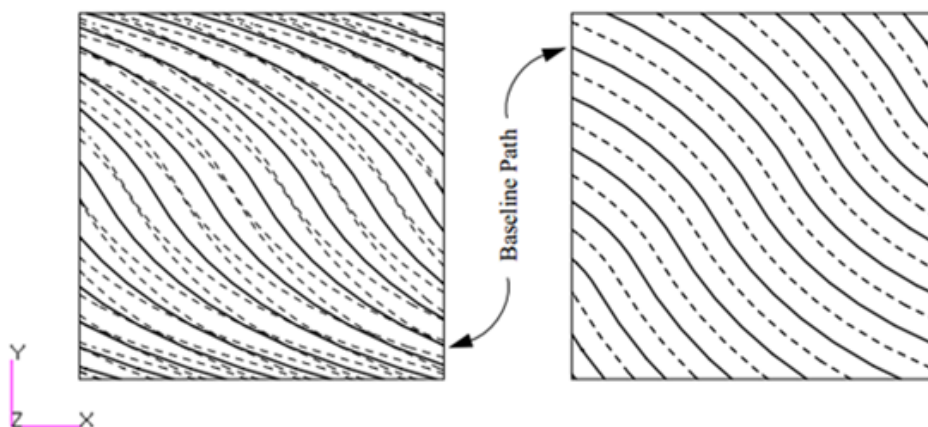


Figure 7 $\langle 0/45 \rangle$ fiber path and orientation [15]

Waldhart proposed two methods for constructing a full variable-stiffness ply based on a curvilinear reference path [14]. According to Waldhart, after the reference fiber path has been defined by Eqn. 2.1 to cover the entire ply, ‘shifted’ fiber paths are formed by shifting the reference path in the y' direction. In Figure 8(a), the shifted reference paths by different amounts along the y' -direction is shown. In other words, this strategy assumes that the shape of the reference path is not changing when shifting in a direction perpendicular to the stiffness variation. The thick solid lines represent the centerline of each individual path, while the thinner dashed lines denote the edges of the finite width strip of material. As a result of the fiber orientation angle variation, considerable overlap occurs at the edges of the plates. The other method was proposed by Waldhart is the parallel method, in which fiber paths are created by placing the new paths parallel to the original fiber path, as shown in Figure 8(b).

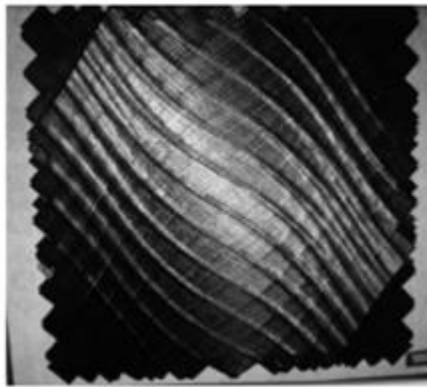


(a) Shifted Fiber Method

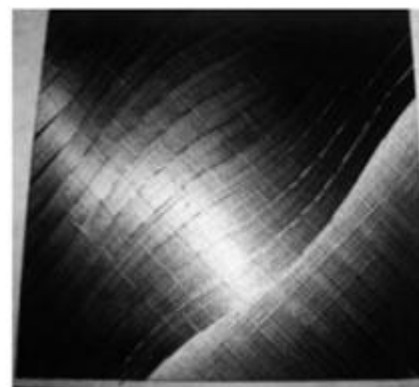
(b) Parallel Fiber Method

Figure 8 Shifted and parallel fiber method, reference path $90 \langle 30/75 \rangle$ [15]

When the shifted and parallel methods are compared, the shifting method proved to be more efficient in redistributing loads than the parallel method, therefore higher improvements in buckling load were obtained. [17] Constraint on the minimum turning radius reduces the feasible design space in case of parallel path; therefore shifting method gave better optimized results. The manufactured panels are shown in Figure 9, compares the panels manufactured by the shifted and the parallel method. [1]



(a) Composite panel manufactured using shifting fiber method



(b) Composite panel manufactured using parallel fiber method

Figure 9 The composite panels [1]

The results of the research mentioned above established the need for experimental validation. Tatting and Gürdal [16] optimized a panel with central hole for compressive buckling load. First, a panel without a hole was considered for the optimization study. Then, a hole was added to the best lay-up and the panel was analyzed in the FE code STAGS (Structural Analysis of General Shells) [14]. Several variable-stiffness panels that are manufactured showed improved performance relative to their straight fiber counterparts. Compared to the baseline panel, the best curvilinear-fiber panel achieved an improvement in the load-carrying capability of over 60% with no appreciable increase in weight. Wu et al. [18] analyzed and tested tow steered panels under compression loads up to failure. When compared to the failure load with baseline design, the improvement is 28%.

The fiber orientation definition for curvilinear fiber paths can be optimized and tailored for various loading conditions by using NURBS (Non-Uniform rational

B-splines) curves as reference fiber paths that was introduced by Nagendra [23]. Using finite elements, Nagendra studied buckling load design of laminated composite plates with a central hole subject to deformation and ply failure. In this study, manufacturing limitations were set active, therefore optimized fiber path design space was limited. In the research, 7-axis AFP machine, developed by Cincinnati Milacron Inc., was used. Their optimization approach was based on the shape optimization formulation for the fiber path optimization problem. The reference fiber paths were NURBS curves.

Inci, worked on the fiber path optimization for rectangular plate via different optimization techniques [20]. Firstly, the optimization was done with the gradient-based numerical optimization solver of MSC.Nastran. It was understood that to solve the design variables for the variable stiffness composite structures, it is necessary to use of a finite element solver, because variable stiffness composites are hard to be modeled analytically. For case studies, different two dimensional problems were defined and discrete fiber orientation angle and continuous fiber path optimizations were performed to minimize the total strain energy at different loading conditions. Results obtained by discrete fiber orientation optimization are satisfactory in theory, but in practice they cannot be used in manufacturing since in actual manufacturing continuity of the curvature of the fiber path is required. To avoid the discontinuities, continuous fiber orientation approach was tried and up to 30% increase was obtained in the first buckling load with respect to the zero degree straight fiber composite plate. It was seen that when the curvature constraint is removed, 43.4% increase in the lowest buckling load was obtained.

Langley et al. worked on the finite element modeling of tow placed variable stiffness laminates. [15] In this study, the process of giving element properties to shell elements was important, since it was required to find the distance between the element center and the reference path. Golden section search algorithm was used by Langley for this process. The method to cover entire plate was achieved by shifting of the reference path. The finite element software GENESIS was used to analyze the variable stiffness laminates.[15] The first case was a square plate and the boundary conditions were uniform end shortening and free upper and lower edges. The

other case was again a square plate but the boundary conditions were uniform end shortening with constrained upper and lower edges. In this research, to decrease the computational time, a quarter plate was utilized. Moreover, many mesh sizes were tried to get proper characterization of the static response, and minimum element number was defined to model the thickness variation throughout the plate.

The application of a cylinder as a structural component has been used for centuries, due to its efficiency as a structural element. Khani et al. studied the elliptical cross section composite cylinders under internal pressure and bending about the major axis. [24] The fiber angle variation was bi-symmetric and linear. The investigation did not show significant improvements over straight fiber case under internal pressure or bending. However, under combined internal pressure and bending load case, small improvement was achieved.

Tatting's studies about the variable stiffness thin circular cylindrical shells achieved performance improvements. [25] Stress analysis and initial buckling solutions were performed for a general variable-stiffness cylinder. Two cases of loading were selected and two different stiffness variations were applied on the cylinders to investigate the possible areas of improvements over constant stiffness cylinders. In the initial phase of the study, axial stiffness variation was considered, and the constant axial compression, pressure and torsion were applied as external loads. The results for this case showed not too much improvement over traditional laminates. In the second case, the stiffness variation was in the circumferential direction and the cylinder was subjected to axial compression, pressure, torsion, bending or transverse shear. As a result of this work, it was concluded that the stiffness variation on the cylinder contributes to increased performance by lowering the stresses in the critical areas and providing a relatively stiff region.

Wu et al. [18] investigated a composite cylindrical shell which was a fuselage section of an aircraft subjected to bending loads. Circumferentially varying fiber orientation was used to create the variable stiffness laminate. The radius of curvature was taken constant and plies were constructed according to the shifted ply method. Designs with gaps and overlaps were analyzed for the described fiber angle variation using

the STAGS finite element models. [14] Results were compared with an 8-ply quasi-isotropic baseline and the conclusion was that the thickness variation due to overlaps improves the buckling load capacity and the structure has higher bending stiffness. In case of gaps in the design, the bending stiffness or buckling load carrying capacity was not increased.

Wu et al. [26] also continued the research by manufacturing two variable-stiffness shells using an Ingersoll fiber placement machine. To minimize the gaps and overlaps, it was required to adjust the nominal circumferential spacing. In addition, variation of the fiber orientation of the reference path was determined to better lay-up to the desired shell geometry. To avoid the formation of wrinkles in the steered plies, lay-up speed was decreased and the compaction force of the fiber placement head was increased. After the manufacturing, the cured shell surface of cylinder was surveyed to determine initial imperfections and thickness variations. It was seen that the cross sections of both shells varied along the length of the cylinder.

Another optimization, design, manufacturing and test research on the fabrication of composite cylinder with circumferentially varying stiffness were conducted by Blom. [4] their objective was to optimize the cylinder for maximum buckling load. The commercial finite element program ABAQUS was used for the structural response of the cylindrical shell. The radius of curvature constraint was applied to get manufacturable fiber path. A reference path was obtained and the entire surface was covered by shifting the reference path. They allowed overlaps but gaps were not allowed. Unwrapped cylinder is shown in Figure 10.

The model was built in ABAQUS and consisted of shell elements. By using the information about the local stacking sequence and material properties, a FORTRAN subroutine was used to calculate the stiffness matrices using the classical laminate theory. Stiffness information was then passed to ABAQUS. The manufacturing constraints; the minimum radius of curvature, tow drop interfaces, minimum cut length and compaction pressure, were taken into account for this study. The buckling loads of the variable stiffness panels were compared with the buckling loads of straight fiber panels of the same weight, and even though the manufacturing

constraint limited the design space, 17% improvement in the buckling load was calculated.

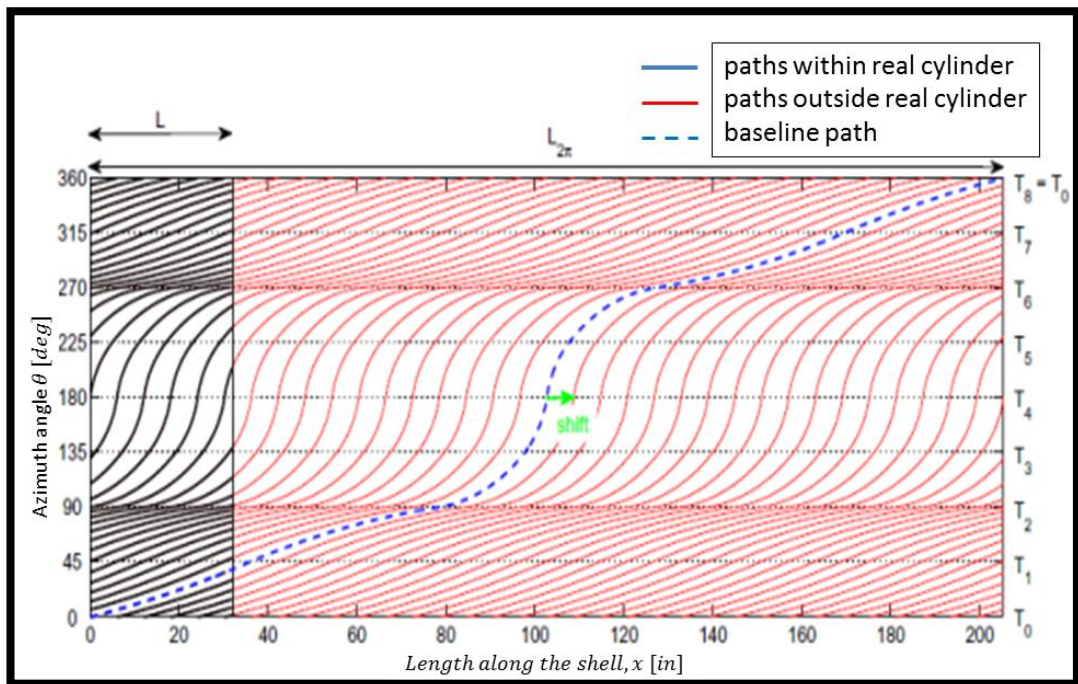


Figure 10 Cylinder model [4]

CHAPTER 3

AUTOMATED FIBER PLACEMENT

3.1. Introduction

The Automated Fiber Placement (AFP) machines first become commercially available in 1980s. This novel technology is stimulated by a using a computer-controlled multi-axis delivery head to place strips of tows. [2] This process allows design and production of parts that would be extremely hard or impossible with tape lay-up or filament winding. In general, the tow placement machine is a computer controlled seven axis fiber placement systems, and it is composed of a sled, a fiber delivery head, and a mandrel. There are three position axes, three rotation axes and an axis to rotate mandrel. [2] The seven axes give more flexibility to the fiber placement machine to move the fiber placement head on the part's surface. This way the production of complicated composite parts can be realized. A picture of an Ingersoll AFP machine is shown in Figure 11.

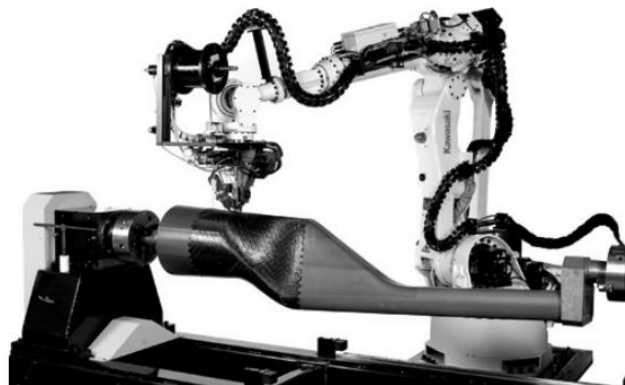


Figure 11 An automated fiber placement machine [22]

Current AFP machines allow up to 32 individually controlled tows, collectively known as course. The tows can be added or dropped at any point along the path of the machine head by using the cut and the restart capability. Tow width varies from 0.125" (3,175mm) to 1" (25.4mm). Different kind of materials such as thermoset prepreg (pre-impregnated) material, thermoplastic material, or dry fibers can be used in AFP machines. Carbon fibers pre-impregnated with thermoset resin are most commonly used in the aerospace industry.

The schematic view of fiber placement head of a typical machine is shown in Figure 12. This head can lay-up fiber following the curvilinear paths, cut and keep individual fibers according to the design of the laminate. Moreover, it provides consolidation with compaction rollers, houses cutting mechanisms which can cut individual tows. A second mechanism allows for the restart capability, and after the cut of the of the tows, fiber placement machine can start laying. As a result, the path width is controlled by increasing or decreasing the number of tows along the curvilinear path.

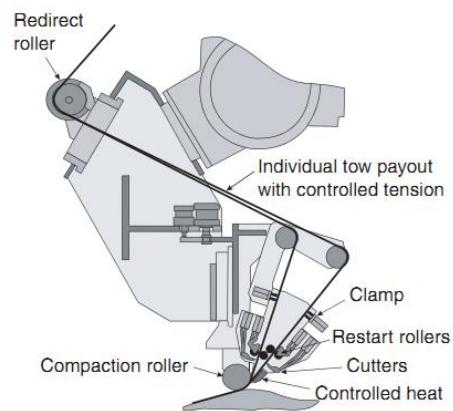


Figure 12 Schematic view of a fiber deposition head used for AFP machine [20]

Each tow is fed from an individual spool by pinching rollers which moves the tows over the tool surface. The head has a special heating mechanism and the tows are generally heated by the infrared light before it is laid over the tool or the part surface. The heating increases the tackiness of the material and heating is also required to overcome the slight tension present in the tow. When the tows reach the tool surface, the tow is pulled forward by the compaction roller and the tool surface, allowing the

tow to move at its own speed. In addition, the tackiness of the material and the compaction enable curved fiber courses to adhere to the tool surface. Figure 13 shows an actual delivery head which is used to manufacture aerospace structures in the industry.

There are many types of composites materials used in aerospace application, therefore tow placement machines must deal with wide range of materials. Boeing 787 and Airbus A350 aircraft have many composite parts, and for these parts resins with low viscosities are used. Low viscosity resins allow for ease of manufacturing, and after the curing operation, low viscosity resins offer the best structural properties. In the Figure 14 fuselage section and nose cone of Boeing 787 manufactured by a tow placement machine is shown. [37] It should be noted that heating and compaction capability of tow placement machines is very important to manufacture primary structures.



Figure 13 An actual fiber placement machine's head while laying down [8]



Fuselage Section



Nose cone

Figure 14 The manufactured fuselage section and nose cone of Boeing 787 Dreamliner by AFP [37]

Airbus also uses the carbon fiber placement process for the production of the barrel for its A350 XWB fuselage which is shown in Figure 15. The barrel, known as section 19, is 5.5 meters long, with an area of 56 square meters, and it is placed at the rear part of the aircraft.



Figure 15 A350 XWB fuselage section manufacturing

Another application is the composite tail boom of a commercialized military helicopter which is manufactured by Automated Dynamic's AFP machine. Figure 16 illustrates the lay down and the final product. The subscale boom is roughly conical in shape, with forward cross-sectional dimensions of about 710 mm by 914 mm, an aft cross section of 622 mm by 80 mm, and a total length of 1,524 mm. [22]

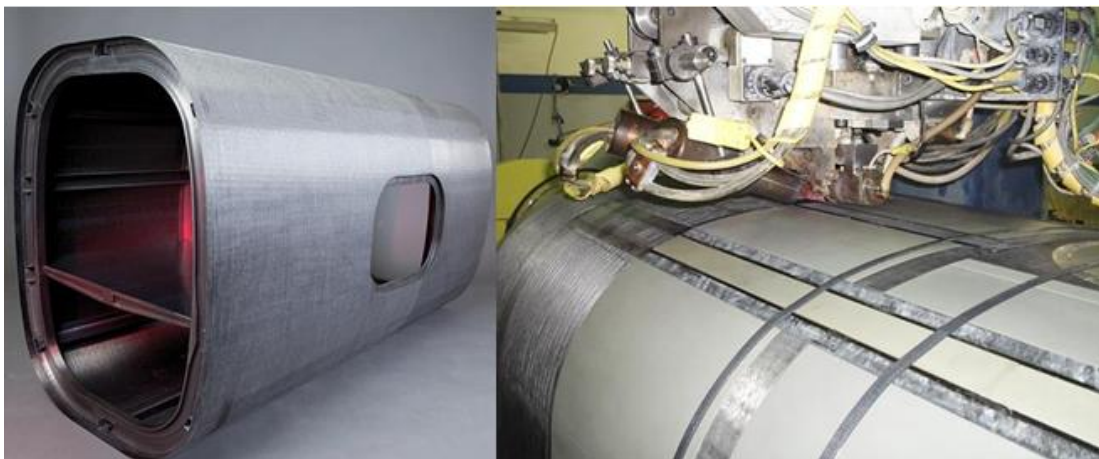


Figure 16 Manufacturing of composite tail boom by AFP, Automated Dynamics [22]

The Boeing JSF's inlet duct, engine nacelle doors and landing gear pod fairings of C17 and Hawker Horizon business jet are other examples of AFP production. [8] With the use of AFP machines in the manufacturing, costs were reduced on all programs compared to the hand layup method as a result of a reduction in part, count reduction in layup time and smaller scrap rates.

3.2. Minimum Turning Radius

The minimum turning radius is a manufacturing constraint and a design parameter in the manufacturing of the composite structure. While steering the tows, they are forced in-plane deformation. Since the inner radius of the tows is smaller than the outer radius, inner side of the tows is compressed and the outer side of tows is in tension as shown in Figure 17. If the compressive forces exceed a specific threshold, local fiber buckling occurs.

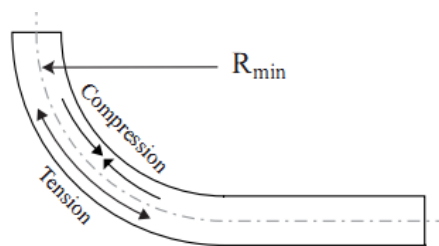


Figure 17 Minimum turning radius is required to prevent local fiber buckling due to excessive compressive forces [4]

Figure 18 shows three tows. The first one is straight tow, and second one is curved tow, which does not violate the curvature constraint. The last one is again curved tow, but it violates the curvature constraint, so wrinkling occurs.

The presence of buckled tows may lead to reduction in laminate quality. As seen in Figure 19, the surface quality of the manufactured plate is affected because of local fiber buckling. Therefore, the curvature constraint is taken into account as a manufacturing constraints. Usually in the design optimization of composite structures, limit on the turning radius is usually imposed in terms of minimum radius of the centerline of the course.

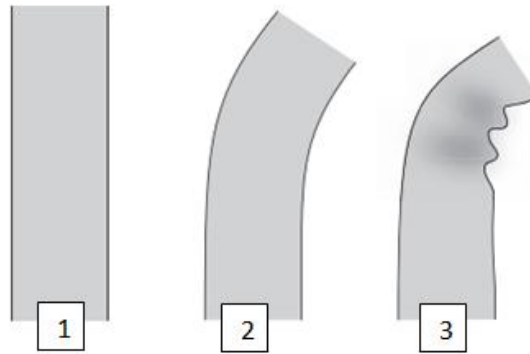


Figure 18 (1) Straight tow (2) Curved tow and (3) Curved tow which violates the curvature constraint [4]



Figure 19 Local fiber buckling due to the violation of the curvature constraint

A typical value for the minimum turning radius for a 32 tow course with 3.175 mm wide tows is 635 mm (25 in). The minimum turning radius is influenced by the tow width. Values for the minimum turning radius of a typical AFP machine for different tow widths are given in Table 1.

Table 1 Variation of minimum turning radius with tow width [23]

| Tow Width(mm) | The Minimum Turning Radius(mm) |
|---------------|--------------------------------|
| 3,175 | 635 |
| 6,35 | 1778 |
| 12,7 | 8890 |

3.3. Gaps and Overlaps

Many tow courses are laid down to cover the entire mandrel surface. During the fiber placement process, fiber angle variation causes gaps and/or overlaps occur between the courses. The formation of overlap and gap regions between tows leads to

changes in laminate thickness throughout the panel. The thickness distribution not only affects the structural response but also the surface quality. Figure 20 gives the schematic representation of overlaps and gaps.

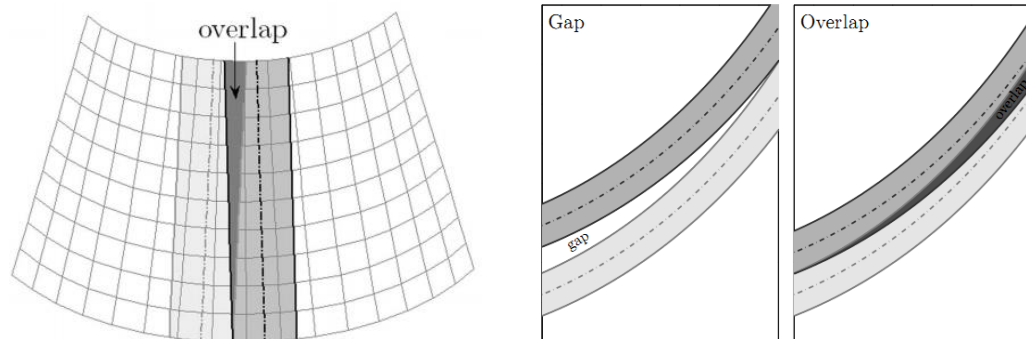


Figure 20 The illustration of overlaps and gaps [4]

The reason for gaps and overlaps is the change of the width of the course. Figure 21 shows the nominal width variation for a course with orientation angle changing from $\theta=0^\circ$ to $\theta=45^\circ$. The width of the tow is taken $1.0w$ at $\theta=0^\circ$, and when the orientation angle increases, the effective width also increases as shown in Figure 21. When the orientation angle θ becomes 45° , the nominal tow width becomes 1.4 times greater than the starting width. The nominal width and tow normal width are equal at the left side of the tow. The nominal width is increasing and becomes $1.4w$, but it is assumed that the normal width becomes constant along the tow.

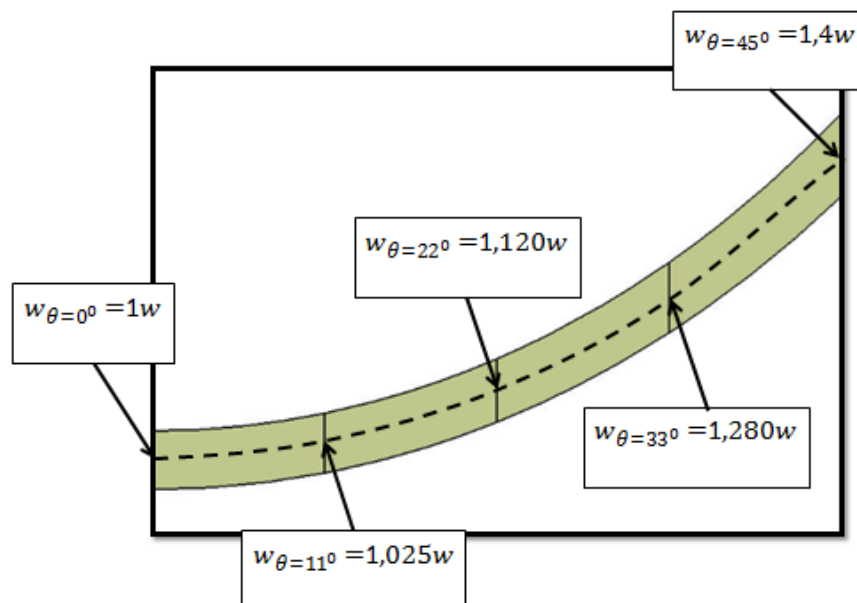
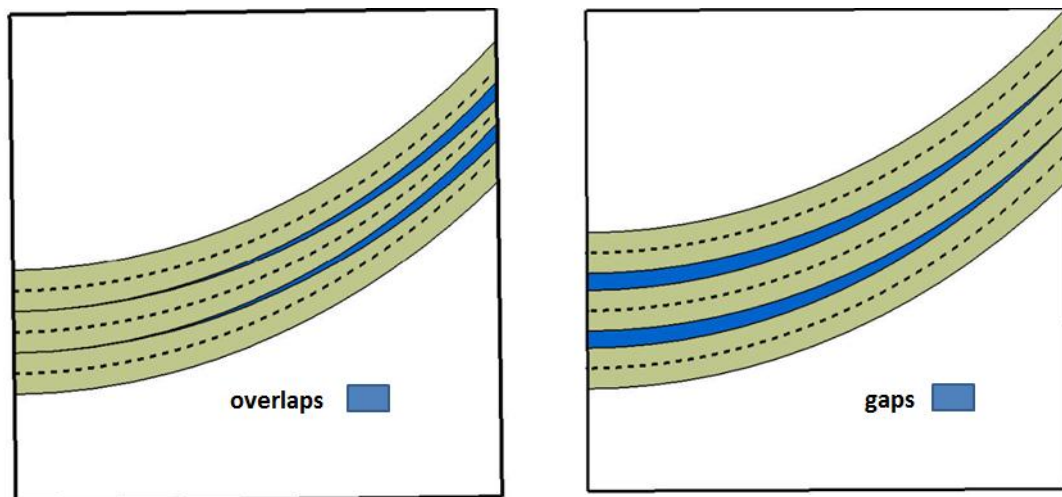


Figure 21 Nominal tow width variation by angle for $\langle 0/45 \rangle$ curved tow

The amount of shift of the fiber course in a certain direction affects gaps and overlaps. For constant tow width, for the example shown in Figure 22 if the shift distance is $1.0w$ at the beginning of the course, the shift distance would have to be $1.4w$ at the end of the course to prevent overlaps. Thus, if the shift distance is $1.0w$, then on the left of the panel, there will not be any overlap or gap, but at the end of the course, tow will not be shifted far enough and tow will overlap with the next path. On the other hand, if the shift distance is taken as $1.4w$, then on the right edge of the panel there will not be overlap or gap. However, this time gaps occur between tows at the left side of the panel. Therefore, according to the chosen shift distance, there will be overlaps or gaps in the panel. The effect of shift distance on the gaps and overlaps in the panel is shown in Figure 22. As shown in Figure 22(a), overlaps occur towards the right end of the panel, and as shown in Figure 22(b), gaps occur at the left end of the panel.



(a) Tow shift is equal to the tow width at the left end of the panel

(b) Tow shift is equal to the tow width at the right end of the panel

Figure 22 The shift distance effect in a lamina resulting in overlaps (a) and gaps (b)

The amount of the shift distance is an important parameter, and it can be defined such that a single thickness region occurs at the left of the panel. It is seen from Figure 22 (a) and (b), the shift distance between the courses and the fiber orientation angles at the left end (T_0) and at the right end (T_1) of the panel affect the size of the overlap or gap regions. The thickness change because of gaps or overlaps could

improve or degrade the mechanical response of the structure. In this research, while optimizing the structure, overlaps are allowed in the design, and it is aimed to investigate how the structural performance changes with overlaps and gaps when the fiber paths are optimized.

3.4. Minimum Cut Length

The minimum cut length is an important constraint in the manufacturing of fiber-placed composites. Minimum cut length is the minimum tow length that needs to be laid down before the tow can be cut after it is laid down. [2] Minimum cut length depends on the design of the fiber placement head, and it varies between 63 and 152 mm. For instance Viper 1200 fiber placement machine has a 100 mm minimum cut length. The fiber placement head does not place any tows that are shorter than the minimum cut length.

During the manufacturing of composite structures by fiber placement machines, the design boundary must sometimes be changed to place longer courses and then the excess material must be trimmed later so that minimum cut length constraint is satisfied. Figure 23 demonstrates the minimum cut length constraint on a rectangular part. From Figure 23, it can be seen that while laying down tows on the top left or on the bottom right corner of the panel, since the corners are shorter than the minimum cut length, longer courses must be placed. [4] Therefore, it can be said that the boundary of the part might be changed according to minimum cut length to satisfy the minimum cut length constraint.

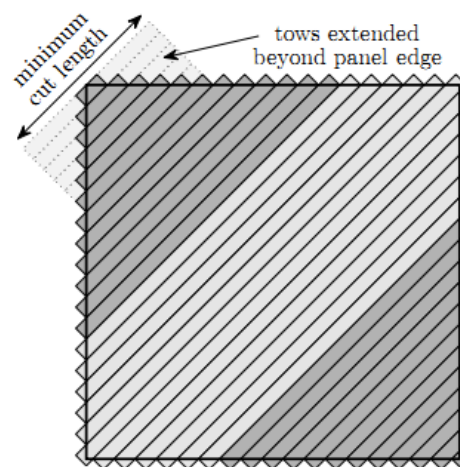


Figure 23 Demonstration of minimum cut length constraint [4]

3.5. Coverage Parameter

Another design parameter in fiber placement technology is the coverage parameter. This parameter has an effect on the strength and on the surface quality of a laminate. Coverage parameter can be defined as the gap/overlap parameter. Composite parts created with 0 % coverage parameter cause gaps between two curved courses. In a laminate with 0 % coverage parameter, since overlap is not allowed between tows, resin rich areas exist in the laminate. Figure 24 shows the ply lay-up with 0 % coverage parameter. The white areas which are seen in Figure 24 are gaps, and they reduce the strength of the composite laminate. On the other hand, coverage of 100 % causes overlaps and the thickness of the laminate vary in the laminate because of the overlaps. Overlaps destroy the surface quality of the part but at the same time overlap regions act like stiffeners which may improve the laminate strength. Fifty percent coverage parameter implies that gaps and overlaps are equal.

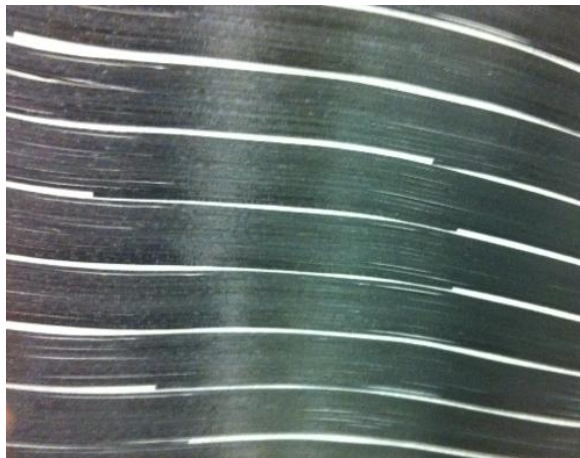


Figure 24 A lamina with 0 % coverage parameter

CHAPTER 4

PARTICLE SWARM OPTIMIZATION AND CONSTRAINED OPTIMIZATION

4.1. Introduction

The chosen optimization method is important to find optimum solution of the problem. The type of the design variables, the type of objective function, shape of design space, the number of design variables, cost of each evaluation is important while choosing the optimization method.

Particle swarm optimization (PSO) is a population based optimization technique introduced by Dr. Eberhart and Dr. Kennedy in 1995. It is based on by social behavior of bird flocking or fish schooling, which collaboratively searches area to find food. [28] The algorithm was simplified and it was observed to be performing optimization. An extensive survey of PSO applications is made by Poli. [31, 32]

PSO shares many similarities with evolutionary computation techniques such as Genetic Algorithms (GA). PSO does not suffer from some of the problems found in genetic algorithm. For instance, the iteration with the group improves the solution, instead of negative impact on the progress of evaluation. PSO has no evolution operators such as crossover and mutation. Moreover, PSO has memory so, knowledge of good solution is retained within all particles; whereas for example in GAs, previous knowledge of the problem will be destroyed once the population changes. Compared to GA, PSO is simple and implementation is easy. Therefore, PSO has gained much attention and has been successfully applied in a variety of

fields such as function optimization, the model classification, machine study, neural network training, the signal procession, vague system control, and automatic adaptation control. Also, PSO does not require that the optimization problem be differentiable as is required by classical optimization methods such as gradient descent and quasi-newton methods.

4.2. PSO Algorithm

In the basic particle swarm optimization algorithm, particle swarm consists of “ D ” candidate solution (called particles), and the position of each particle stands for the potential solution in D -dimensional space. The particles change its condition according to the following three principles:

- (1) To keep its inertia ; each particle is treated as a point in a D -dimensional space
- (2) To change the condition according to its best position ; each particle keeps track of its coordinates in the solution space
- (3) To change the condition according to the swarm’s best position; another best value that is tracked by the PSO is the best value obtained so far by any particle in the neighborhood of that particle. This value is called *gbest*.

The basic concept of PSO lies in accelerating each particle toward its *pbest* and the *gbest* locations, with a random weighted acceleration at each time step as shown in Figure 25.

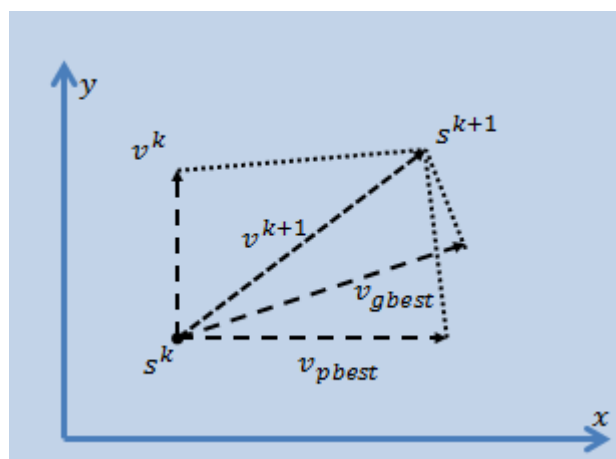


Figure 25 Concept of modification of a searching point by PSO

In Figure 25, parameters $s^k, s^{k+1}, v^k, v^{k+1}, v_{pbest}$ and v_{gbest} :

- s^k :Current searching point
- s^{k+1} :Modified searching point
- v^k :Current velocity
- v^{k+1} :Modified velocity
- v_{pbest} :Velocity based on $pbest$
- v_{gbest} :Velocity based on $gbest$

Consider a minimization problem :

Minimize $F(s)$

With $s_{min} < s < s_{max}$

Where s_{min} and s_{max} denote the lower and upper bounds.

The maximum velocity of the particles is defined at the beginning, is given in Eqn. 4.1

$$v_{max} = \sigma * (s_{max} - s_{min}) \quad (4.1)$$

Where σ is the coefficient to determine maximum velocity.

The basic algorithm of PSO is described below in steps.

For each particle $i=1, \dots, D$;

1. Create and initialize a population of particles with random positions and velocities on D dimensions in the problem space.
2. Evaluation of each particle's position
3. Update of the particle position if a particle's current position is better than its previous best position
4. Determine the best particle
5. The particles' velocities are updated according the Eqn. 4.2

$$v_i^{k+1} = w * v_i^k + c_1 * r_1(\dots) * (s_{pbest}^k - s_i^k) + c_2 * r_2(\dots) * (s_{gbest}^k - s_i^k) \quad (4.2)$$

Velocity v_i^{k+1} (which denotes the amount of change) is a function of the difference between the individual's personal best s_{pbest}^k and its current position, and the differences between the neighborhood's best s_{gbest} and its current position. c_1 and c_2 are the cognitive (individual), and social (group) learning rates. r_1 and r_2 are uniformly distributed random numbers in the range 0 and 1. The values of c_1 and c_2 are usually assumed to be 2 so that $c_1 * r_1$ and $c_2 * r_2$ ensure that the particles would overfly the target. [29]

Where v_i^{k+1} , w , v_i^k , s_{pbest}^k , s_i^k , s_{gbest} ;

- v_i^{k+1} : New velocity of particle i at iteration $k+1$
- w : Weighting function
- v_i^k : Particle velocity of i at iteration k
- s_i^k : The position of particle i at iteration k
- s_{pbest}^k : The best position of particle i
- s_{gbest} : The best position of the swarm

Selecting PSO parameters that yield good performance has therefore been the subject of much research. The weighting function is usually utilized, w is the inertia factor and α is the decreasing factor of inertia formulated in Eqn. 4.3.

$$w = \begin{cases} w_{min} & \text{if } w < w_{min} \\ w_{max} * \alpha & \end{cases} \quad (4.3)$$

A large inertia weight, w facilitates a global search. By decreasing the inertia weight from a relatively large value to a small value through the course of the PSO run gives the best PSO performance compared with fixed inertia weight settings.

6. Update particles position according to Eqn. 4.4

$$s_i^{k+1} = s_i^k + v_i^{k+1} \quad (4.4)$$

7. Loop to step 2 until a criterion is met.

The schematic representation of particle swarm optimization is shown in Figure 26.

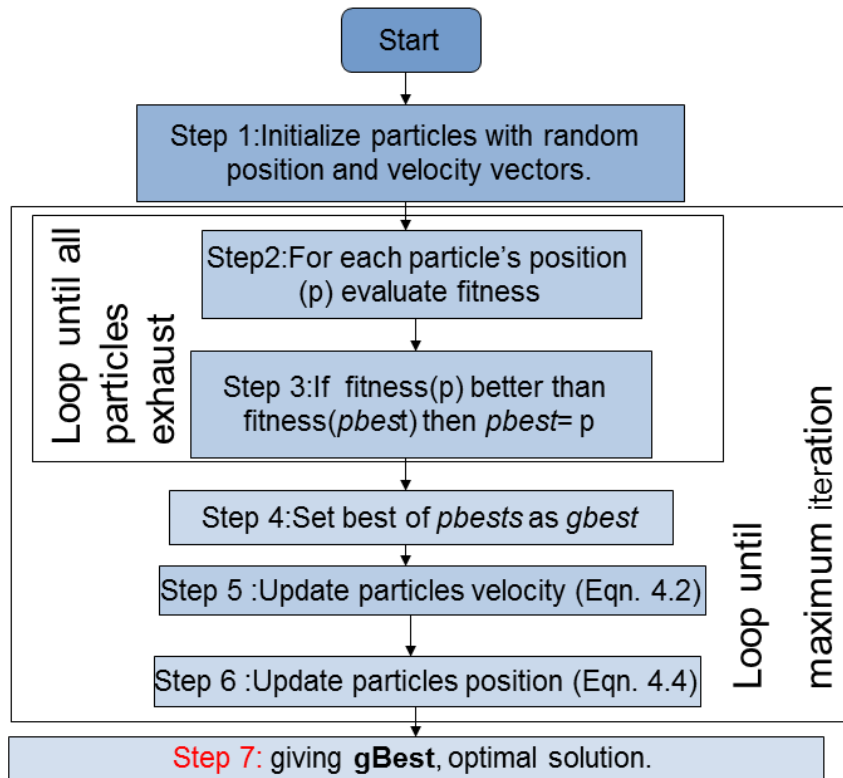


Figure 26 Particle Swarm Optimization Algorithm

In this thesis, the convergence criterion is taken as getting the same value for the swarm's best known position twice. When the PSO code determines the swarm's best known position, PSO algorithm does not terminate. The program passes the swarm's best known position inside the initial swarm like a randomly created swarm and the optimization cycle starts again. If the passed the swarm's best known position is obtained again at the end of the new cycle, the program terminates. By using this approach, it is aimed to prevent getting local optimum point, and to give a second chance to find the global optimum, if found, to be sure about the global optimum. This approach assumes that instead of using a big population, small but repeated and fast generation of population might be beneficial to reach to global optimum.

4.3. The Constrained Problem

A general optimization problem is about determining design variables to minimize or maximize the objective function. The objective function is a function returns a single value from which different designs can be compared. It is a scalar

quantity that is either minimized or maximized by the optimizer. The optimal design is the design with a minimum (or maximum) value of the objective. Design characteristics that are varied to achieve the objective are called as design variables. Discrete design variables can take only discrete values, typically from a list of permissible values. In this thesis, the design variables are taken as discrete values to decrease time cost.

In optimization problems, there can be some constraints that have to be satisfied while minimizing (or maximizing) the objective function. Conditions that the designs must meet are called as design constraints. If $F(x)$ is objective function subjects to a set of inequality constraints $g(x)$ and equality constraints $h(x)$, then a typical minimization optimization problem is defined as in Eqns. 4.5, 4.6, 4.7 and 4.8:

$$\text{Minimize } F(x) \tag{4.5}$$

$$\text{Subject to; } g_i(x) \geq 0 \quad i = 1, 2, \dots, n_g \tag{4.6}$$

$$h_i(x) = 0 \quad i = 1, 2, \dots, n_h \tag{4.7}$$

$$x_i^L \leq x_i \leq x_i^U \quad i = 1, 2, \dots \tag{4.8}$$

Constrained optimization (CO) problems are encountered in many applications. Although Evolutionary Algorithms have been developed primarily as unconstrained optimization methods, they are considered as a good alternative for solving constrained optimization problem. [36]

The most common approach for solving CO problems is the use of a penalty function. The constrained problem is transformed to an unconstrained problem, by penalizing the constraints. [33] This is the main reason behind the popularity of the penalty function. In this thesis, PSO code performed in solving the constrained problem by using the penalty function. The advantage of the penalty function approach is that many constraints in the real world are "soft", in the sense that they need not be satisfied precisely. The penalty function approach is well-suited to this type of problem.

Penalty function approach converts the constrained optimization problem into an unconstrained optimization problem. Then, the optimization problem can be solved

as an unconstrained problem. Modification of the objective function is achieved by adding penalty function $P(x)$ to the objective function and defining r_h and r_g which are the penalty function multiplier. This additional function should penalize the objective function only outside the feasible region. In order to achieve this, penalty function can be chosen as Eqns. 4.9 and 4.10. [30]

$$F(x, r_h, r_g) = F(x) + P(x, r_h, r_g) \quad (4.9)$$

$$P(x, r_h, r_g) = r_h * \sum_{i=1}^l h_i(x)^2 + r_g * \sum_{i=1}^m \max(0, g_i(x))^2 \quad (4.10)$$

Definition of the penalty function by Eqn. 4.10 assures that when the constraints are violated the new objective function becomes large, thus objective function is penalized. Also, constants “ r_h ” and “ r_g ” are used to adjust the weight of the penalty function. These constants are called weighting factors or penalty parameters and it is not necessary to change them in each iteration.

In this part of the thesis, the general information is given about Particle Swarm Optimization. In Chapter 5, the application of PSO to the optimization of composite laminate, which constraint are applied and how the objective function is formulated are given in detail. The code is specific for the optimization of variable stiffness laminates, the parameters definitions are only for the defined problems.

4.4. The Verification of PSO Code

In this section, two test problems are demonstrated in order to test the performance of the PSO algorithm. The PSO parameters and the penalty multiplier r_g are taken from Table 2 for optimization.

Table 2 The PSO and penalty multiplier

| | <i>PSO Parameters</i> |
|-----------|-----------------------|
| c_1 | 2 |
| c_2 | 2 |
| w_{max} | 1 |
| w_{min} | 0,4 |
| α | 0,99 |
| σ | 0,4 |
| r_g | 10^4 |

4.4.1. The Test Problem 1

The first test problem is defined in Figure 27. The objective is to minimize the function defined in Eqn. 4.11 subject to the constraint defined in Eqn. 4.12. The design variables are X_1 and X_2 . Firstly, the constrained problem is converted to unconstrained problem by using penalty approach.

$$f(X_1, X_2) = 0.25 * X_1^4 - 3 * X_1^3 + 11 * X_1^2 - 13 * X_1 + 0.25 * X_2^4 - 3 * X_2^3 + 11 * X_2^2 - 13 * X_2 \quad (4.11)$$

$$g_1(X_1, X_2) = 4 - X_1 - X_2 \leq 0 \quad \text{and} \quad 0 < X_1, X_2 < 6 \quad (4.12)$$

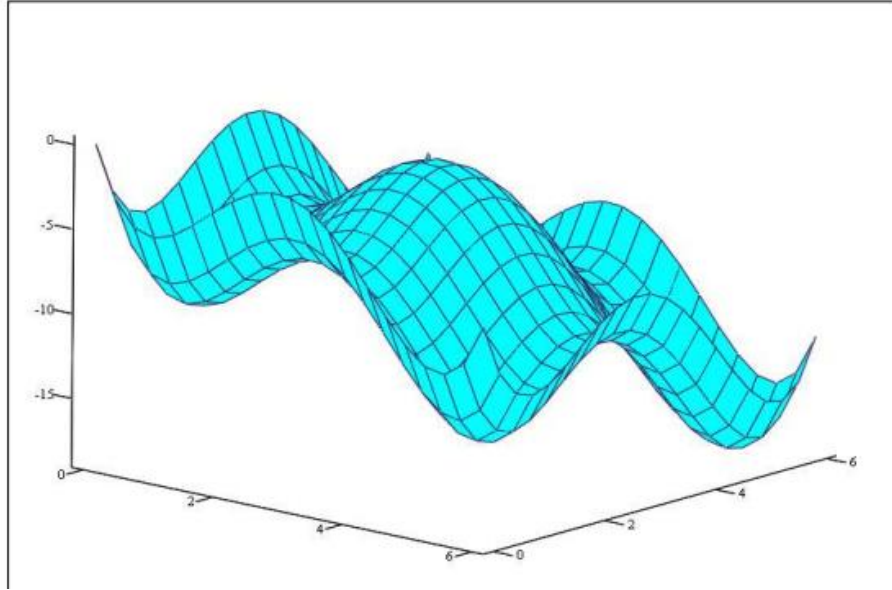


Figure 27 Test Problem 1

The constrained problem converted to unconstrained problem in Eqns. 4.13 and 4.14, and solved by PSO algorithm and the results are given at Table 3

$$F(X_1, X_2, r_g) = f(X_1, X_2) + P(X_1, X_2, r_g) \quad (4.13)$$

$$P(X_1, X_2, r_g) = r_g * \max(0, g_1(X_1, X_2))^2 \quad (4.14)$$

If $g_1(X_1, X_2)$ is less than zero, the constraint is satisfied and the penalty is not applied. If $g_1(X_1, X_2)$ is greater than zero, the constraint is violated and the penalty is applied and the penalty is multiplied by r_g .

Table 3 Comparison of optimization results for the test problem 1

| | <i>Exact Global Optimum Point</i> | <i>Exact Fitness Value</i> | <i>PSO, Global Optimum Point</i> | <i>Objective Function</i> | <i>% Error</i> |
|-----------|-----------------------------------|----------------------------|----------------------------------|---------------------------|----------------|
| X1 | 5,33 | -18,568 | 5,4035 | -18,5365 | 0,12 |
| X2 | 5,33 | | 5,3345 | | |

The PSO algorithm gives the minimum at point (X_1, X_2) at (5.4035, 5.3345) with $f(X_1, X_2) = -18.5365$. The exact minimum is -18.568 for this problem. Error is determined as 0.12 % compared to the exact minimum of the function.

4.4.2. The Test Problem 2

The second test problem is defined in Figure 28. The objective is to maximize the function defined in Eqns. 4.15, 4.16 and 4.17. The design variables are x and y .

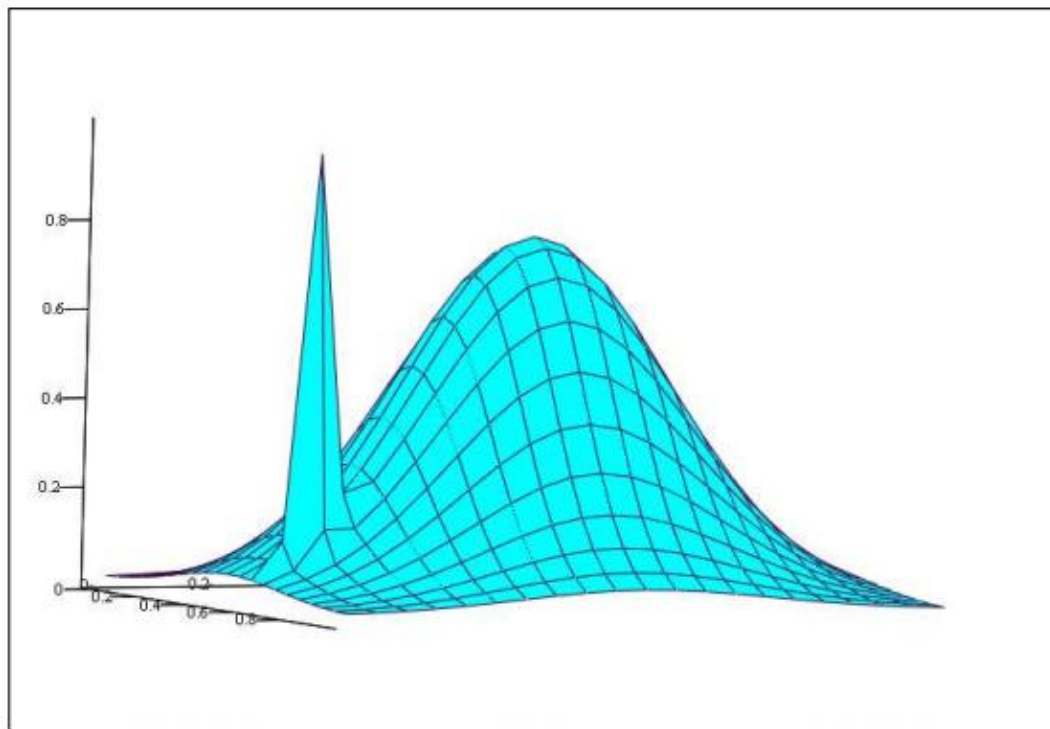


Figure 28 Test Problem 2

$$f(x, y) = 0.8 * \exp\left(\frac{r_1^2}{0.09}\right) + 0.8 * \exp\left(\frac{r_2^2}{0.0009}\right) \quad (4.15)$$

$$r_1^2 = (x - 0.5)^2 + (y - 0.5)^2 \quad x, y \in [0,1] \quad (4.16)$$

$$r_2^2 = (x - 0.6)^2 + (y - 0.1)^2 \quad (4.17)$$

The problem was solved by PSO algorithm and the results obtained with the PSO algorithm, is compared with exact results in Table 4.

Table 4 Comparison of optimization results for the test problem 2

| | <i>Exact Global Optimum Point</i> | <i>Exact Fitness Value</i> | <i>PSO, Global Optimum Point</i> | <i>Objective Function</i> | <i>% Error</i> |
|----------|-----------------------------------|----------------------------|----------------------------------|---------------------------|----------------|
| x | 0,6 | 1 | 0,602 | 0,9917 | 0,82 |
| y | 0,1 | | 0,1026 | | |

The PSO algorithm gives the maximum at point (x, y) at $(0.602, 0.1026)$ with a function value of $f(x, y) = 0.9917$. Exact maximum is 1 for this problem. Error is determined as 0.82 % compared to the exact maximum of the function.

The test results show that PSO code works properly and can be used to optimization problems.

CHAPTER 5

FINITE ELEMENT MODELLING AND OPTIMIZATION OF VARIABLE STIFFNESS COMPOSITE CYLINDER STRUCTURES

5.1. Introduction

Optimization of variable-stiffness laminates and determining the structural response are difficult tasks. Besides the continuously varying fiber orientation within a ply, another difficulty is associated with the formation of gaps or overlaps between courses, resulting in varying thickness in a laminate from point to point. To develop an analytical closed-form solution to a problem with spatially varying fiber orientations and thickness is almost impossible. Therefore, in the present research, the finite element method is used to analyze the variable-stiffness laminates with continuously varying fiber orientation as a function of position only in one direction. For the cylindrical shell structures, the variation direction of the fiber orientation is taken as either axial or circumferential, and the shifted course method is used to shift the fibers in the perpendicular direction to the variation direction of the fiber orientation. In the study, hybrid laminates which consist of constant stiffness and variable stiffness plies are also investigated. The finite element model of variable stiffness laminates, and coupling of finite element solver and optimization algorithm are explained in detail in this chapter. PSO algorithm is used for the optimizer and MSC.Nastran as the finite element solver. PSO and MSC.Nastran are coupled with a MATLAB code.

5.2. Determination of Optimum Fiber Paths of Variable Stiffness Composite Cylinder Structures

5.2.1. Nomenclature of Variable Stiffness Lamina

Variable stiffness ply is designed by curvilinear fiber paths parameters which cannot be described by a single orientation angle. A continuous fiber path is assumed that the fiber orientation of the reference fiber path varies linearly from one value at the beginning of the cylinder to another value at the end of the cylinder.

The fiber orientation of the composite lamina can be determined with two variables. These variables are defined as T_0 and T_1 . [10] For the axially varying fiber orientation case, T_0 is the fiber orientation angle of the reference fiber path calculated at the beginning of the cylinder, T_0 and T_1 is the fiber orientation angle measured at the end of the cylinder. Parameters T_0 and T_1 are shown in Figure 29.

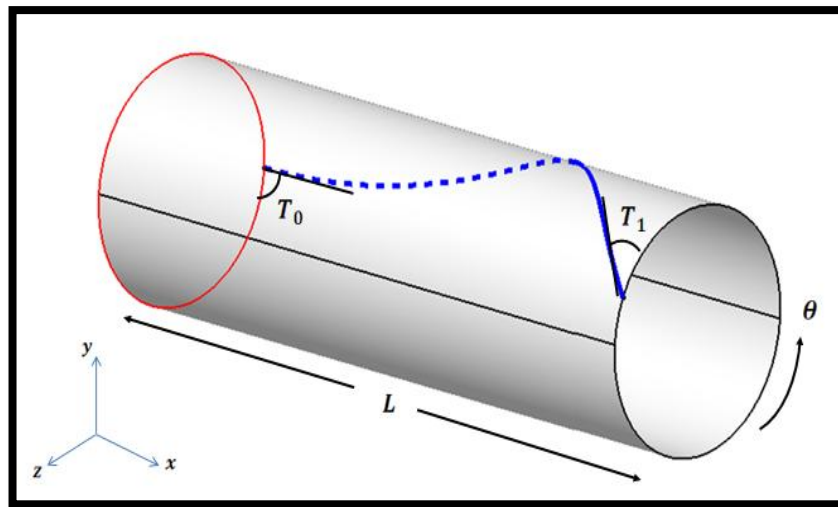


Figure 29 Fiber path parameters, T_0 and T_1 for the axially varying fiber orientation case

The stacking sequence is used to form a composite laminate. Variable-stiffness lamina cannot be stacked like traditional composite laminate to form a variable-stiffness laminate because the thickness and orientation angles of a variable-stiffness

laminate vary. Variable-stiffness laminates also require special nomenclature to specify the stacking sequence.

The stacking sequence is used to form a composite laminate. Variable-stiffness lamina cannot be stacked like the traditional composite laminate to form a variable-stiffness laminate, because the thickness and the orientation angle of variable-stiffness laminates vary. Variable-stiffness laminates also require special nomenclature to specify the stacking sequence.

In the traditional composite laminates' stacking sequence nomenclature, fiber-orientation angles are listed inside a set of square brackets and each layer is separated by slashes. As an example, stacking sequence of a traditional composite laminate could be defined as $[45/-45/0/90/90/0/-45/45]$. In this example, design represents an eight-layer laminate. The laminate could also be summarized in a shorter form as $[\pm 45/0/90]_s$. The subscript "s" means that the laminate is symmetric with respect to a reference plane which is commonly taken as the mid plane of the laminate. Traditional composite notation is not enough to define variable stiffness laminate, therefore it is necessary to use a modified version of the notation used for traditional laminates. To designate a variable stiffness composite laminate, instead of using multiple constant-orientation angles offset by slashes, the special angled brackets for each variable-stiffness lamina are placed inside square brackets and offset by slashes, given in Eqn. 5.1.

$$[\langle 15|60 \rangle / \langle -15| - 60 \rangle / \langle -15| - 60 \rangle / \langle 15|60 \rangle] \quad (5.1)$$

In Eqn. 5.1 fiber orientation angle defined by T_0 is equal to 15^0 and T_1 is 60^0 . Variable stiffness laminate defined by $[\pm \langle 15|60 \rangle]_s$ is exactly the same as the laminate listed explicitly shown in Eqn. 5.1 above. A \pm outside of the square brackets or angle brackets denotes two variable stiffness layers. The first layer would have the signs shown in the brackets and the second layer would have the opposite of the signs shown in the brackets. Thus a $[\pm \langle 15|60 \rangle]$ would define two layers, a $\langle 15|60 \rangle$ layer and a $\langle -15|-60 \rangle$ layer. Additionally, a subscript "s" is used to denote that each layer in a laminate has a symmetric layer associated with it.

5.2.2. Variation of fiber orientation angle in the axial direction for the cylindrical shell

The fiber orientation angle on the cylindrical shell is defined by the parameters T_0 and T_1 . Fiber orientation angle varies linearly along the shell axis x from T_0 at the beginning of the cylinder to T_1 at the end of the cylinder. Eqn. 5.2 shows the formulation of fiber orientation angle φ where L is the length of the cylinder. [4]

$$\varphi(x) = T_0 + \frac{(T_1 - T_0)x}{L} \quad (5.2)$$

The formulation for the three dimensional path definition over the cylinder and the curvature of path κ are given Eqn. 5.3 and Eqn. 5.4. [4]

$$\theta(x) = -\frac{L}{R(T_1 - T_0)} \ln(\cos \varphi) + \frac{L}{R(T_1 - T_0)} \ln(\cos T_0) \quad (5.3)$$

$$\kappa(x) = \frac{T_1 - T_0}{L} \cos \varphi \quad (5.4)$$

Where $\theta(x)$ is the circumferential coordinate, and R is the radius of the cylinder.

5.2.3. Variation of fiber orientation angle in the circumferential direction for the cylindrical shell

The orientation for a fiber path on a cylindrical shell with a circumferentially varying fiber orientation angle is defined in Eqn. 5.5. [4]

$$\varphi(\theta) = T_0 + (T_1 - T_0) \frac{(\theta - \theta_1)}{(\theta_1 - \theta_0)} \quad (5.5)$$

where θ_0 and θ_1 are the circumferential locations at which the linear angle variation starts and ends, respectively.

The fiber path formula is given in Eqn. 5.6 [4]

$$x = \frac{\theta_1 - \theta_0}{T_1 - T_0} (\ln(\sin \varphi) - \ln(\sin T_0)) \quad (5.6)$$

The expression for the in-plane curvature in Eqn. 5.7. [4]

$$\kappa(\theta) = \frac{(T_1 - T_0)}{R(\theta_1 - \theta_0)} \sin\varphi \quad (5.7)$$

The path and curvature definitions for the axial and the circumferential directions, which were introduced by Bloom [4], are used to define variable-stiffness plies in this thesis.

The goal for this thesis is to design and analyze variable stiffness composite cylinder by employing fiber paths such that the composite cylinder can also be manufactured. For this purpose, Eqn. 5.4 and Eqn. 5.7 are used to define curvature constraints for the fiber path which varies either along the axial or along circumferential direction. A curvature constraint for the tows is taken from the Reference 23 given in Table 1 before in Chapter 2. The maximum allowable curvature for the 3,175mm width tow is 1/635mm. Therefore, in the present study, minimum turning radius is taken as 635 mm. If this value is violated, the solution is unfeasible because laminate is not manufacturable. In the optimization process of the fiber path, unfeasible solutions are handled by penalizing the objective function by a very large number in the taking the manufacturing constraint into account. The detail formulation of objective function and constraint is given in this chapter.

5.2.4. Shifted fiber path

In order to create variable-stiffness composite laminate, reference fiber path method, is commonly employed in the literature. The shifted fiber paths are used to define the remaining fiber paths based on the reference fiber path definition. [10]

In this thesis, shifted fiber path definition is used in the fiber path optimization study. Shifted fiber path can simply be defined as the shifting of the reference fiber path by a fixed amount in the perpendicular direction to variation direction of the fiber orientation angle. Figure 30 shows a reference path that varies axially and all the shifted paths are generated based on this reference fiber path to cover the entire surface of cylinder.

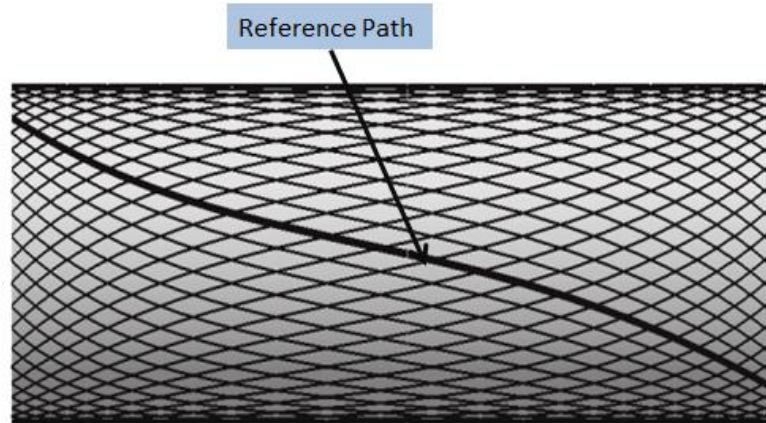


Figure 30 Reference path and shifted fiber paths along the axial direction

The direction of variation of the fiber orientation angle changes along the axial direction, x and the reference path is shifted along the circumferential direction, as shown in Figure 31. Therefore, the cylinder manufactured using the first method is called as axially varying variable stiffness cylinder.

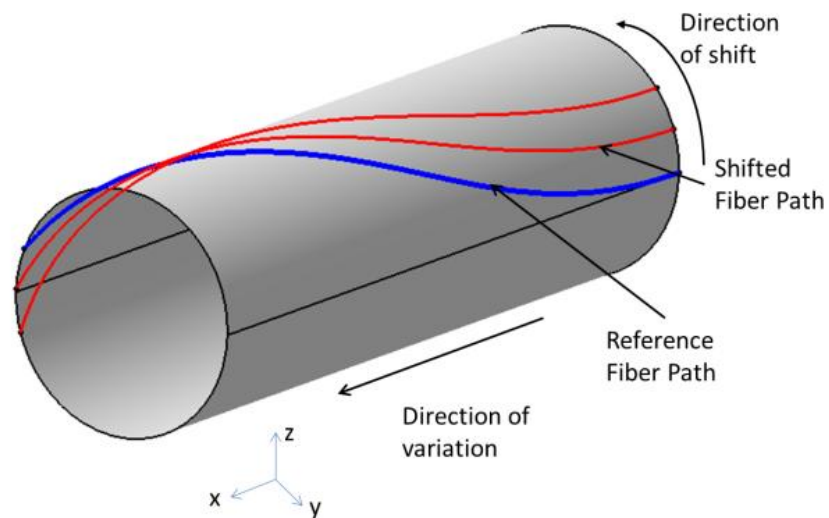


Figure 31 Variable stiffness cylinder with axially varying fiber orientation angle

The number of the shifted paths and the shift distance is important parameters which for axially variable stiffness laminates depend on the path parameters T_0 and T_1 . Number of the shifted path and the shift distance for axially variable stiffness lamina

is given in Eqns. 5.8 and 5.9. The shift distance is actually the shift orientation for axially variable stiffness laminate because the shift is around the cylinder.

$$Shifted_number = \max\left(\frac{Cyr_length * \cos T_0}{2 * Tow_width}, \frac{Cyr_length * \cos T_1}{2 * Tow_width}\right) \quad (5.8)$$

$$Shift_orientation = 2\pi / (2 * Shifted_number) \quad (5.9)$$

The gaps are not allowed by using Eqn. 5.8 and Eqn. 5.9 because the shift number formula gives the maximum and an integer number. The shift direction is circumferential direction, and the shift orientation is calculated around the circumferential direction for axially variable stiffness laminates. The cylinder length is 635mm and tow width is 38.1 mm.

The second type of variable stiffness cylinder is the one with circumferentially varying fiber orientation angle shown in Figure 32. In this case, the direction variation of the fiber orientation angle is around the cylinder, in the direction, and the reference path is shifted along the axis of the cylindrical shell.

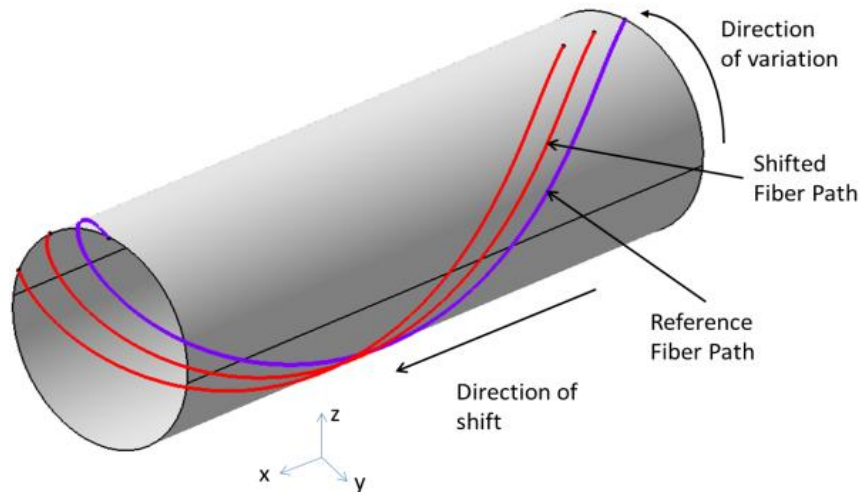


Figure 32 Variable stiffness cylinder with circumferentially varying fiber orientation angle

The shift number is taken as a constant value because the shift distance is independent from the shift direction for circumferential variable stiffness laminate because the shift direction is along the axial direction. The shift number is taken 30 and the shift distance formula is given in Eqn. 5.10 along the axial direction for circumferential variable stiffness laminates.

$$Shift_distance = \frac{Tow_width}{\max(\sin T_0, \sin T_1)} \quad (5.10)$$

The shift distance is minimum to prevent gaps according to T_0 and T_1 reference path parameters.

5.2.5. Cylinder Shell Geometry

In the present study, the cylindrical shell geometry, mesh of the cylinder, material property definition, load and boundary conditions are all prepared in the commercial pre-processor MSC.Patran. The cylindrical shell is 635 mm (25") in length and radius of the cylinder is 101 mm (4"), as seen in Figure 33

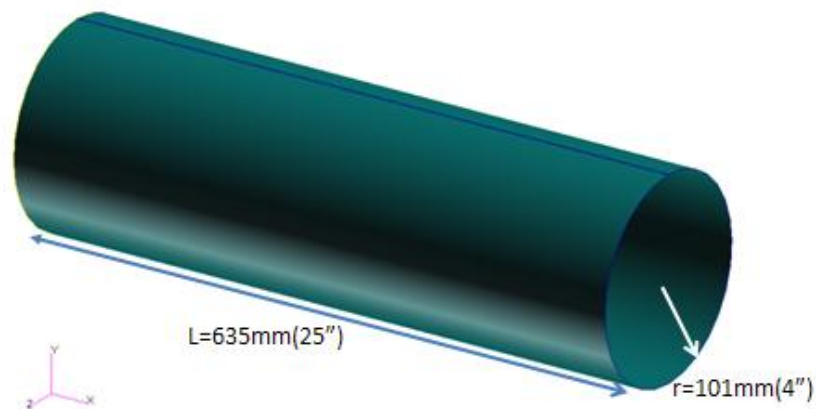


Figure 33 Dimensions of the cylindrical shell

In the study, 2500 quadrilateral shell elements with four corner nodes are used to generate the finite element mesh on the surface of the cylinder. The mesh size is 12.7 mm x 12.7 mm on the cylinder is illustrated in Figure 34.

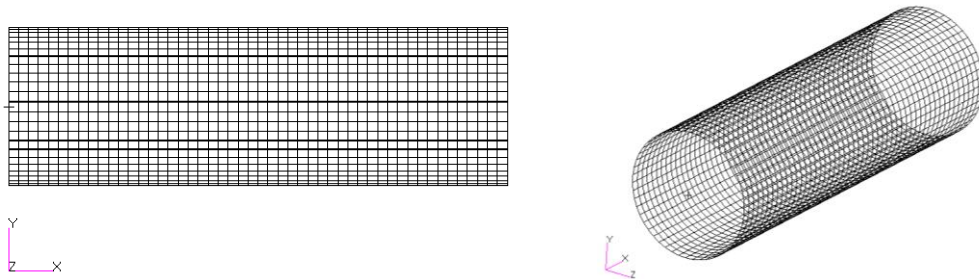


Figure 34 The mesh of the cylinder shell

5.2.6. Material Properties

For this research, all layers are made of the same composite material. In order to properly characterize a composite material, many material properties must be known. The material properties listed below at Table 5.

Table 5 Material Properties of AS4/855-2, Graphite Epoxy [38]

| Property Name | Property Definition | |
|---------------|--|-----------|
| E_1 | Modulus in the fiber direction | 129 GPa |
| E_2 | Modulus perpendicular to fibers | 9.1 GPa |
| ν_{12} | Poisson's ratio | 0.32 |
| G_{12} | In-plane shear modulus | 5.3 GPa |
| X_T | Tensile strength in fiber direction | 2070 MPa |
| X_C | Compressive strength in fiber direction | 1160 MPa |
| Y_T | Tensile strength transverse to fiber direction | 132.7 MPa |
| Y_C | Compression strength transverse to fiber direction | 199.8 MPa |
| S | Shear strength | 117.1 MPa |
| t | Thickness of ply | 0.183 mm |

5.2.7. Finite Element Solver

In the present study, solver which is used in the optimization process is the finite element solver MSC.Nastran. MSC Nastran is a finite element analysis (FEA) program that was originally developed for NASA in the late 1960s. NASTRAN software application was written to help design more efficient space vehicles such as the Space Shuttle. [34]

5.2.8. Failure Criteria

MSC.Nastran calculates the stresses in each layer of each element in the fiber and transverse to the fiber directions. As such, these stresses can be employed in a failure criterion to calculate the failure indices to predict failure in each layer. Nastran also has the ability to automatically calculate failure indices based on many different failure criteria commonly used in composite material analysis. The methods available include maximum strain, maximum stress, Tsai-Hill, Hoffman and Tsai-Wu failure theories. For each of the failure criterion, it is necessary to give the failure strength in tension and compression for both the fiber direction and transverse to the fiber direction and the shear failure strength as input. The failure index is then calculated according to each theory. If the failure index reaches a value of 1.0, then failure is assumed to have occurred. In this thesis, Tsai-Wu failure criterion is applied to calculate the failure indices which were calculated by using the stress information which comes from Nastran output file.

Tsai-Wu Failure Criteria allows for the failure strengths to differ in tension and compression. The failure can occur due to a combination of failure modes. The formulation of failure indices calculation is given Eqns. 5.11 to 5.17. [27]

$$F_1 = \left(\frac{1}{X_t} - \frac{1}{X_c} \right) \quad (5.11)$$

$$F_2 = \left(\frac{1}{Y_t} - \frac{1}{Y_c} \right) \quad (5.12)$$

$$F_{11} = \left(\frac{1}{X_t} * \frac{1}{X_c} \right) \quad (5.13)$$

$$F_{22} = \left(\frac{1}{Y_t} * \frac{1}{Y_c} \right) \quad (5.14)$$

$$F_6 = \left(\frac{1}{S^2}\right) \quad (5.15)$$

$$F_{12} = -0.5(F_1 * F_2)^{0.5} \quad (5.16)$$

$$FI = \sigma_1 * F_1 + \sigma_2 * F_2 + \sigma_1^2 * F_{11} + \sigma_2^2 * F_{22} + \sigma_3^2 * F_6 + 2F_{12} * \sigma_1 * \sigma_2 \quad (5.17)$$

5.2.9. The Buckling Load Factor

The objective of the optimization of variable stiffness cylinder that is investigated the next chapter is to maximize the buckling load factor while satisfying certain stress constraints under different load cases. The buckling load factor is also calculated by MSC.Nastran by the solution sequence Sol 106. The buckling load factor (BLF) is a factor of safety against buckling or a ratio of the buckling loads to the currently applied loads. Table 6 illustrates the interpretation of the Buckling Load Factor (BLF) values.

Table 6 Description of Buckling Load Factor values

| BLF | Buckling Status | Remark |
|--------------|------------------------|--|
| 1 < BLF | Buckling not predicted | The applied loads are less than the critical loads. |
| 0 < BLF < 1 | Buckling predicted | The applied loads exceed the critical loads. |
| BLF = 1 | Buckling predicted | The applied loads are exactly equal to the critical loads. |
| BLF = -1 | Buckling not predicted | The model is in tension and buckling is not expected. |
| -1 < BLF < 0 | Buckling not predicted | Buckling is predicted if you reverse all loads. |
| BLF < -1 | Buckling not predicted | Buckling is not expected even if you reverse all loads. |

5.2.10. Creation of Variable Stiffness Finite Element Model

The finite element method is an excellent tool for determining the structural response of systems with complex geometry or boundary conditions, such as variable-stiffness laminates. The input file of the finite element model of the cylindrical shell having complex geometry and variable stiffness can be easily prepared in MSC.Nastran which performs finite element analysis. The task is to develop a method that can be used to generate finite element input accurately with enough detail in the model for a wide range of designs. In this section, the approach used to generate the finite element model, and how this approach is implemented in the present study is described in detail.

5.2.10.1. Finite Element Modeling of a Reference Path

The first step in creating the finite element model of the variable stiffness cylindrical shell is to create a continuous reference path. Reference path on the surface of the cylinder is generated by using the reference path parameters T_0 and T_1 . After the path is defined, the distance between the center of each element and the reference fiber path must be determined. The distance is determined using a Golden Section search to minimize the distance between the element center and the reference fiber path [15]. The Golden Section search is a very computationally efficient interval search method that is carried out in two stages. The first stage involves bracketing the unimodal minimum. The second step is to reduce the interval of uncertainty by comparing function evaluations at different points in the interval. The advantage of a golden section search is that it requires only one function evaluation between iterations, and convergence is very rapid. The Golden Section Method algorithm is given in Appendix B.

While calculating the fiber orientation angles for each element in the fiber path optimization, the element locations must be read in so that fiber orientations angle of each element can be calculated. Therefore, nodal information of all elements is needed to calculate the fiber orientation angle as a location. The nodal information is taken from MSC.Patran as an output. The distance between the center of each element and the centerline of the reference path centerline is

determined to decide if the element belongs overlaps equal or more than %50 with to the reference tow path. If the distance between the element center and the reference path was is less than half of the tow width, then the thickness of that element is increased to a single thickness by the thickness of the tow that the element overlaps with more than %50. The result is a tow path of a single layer of composite material which goes through that has complete variation of varying fiber orientation angle either in the circumferential direction or in the axial direction of the cylinder, depending on the definition of the reference fiber path and the shift direction fiber angle. A single $\langle 0|45 \rangle$ axially varying reference tow path discretized over cylinder, is shown in Figure 35. The discrete nature of the tow path model is apparent along the top and bottom edges of the tow path.

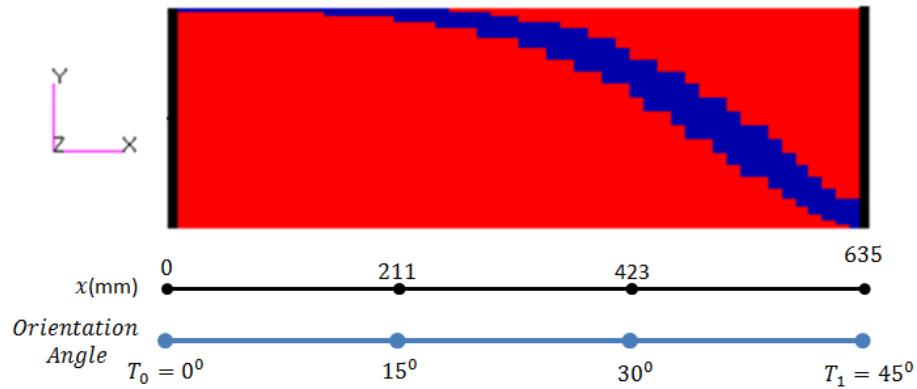


Figure 35 Single $\langle 0|45 \rangle$ Axially Varying Reference Tow Path Discretized over the Cylinder

The tow width is 38.1 mm and element mesh size is 12.7mmx12.7mm. Therefore, one tow path width includes at least 3 quad shell elements. The mesh size can be enough to model finite element model of variable stiffness cylinder structure. For a panel as seen at Figure 36 shows that a $\langle 0|45 \rangle$ axially varying fiber tow includes 3 elements at the left side of the panel and 5 elements at the right side of the panel.

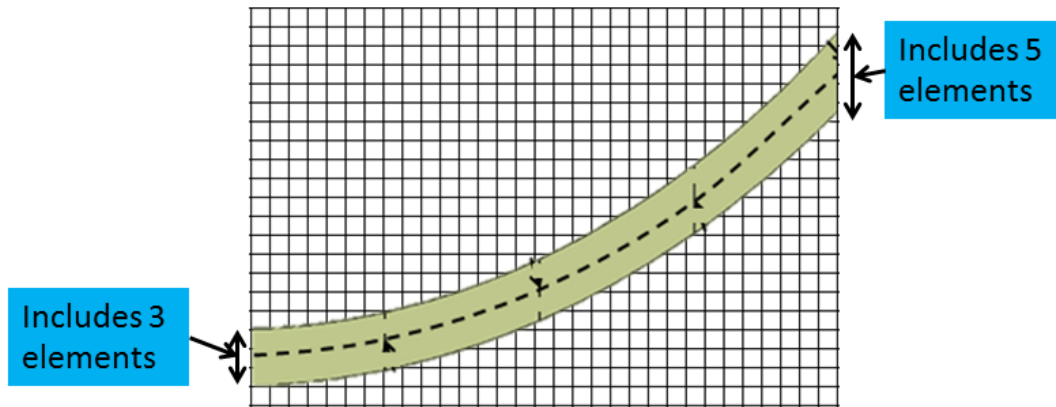


Figure 36 $\langle 0/45 \rangle$ Axially varying fiber tow through the panel.

Once the continuous reference path has been developed, it is necessary to use it to create the entire ply. Because all tow paths will be identical, all that is necessary to model the rest of the variable stiffness ply is to duplicate the reference tow path and shift the duplicate tow paths the correct distance. If the elements are filled by the reference path then an additional layer is created. The information for the reference fiber path and shifted paths are stored, and then the thickness and the orientation angle information for every element are written to the Nastran input file.

Thickness plot of an 8-layer $[\pm\langle 0/45 \rangle]_s$ laminate that has fiber, orientation angle varying along the axial direction is shown in Figure 37.

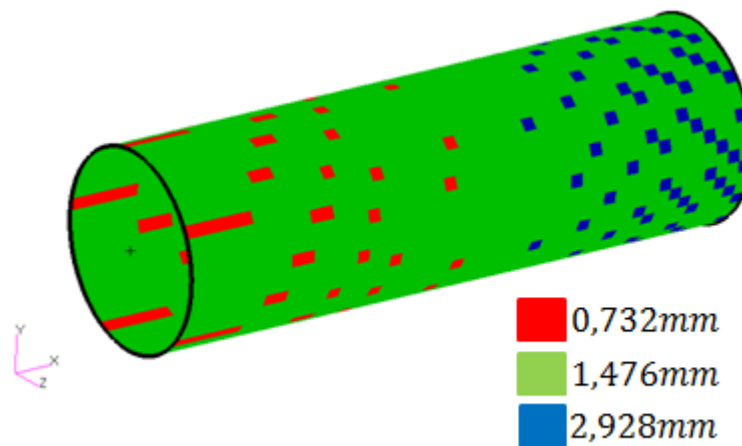


Figure 37 Thickness distribution of the $[\pm\langle 0/45 \rangle]_s$ laminate with axially varying fiber orientation angle

It is seen from the Figure 37 that the thickness of the shell is varying along the x axis. It should be noted that although the thickness of a single ply of the 8 ply laminate is 0.183mm, the red regions are only 0.732 mm, which is equal to the total thickness of 4 plies because of the existence of gaps between the tows, and blue regions have a thickness which is equal to the thickness of 16 plies because of the overlaps.

After the thickness and element orientation are determined, these values are written in Nastran input file as a property called PCOMP card. The detail of the PCOMP card is given in Appendix A.

5.2.10.2. Nastran input file

Nastran input file which has an extension of .bdf, includes the information about geometry, mesh, material, load and boundary condition. The mesh properties are different for all elements. In the .bdf file, the properties are written one by one for all elements by using the information about the reference fiber path.

PCOMP cards have information about the thickness of each ply and its fiber orientation angle. In variable stiffness laminates, since each element may have different thickness and fiber orientation angle, for each element a distinct PCOMP card has to be defined. During the structural analysis phase of the optimization process, based on the definition of the reference path, fiber orientation angle is calculated for each element and fiber orientation angle along with the thickness of the element are written in the PCOMP card of Nastran. An example of the Nastran input file and explanations related to the critical card entries used in the input file are given in the Appendix A.

5.3. Optimization Procedure by Coupling the Nastran Finite Element Solver and Particle Swarm Optimizer in MATLAB

Due to the large number of design parameters and space requirement, the optimization of the composite material orientation is complicated. Utilizing computer integrated optimization algorithms allow designers to explore the design space and find the optimum design of a composite structure. [23] Evolutionary algorithms such as PSO can be used to optimize composite structures, because the formulation of design parameters is complex and very hard to handle. And, finite

element analysis is usually the preferred analysis method for geometrically complex laminate composite parts.

In this part of the thesis, the fiber path optimization procedure is explained. As explained before, the design variables that are to be optimized are the parameters of the reference fiber path which are defined by T_0 and T_1 . Optimization process by the PSO is explained in Chapter 4. In this thesis, PSO code is developed for the case studies are presented in next chapter. The PSO code is special for the variable stiffness composite structure optimization. The design variable is T_0 and T_1 . The objective function which is to maximize the buckling load factor, is given as input to the algorithm as a MATLAB code. The MATLAB code is prepared to couple the Nastran finite element solver and the PSO code developed.

Consider a maximization of buckling load factor of the variable stiffness laminate problem with, maximum failure indices and curvature constraints defined in Eqns. 5.18 to 5.21. The maximization problem is converted to minimization problem by multiplying -1 to the absolute buckling load factor because PSO code is a minimization code.

$$\text{Minimize } (F_BLF(T_0, T_1)) \quad (5.18)$$

$$3^0 < T_0, T_1 < 90^0 \quad (5.19)$$

$$g_1(T_0, T_1) = \text{Maximum failure indices} - 1 \quad (5.20)$$

$$g_2(T_0, T_1) = \frac{\text{Maximum curvature}}{\text{Allowed curvature}} - 1 \quad (5.21)$$

The constrained problem is converted to unconstrained problem by using penalty approach mention in Chapter 4. The unconstrained problem formula for variable stiffness laminate is given in Eqns. 5.22 and 5.23.

$$F_BLF(T_0, T_1, r_g) = -\text{absolute}(f_BLF(T_0, T_1)) + P(T_0, T_1, r_g) \quad (5.22)$$

$$P(T_0, T_1, r_g) = r_g * \max(0, g_1(T_0, T_1))^2 \quad (5.23)$$

The maximum failure indices which are the output of the Nastran, are read from .f06 file. To obtain maximum failure indices, the input .bdf file must be solved by MSC.Nastran but the maximum curvature is calculated by analytically and there is no need to solve by MSC.Nastran. The most time consuming part of the optimization is Nastran solver part. To make optimization time shorter, if curvature constrained is violated, the Nastran solver part of the code is by-passed and given a high buckling load factor. The formulation is given in Eqns. 5.24 and 5.25.

$$F_{BLF}(T_0, T_1, r_g) = 10^{10} \quad (5.24)$$

$$\text{if } g_2(T_0, T_1) > 1 \quad (5.25)$$

Before the optimization process, general inputs are given the main matlab code, listed below and an example of input parameters listed in Table 7.

- The number of swarms to determine the size of the swarm, n_swarm
- How many times the iteration of swarm is done, n_ite
- The laminate configuration, lam_con
- Direction of the variation for the fiber path, var_dir
- The load condition, $load_c$
- Discretization value to decrease the design space, $disc_val$

Table 7 An example of Main Matlab code input parameters

| | |
|-------------|--------------------------|
| n_swarm | 8 |
| n_ite | 4 |
| lam_con | $[\pm 45 < T_0/T_1 >]_s$ |
| var_dir | Axial Direction |
| $load_c$ | Bending Load |
| $disc_val$ | 3 |

Another general input is the center of the each element. In the main matlab code, for a more robust solution procedure, all the grid and element information are taken from MSC.Nastran once, and connectivity information of the grids and finite elements is processed with a different “element_center.m” file to calculate the coordinates of the centroids of each element. Then, fiber orientation angles of every quadrilateral element are calculated at the element centroids.

After above parameters are given input the main matlab code, it is called to PSO code, and the parameter of the PSO code is listed in Table 8.

Table 8 The PSO code parameters

| | <i>PSO Parameters</i> |
|-----------|------------------------------|
| c_1 | 2 |
| c_2 | 2 |
| W_{max} | 1 |
| W_{min} | 0,4 |
| α | 0,99 |
| σ | 0,4 |
| r_g | 10^4 |

The maximum velocity of T_0 and T_1 is defined at the beginning of PSO, is given in Eqns. 5.26 and 5.27.

$$T_0, v_{max} = \sigma * (T_{0max} - T_{0min}) \quad (5.26)$$

$$T_1, v_{max} = \sigma * (T_{1max} - T_{1min}) \quad (5.27)$$

The algorithm of PSO is described below in steps for the variable stiffness optimization.

For each particle $i=1, \dots, n_swarm$;

1. Create and initialize a population of T_0 and T_1 with random positions and velocities on n_swarm dimensions in the defined problem space.

The design space is discrete so MATLAB creates the population in a discrete manner to reduce the design space for the fiber path optimization problems studied. The created “discrete” values are multiplied with a coefficient *disc_val*. For instance, *disc_val* is equal to 3 and, T_0 and T_1 can take the values between 3^0 and 90^0 . The design space is discretized by 3 and becomes 1 to 30. Therefore, T_0 and T_1 can take 30 different values to create a variable stiffness lamina. The initial population is created with random positions and velocities, T_0 and T_1 can take values between 1 and 30.

2. Evaluate each (T_0, T_1) according to the objective function, *fx_BLF.m*

fx_BLF.m is the function, calculate the orientation angles of each element for each ply according to the parameters T_0 and T_1 but firstly, T_0 and T_1 is multiplied by *disc_val*. The reference path and shifted paths are determined by using T_0 and T_1 . Then, call the *GSO.m* to calculate the distance between the paths and element center, and return with the distance information to *fx_BLF.m*. According to the distance information, the thickness of each element for each ply is determined. After orientation angle and thickness values are determined, the PCOMP cards are created for each element. *fx_BLF.m* creates the input file for MSC.Nastran. After this step, *fx_BLF.m* calls for a Nastran execution. The input file of Nastran, which is prepared, is used in the Nastran run to produce the output file which has all the results. For the case studies, linear static and buckling analysis are performed for the composite cylindrical shells. The output .f06 files are read by *fx_BLF.m* to target Von Mises stress of each element of each layer and buckling load factor. The stress information is used to calculate failure indices by using Tsai-Wu failure criteria. By using the unconstrained problem formulation, the buckling load factor is calculated again and returned the *PSO.m*.

Note that, at the beginning of the Step 2, the curvature constraint is calculated, if the allowed curvature is violated, the rest of the Step 2 is not evaluated, and directly returned the *PSO.m* with a buckling load factor value 10^{10} .

3. PSO operations, if a particle's current position is better than its previous best position, update it.

4. PSO operations, determine the best particle (T_0, T_1)
5. PSO operations, update particles' velocities
6. PSO operations, update particles position (T_0, T_1)
7. Loop to step 2 until a criterion is met.

When the PSO code determines the swarm's best known position (T_0, T_1) , PSO algorithm does not terminate. The program passes the swarm's best known position (T_0, T_1) inside the initial swarm in Step 1 like a randomly created swarm and the optimization cycle starts again. If the passed the swarm's best known position (T_0, T_1) is obtained again at the end of the new cycle, the program terminates. By using this approach, it is aimed to prevent getting local optimum point, and to give a second chance to find the global optimum and to be sure about the global optimum. This approach assumes that instead of using a big population, small but repeated and fast generation of population might be beneficial to reach to global optimum.

After PSO.m operations, the main matlab code writes the optimum (T_0, T_1) to results file and optimization is finished. A flowchart for the continuous fiber path optimization procedure is given in Figure 38. The detail of optimization procedure is also given in Appendix C.

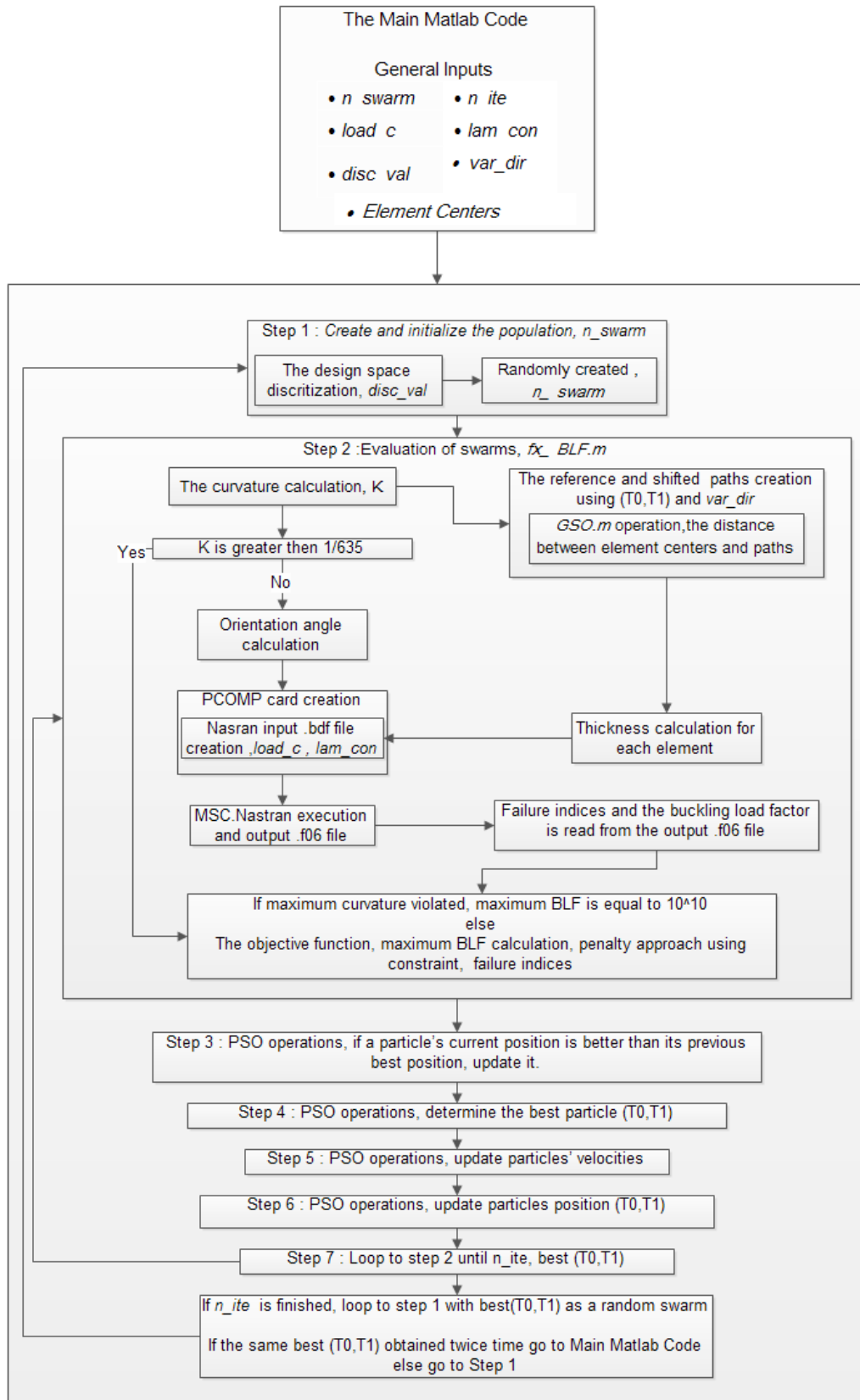


Figure 38 The fiber path optimization procedure flowchart

CHAPTER 6

RESULTS OF FINITE ELEMENT ANALYSIS AND OPTIMIZATION

6.1. Introduction

In the literature, the variable stiffness approach is commonly used for maximizing the buckling load.[12, 13, 17] Therefore, in the present study, to demonstrate the variable stiffness design concept, cylindrical shell with different load conditions are optimized for the maximum buckling load factor, using the fiber path definitions introduced in Chapter 4. Before the optimization of variable stiffness cylinder, the finite element model verification is performed to check effectiveness of the developed code. [17, 20]

Many different forms of response data can be generated by MSC.Nastran finite element analysis. The most basic outputs are the maximum failure indices and the buckling load factor. This section first demonstrates the baseline design and analysis for the straight fiber laminates with constant fiber traditional orientation angles for each ply. In the second part of the analyses and optimization of hybrid laminates are carried out. Hybrid laminates are composed of combination of constant stiffness plies with constant fiber orientation angles and variable stiffness plies with curvilinear fiber paths. In the last party of the analysis, optimization of variable-stiffness composite cylindrical shells having plies with axially and circumferentially varying fiber orientation angles are performed. Results of the three different set of analyses are compared with the baseline designs and conclusions are inferred with regard to the advantages of variable stiffness concept. Again for the case studies performed in

this section of the thesis, to improve the manufacturability, the curvature constraint is also added to optimization process. Conclusions are drawn based on the numerical examples.

6.2. Problem Definition and Optimization Procedure

The optimization problem is formulated as the maximization of the buckling load factor for the laminated cylindrical shell that is introduced in Chapter 5. Since PSO is a minimization algorithm, in the buckling load factor evaluation, buckling load determined by the finite element analysis is multiplied by minus one to make the optimization a minimization problem. Thus, the best value of the objective function has to be multiplied by -1 to get the true value of the optimized buckling load. There are two input file of Nastran which are evaluated by the linear buckling analysis and the linear static analysis. Linear buckling and static analyses are carried out and the output files are read separately. The buckling load factor is read from the Nastran output file that is generated as a result of linear buckling analysis. One of the constraints is defined as the maximum failure index value which is read from Nastran output file of the linear static analysis. To check to material failure, failure index is used as constraints of the optimization problem. If a failure index exceeds a value of 1.0, then it means that the particular ply has exceeded the specified failure strength. The failure theory used is the Tsai-Wu Failure Criteria which requires the tensile and compressive strengths to be the different for both in the fiber direction and in the transverse direction to the fiber direction.

Another constraint that is implemented for the optimization of variable stiffness cylinder is the curvature κ of the fiber paths. Because composite shells are designed to be built using a fiber placement machine, the curvature of fiber paths has to be smaller than the maximum allowed curvature κ . It should be noted that run times are long for the PSO case studies. Because, in every function evaluation of the PSO algorithm, which consists of linear buckling and linear static analysis, to calculate the buckling load factor and the maximum failure index, Nastran input file is read, variables are placed in the Nastran input file, and an analysis is performed in Nastran. After the Nastran analysis is completed, MATLAB code developed searches the objective function value, which is the buckling load factor, in the output file of

Nastran. All these operations take time and when the computational costs add up, the execution of each function evaluation takes longer time. Therefore, if the curvature constraint is violated, objective function is penalized by means of a very large number. The details are given in Chapter 5. Therefore, if the curvature constraint is violated, steps involving the writing of the input file and reading of the output file are skipped. As a result of skipping the writing and reading of the input and the output files, optimization run becomes shorter whenever a curvature constraint is violated. It should also be noted that by taking the curvature constraint into account, laminated cylindrical shell can be manufactured by means of fiber placement machines.

In the present study, the design optimization problem is defined as given by Eqns. 6.1, 6.2, and 6.3:

$$\text{Objective ; Maximize Buckling Load Factor} \quad (6.1)$$

$$\text{Subjected to; Maximum Failure Index} \leq 1 \quad (6.2)$$

$$\text{Maximum Curvature} \leq \frac{1}{635} \quad (6.3)$$

Fiber path parameters T_0 and T_1 , which are the design variables of the design optimization problem, are defined as given by Eqn. 5.3 and Eqn. 5.6 for the axially and the circumferentially varying fiber orientation cases described in Chapter 5. Design variables T_0 and T_1 are discretized so that they can take on values ranging from 3^0 to 90^0 in an increment of 3^0 as shown in Eqn. 6.4. Thus, the design space is discretized to decrease computational cost of the optimization.

$$3^0 \leq T_0, T_1 \leq 90^0 \quad (6.4)$$

In countless engineering applications, the structural members are subjected to many different loads. Four load cases are considered in the design study described in this chapter. The dimensions of the cylinder are given in Chapter 5. Load cases used in the design optimization of the tow placed cylindrical shell structure are:

- Bending load
- Torsional load

- Combined bending and torsion load
- Axial load

6.3. Design of the Laminated Shell Wall

Laminated shell wall is assumed to be composed of 8 plies with symmetric and balanced lamination scheme. Initially, a conventional 8-ply laminated shell wall consisting of combination of 0° , 90° and $\pm 45^\circ$ plies is analyzed, and stacking sequence optimization is performed to maximize the buckling load factor subject to four different load cases defined above. Conventional design is performed to serve as the baseline design. Furthermore the laminate is required to be symmetric and balanced to avoid extension-shear and extension-bending coupling.

Firstly, constant stiffness laminate designs, which are composed of the classical $0^\circ/\pm 45^\circ/90^\circ$, maximum failure index and buckling load factor values are calculated. The designs that are analyzed are;

- TL-1 design, $[0/90/\pm 45]_s$
- TL-2 design, $[\pm 45/\pm 45]_s$
- TL-3 design, $[0/90/0/90]_s$

Secondly, stacking sequence optimization is performed for designs which also include non-traditional fiber orientation angles which can be different from 0° , 90° and $\pm 45^\circ$;

- CS-1 design, $[0/90/\pm \emptyset]_s$
- CS-2 design, $[\pm 45/\pm \emptyset]_s$
- CS-3 design, $[\pm \emptyset_1/\pm \emptyset_2]_s$

In the second party of analyses, the orientation angle \emptyset is optimized to maximize the buckling load factor subject to maximum failure index and curvature constraints. Fiber orientation angle, \emptyset is taken between 0° and 90° , and the range of the fiber orientation angle is discretized by 3° to reduce the design space.

Results of the first and the second optimization are considered as baseline designs for the comparison of the constant stiffness and variable stiffness laminated cylindrical shells.

The third party of optimization is performed for the variable stiffness laminated cylindrical shells. In the first two designs, hybrid laminated cylindrical shell designs are optimized. Hybrid designs consist of combination of constant stiffness and variable stiffness plies. The third design consists of plies all of which are variable stiffness plies. For the variable stiffness laminated cylinders, optimizations are performed for two different designs. In the first design, fiber orientation angle is varied in the axial direction (VA-I design) and in the second design fiber orientation angle is varied in the circumferential direction (VC-I design). Variable stiffness laminated cylinder design that are studied are given below.

- VA-1 and VC-1 designs, $[0/90/\pm\langle T_0/T_1 \rangle]_s$
- VA-2 and VC-2 designs, $[\pm 45/\pm\langle T_0/T_1 \rangle]_s$
- VA-3 and VC-3 designs, $[\pm\langle T_0^1/T_1^1 \rangle/\pm\langle T_0^2/T_1^2 \rangle]_s$

It should be noted that laminates which consist of combination of constant and variable-stiffness plies, may offer advantages that straight fiber laminates cannot. Therefore, in the third party of analyses, the performance of hybrid laminates designs VA-1, VA-2, VC-1 and VC-2 are also investigated. The abbreviation VA is used for axially variable stiffness laminate design and VC is used for circumferential variable stiffness laminate designs. The definitions of axial and circumferential stiffness variation for laminates are given in Chapter 5.

Material properties and the thickness of one ply are given Chapter 5, so they are not repeated here.

In the analyses, laminated shell wall thickness is taken as constant and for constant stiffness laminates, thickness is 1.464 mm. However, it is shown in the following analyses that due to overlaps, thickness is not constant throughout the entire ply for variable stiffness laminates which form the wall thickness of the cylindrical shell. Therefore, before comparing the results of cylinders with variable stiffness and constant stiffness laminated cylindrical shell, the buckling load factor is normalized

with the thickness ratio to account for the mass increase or decrease due to the overlaps. It is known that buckling load factor is proportional to the square of thickness of the laminate; therefore buckling load factor of the variable stiffness laminated shell wall is divided by square of the thickness ratio which is defined by the ratio of the mean thickness of the variable stiffness shell to the thickness of the constant stiffness shell. Thus, constant stiffness and variable stiffness shells can be compared with each other on equal terms. The specific buckling load factor and thickness ratio are given in Eqn. 6.6 and Eqn. 6.7.

$$sBLF = \frac{BLF}{TRatio^2} \quad (6.6)$$

$$TRatio = \frac{Mean\ Thickness}{1,464} \quad (6.7)$$

It should be noted that the mean thickness is calculated only for variable stiffness laminates. Mean thickness is calculated by summing the thicknesses of all elements and dividing it by the total number of elements, as shown in Eqn. 6.8.

$$Mean\ Thickness = \frac{\sum_{m=1}^{Number\ of\ Element} Element\ Thickness(m)}{Element\ Number} \quad (6.8)$$

For the buckling optimization of variable stiffness cylindrical shells, after the buckling load factor is calculated, specific buckling load factor, which is calculated by Eqn. 6.6, is compared with the buckling load factor of constant stiffness laminated cylindrical shell.

For verification purpose, before the variable stiffness cylinder optimization cases studies are performed, a variable stiffness panel is created and the response of this panel is compared the response given by the case studies in the literature. [17, 20]

6.4. Finite Element Model Verification Case Study

The aim of this section is to show the effectiveness and usefulness of the code developed by using Matlab to create finite element model of the variable stiffness

laminate. The geometry of the composite plate in Reference 17 is taken as the reference. In Reference 17, in one of the case studies that is studied composite plate is subjected to the load in the x direction. The same case was also investigated by Inci [20], a square plate that is studied is 4 meter by 4 meter. In the finite element model, four hundred CQUAD4 elements are used and, the loads and boundary condition applied are illustrated in Figure 39.

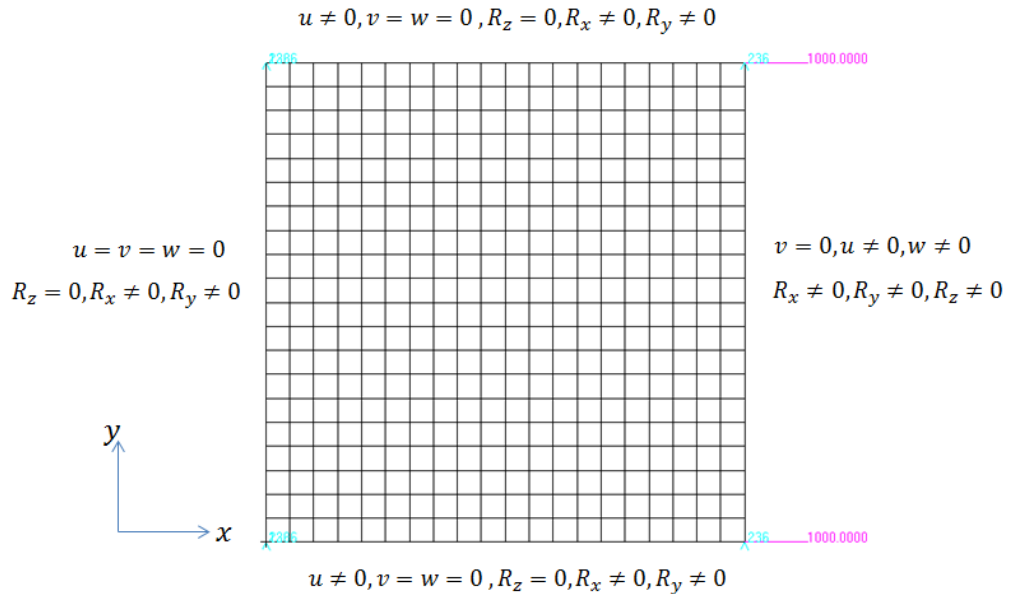


Figure 39 Applied loads and the edge displacement boundary conditions for the case study

The material properties of the layer material are given below [20]:

$$E_1 = 181 \text{ GPa} \quad E_2 = 10,27 \text{ GPa} \quad G_{12} = 7,17 \text{ GPa} \quad \gamma_{12} = 0,28$$

$$t = 0.1524 \text{ m}$$

The case study is a single layer composite plate with the total thickness of the plate given as 0.1524 m. The finite element model is created and the linear buckling analysis is performed to see that how the developed code works.

The baseline design is composed of zero degree orientation angle for all the elements. The buckling load factor of baseline design is determined as 10.21. The maximum buckling load factor of the variable stiffness plate is obtained for the value of 0^0 orientation for T_0 and 50^0 for T_1 , and the orientation angle of direction of

variation \emptyset is taken as 0^0 for this case. [17] Stacking sequence of the laminate is shown as $[\pm < 0/50 >]$. As a result, the finite element model of the variable stiffness square plate is created and the linear buckling analysis is performed. The buckling load factor is determined as 19.17 for $[\pm < 0/50 >]$ laminate design. The increase of the buckling load factor with respect to the baseline design is 88 %. However, it cannot be concluded that the buckling load factor is improved 88 % because the weight of the baseline design and the variable stiffness design are not equal. Thickness of the variable stiffness plate varies along the x-direction and because the curved paths near the right edge of the plate overlaps occurs as shown in Figure 40. Therefore, laminate becomes thicker locally. In Figure 40, dark elements denote overlaps which have higher thickness.

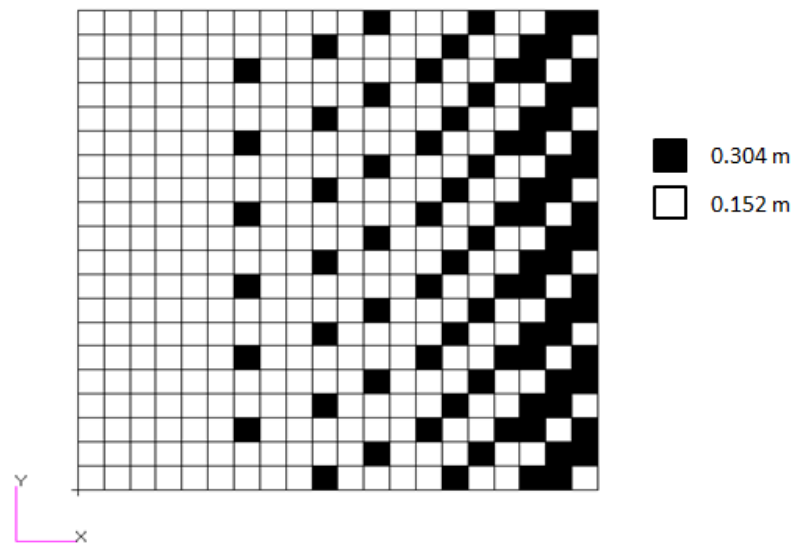


Figure 40 Thickness distribution of $[\pm < 0/50 >]$ plate design

The mean thickness of the variable stiffness laminate is calculated by using Eqn. 6.8 as 0.185 m and, the thickness of the baseline design is equal to 0.152 m and constant for the constant stiffness laminate design. The thickness ratio of variable stiffness and baseline design is calculated using Eqn. 6.7 as 1.215 and the basic assumption is that the buckling load factor is proportional to the square of the thickness ratio. The buckling load factor of variable stiffness plate (19.17) is then divided by the square of thickness ratio to normalize the buckling load factor so that the baseline design and variable stiffness design can be compared on equal terms. The normalized buckling load factor is named as specific buckling load factor which is calculated for

as 12.99 for the particular laminated plate studied. When the specific buckling load factor of the variable stiffness design and the buckling load factor of the baseline design are compared, the improvement in buckling load factor is calculated as 27 %. In other words, the variable stiffness plate buckles at 27 % higher load when compared to the zero degree orientation baseline design. The improvement of the original work in Reference 17 is 19 % and in this work the improvement is calculated as 27 %. These results show that the developed code works fine for the creation of finite element model of the variable stiffness laminate. The difference of results can be attributed to the parameters used to create the finite element model variable stiffness plate. For instance, the tow width, the shift distance, radius of curvature and the mesh size are some of the parameters which may affect the results. These parameters affect the overlap distribution and change the response of the plate under axial load.

For the same plate, fiber orientation angle varies linearly from 0° to 50° and thickness varies linearly along the x-direction. The variable stiffness plate's finite element model is again created to show effect of the thickness variation. For this model, only fiber orientation angle variation is applied and the thickness of each element is taken as constant in the new finite element model. Thus, the thickness of the variable stiffness plate is equal to 0.152 m like the baseline design. The buckling load factor of the variable stiffness plate with only fiber orientation angle variation is 7.92 which is 22 % less than the buckling load factor of the baseline design. It showed that not only the fiber orientation angle variation but also the thickness variation is also important for the effectiveness of variable stiffness laminates.

In Reference 20, Inci's study about the same rectangular plate show that the improvement of the buckling load factor is 30% compared the baseline design. However, Inci used different angles other than $[\pm < 0/50 >]$ and overlaps are not allowed in the finite element model. The optimum fiber orientation angle variation is $[< 14.27/24.30 >]$ and laminate thickness is constant through the entire ply. In the present study, with the orientation angle $[< 14.27/24.30 >]$ and allowing no overlaps finite element model is again created to check the output of the developed code with the result of the independent study of Inci [20]. As a result of finite

element analysis, it is seen that the improvement in the buckling load factor is about 27 %. The percent-improvement achieved in buckling load is very close to the improvement achieved by Inci [20]. Therefore, it can be concluded that the developed code that generates finite element model of variable stiffness laminates and laminated cylinders, with overlaps or no overlaps, can be used reliably in the further studies in this thesis.

For the variable stiffness cylinder design, the overlaps are allowed in the next section for different cases studies that are considered. Four load cases are investigated by using the same approach to create variable stiffness cylindrical structure.

6.5. Results of Bending Load Case

When the cylindrical structure is bent, it is subjected to both tensile and compressive stresses. In practice, because of the compressive stress, the buckling failure can be more probable when the actual compressive stress at the point of failure is less than the ultimate compressive stress that the material is capable of withstanding.

Figure 41 shows the cylindrical structure which is fixed at the left end and loaded by bending forces which are distributed to the cylindrical structure by using multi point constraints (MPCs). Through the use of MPCs, the loads that are applied at the center of the cylinder in different axial locations are distributed the nodes along the circumference of the cylinder, as seen in Figure 41. The buckling load factor is independent for the applied load and is only a coefficient relating the actual load to the buckling load.

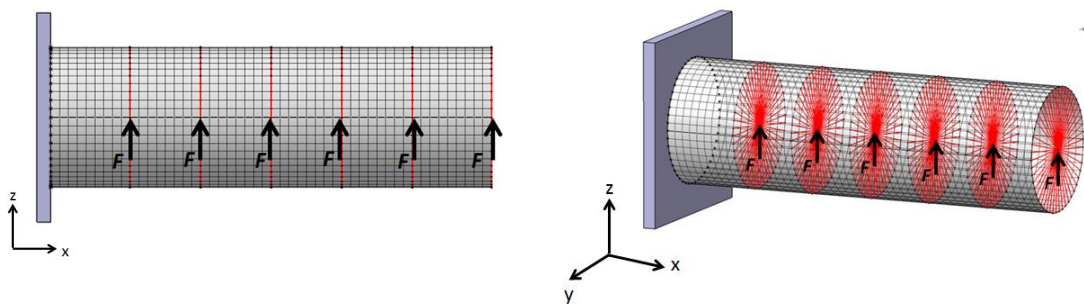


Figure 41 Bending loads applied to the cylindrical structure

Constant stiffness laminated shell designs with plies having traditional fiber orientations of 0° , 90° and $\pm 45^\circ$ are introduced as the baseline designs.

Table 9 gives the structural response of constant stiffness laminated shell designs with traditional fiber orientation angles of 0° , 90° and $\pm 45^\circ$ under bending loading. The thickness of the designs in Table 9 is 1.464 mm.

Table 9 Buckling load factor results of constant stiffness laminated shell designs under bending loading

| | TL-1 | TL-2 | TL-3 |
|----------------|-------------------|---------------------|-----------------|
| | $[0/90/\pm 45]_s$ | $[\pm 45/\pm 45]_s$ | $[0/90/0/90]_s$ |
| Max. FI | 0,2 | 0,46 | 0,13 |
| BLF | 3,12 | 1,9 | 2,1 |

TL-1 design's buckling load factor is highest and maximum failure indices are less than 1. Based on the results given in Table 9, the best laminate design is seen to be TL-1 when compared to TL-2 and TL-3.

The fiber placement machines are capable to lay down fibers in non-traditional orientation. Therefore, to improve the structural capacity of cylinder, the orientations other than 0° , 90° and $\pm 45^\circ$ can also be used to design the laminate. For this purpose, stacking sequence optimization for three laminate designs which are denoted as $[0/90/\pm\phi]_s$, $[\pm 45/\pm\phi]_s$ and $[\pm\phi_1/\pm\phi_2]_s$, are performed to maximize the buckling load factor under bending loading. The only constrain for the stacking sequence optimization is failure index which is calculated by Tsai-Wu failure criteria. ϕ is the fiber orientation angle that is defined between 0° and 90° . Table 10 shows optimization results for cylinders which also include of non-traditional ply angles different from 0° , 90° and $\pm 45^\circ$. The thickness of laminates in Table 10 is 1.464 mm.

Table 10 Optimization results of laminated cylinders composed of non-traditional fiber orientation angles under bending loading

| | CS-1 | CS-2 | CS-3 |
|----------------|-------------------|-------------------|-------------------|
| | $[0/90/\pm 33]_s$ | $[\pm 45/0/90]_s$ | $[0/90/\pm 33]_s$ |
| Max. FI | 0,23 | 0,19 | 0,23 |
| BLF | 3,29 | 2,88 | 3,29 |

The failure index and BLF values are given in Table 10. When the results given in Table 9 and Table 10 are compared, it is seen that by using other orientation angles other than traditional orientations, the buckling load factor increases. When the results of CS-1 and TL-1 designs are compared, the improvement of the buckling load factor is 5 %. For the CS-1 design, by using a non-traditional angle of 33° structural performance of the cylinder improves. Since CS-1 has the best performance among the constant stiffness laminates given in Table 9 and Table 10, CS-1 is chosen as the baseline design. When CS-3 design is considered, it is seen that the resulting optimized stacking sequence is same as the CS-1 design. The Von Mises stress distribution of CS-1 design under bending loading is given in Figure 42. The maximum stresses are seen at the root of the cylinder as expected. Figure 42 gives maximum Von Mises stress. The maximum Von Mises stress is calculated as 437 MPa at the root region. It is noted that the Von Mises stress distribution is composed of maximum Von Mises of each layer.

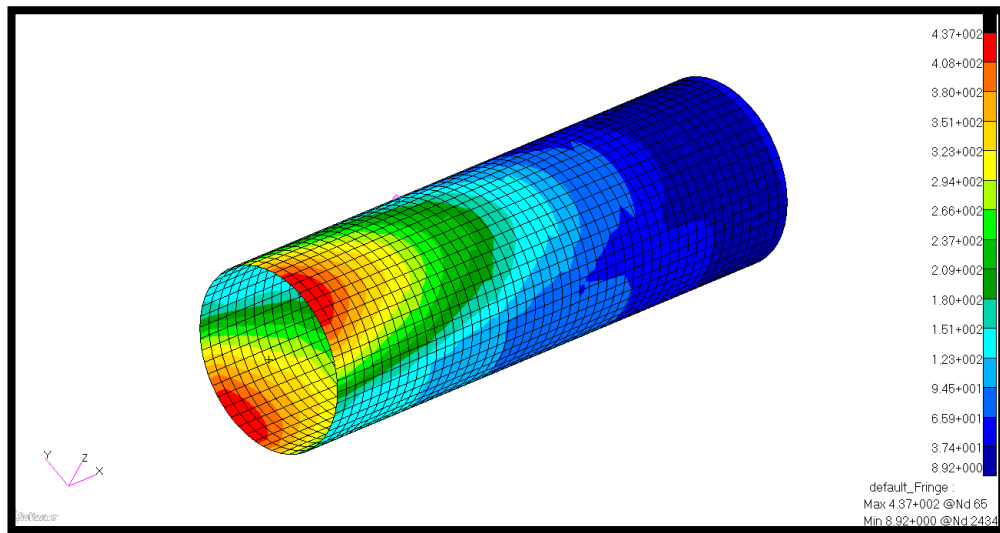


Figure 42 Maximum Von Mises stress distribution (MPa) of the CS-1 design under bending loading

Two approaches to create variable stiffness cylindrical shells that are discussed in Chapter 5, are the variable stiffness cylinder with fiber angle changing in the axial direction and variable stiffness cylinder with the fiber angle changing in the circumferential direction. Optimizations are performed by applying these two

methods. The aim is to find optimum fiber path to create variable stiffness laminated cylindrical shell. The optimization parameters are taken as T_0 and T_1 as discussed before. The hybrid laminated cylindrical shell design with constant and variable stiffness plies, and laminated cylindrical shell with full variable stiffness plies are optimized by using the PSO, and the penalty method approach mentioned in Chapter 4. The laminate designs that are studied are two hybrid designs $[0/90/\pm < T_0/T_1 >]_s$, $[\pm 45/\pm < T_0/T_1 >]_s$ and one full variable stiffness laminate design $[\pm < T_0^1/T_1^1 > / \pm < T_0^2/T_1^2 >]_s$.

It should be noted that as a result of the optimization, the cylinders can also be manufactured, because manufacturing constraint is also taken into account in the definition of the optimization problem. Results of the optimizations performed for the laminated cylindrical shell designs, with axially and circumferentially varying fiber orientation angle, under bending loading by the PSO algorithm are summarized in Table 11 and Table 12, respectively. The failure indices are calculated as constraint to prevent material failure.

Table 11 Optimization results of variable stiffness cylinders with axially varying fiber orientation angle under bending loading

| | VA-1 $[0/90/\pm < 57/21 >]_s$ | VA-2 $[\pm 45/\pm < 3/3 >]_s$ | VA-3 $[\pm < 54/3 > / \pm < 3/3 >]_s$ |
|---------------------------|----------------------------------|----------------------------------|--|
| Max. FI | 0,11 | 0,36 | 0,22 |
| BLF | 5,02 | 2,58 | 4,05 |
| Mean Thickness(mm) | 1,67 | 1,46 | 1,68 |
| sBLF | 3,84 | 2,58 | 3,07 |

Table 12 Optimization results of variable stiffness cylinders with circumferentially varying fiber orientation angle under bending loading

| | VC-1 $[0/90/\pm < 33/33 >]_s$ | VC-2 $[\pm 45/\pm < 3/3 >]_s$ | VC-3 $[\pm < 30/48 > / \pm < 78/90 >]_s$ |
|---------------------------|----------------------------------|----------------------------------|---|
| Max. FI | 0,23 | 0,36 | 0,16 |
| BLF | 3,29 | 2,58 | 2,24 |
| Mean Thickness(mm) | 1,46 | 1,46 | 1,47 |
| sBLF | 3,29 | 2,58 | 2,24 |

When Table 11 and Table 12 are examined, the maximum buckling load factor is seen to be 5.02 which is obtained for the hybrid design VA-1 having constant 0° and 90° plies with axially variable stiffness ply. The cylinder with axially variable stiffness plies does not violate the curvature constraint and the laminate ensures that the failure index is less than maximum allowed value of one. The mean thickness of the laminate VA-1 is determined as 1.67 mm. The buckling load factor of VA-1 is 5.02 while the buckling load factor of the baseline design CS-1 is 3.29. However, VA-1 and CS-1 designs do not have equal thicknesses. To compare the variable stiffness laminates and constant stiffness laminates on equal terms, specific buckling load factor, which is denoted by sBLF, is defined. With the definition of the specific buckling load factor, different variable stiffness designs which have different mean thicknesses can be compared on equal terms.

As shown in Table 10, the buckling load factor of the baseline design is calculated as 3.29 for the CS-1 design. When specific buckling load factor of the VA-1 design and buckling load factor of the baseline design CS-1 are compared, it is seen that the improvement in the buckling load factor is approximately 17 %. The reason for this improvement can be attributed to the local thickness and fiber orientation angle variation which results in better structural performance. The local thickness variation causes increase in thickness, and this creates stiffer region to support the cylindrical structure against buckling. Axially varying fiber orientation accounts for the redistribution of the stress, and failure indices decrease as a result of the redistribution of the stress.

Figure 43 shows the thickness variation of the optimized laminated cylindrical shell design VA-1. From Figure 43, it can be seen that as a result of the optimization, the root of the cylinder is thicker than the tip section, because the root of the cylindrical shell is more critical for buckling under the bending loading. The left side of the cylinder is root of the cylinder and right side of the cylinder is the tip of the cylinder for all captures of cylinders.

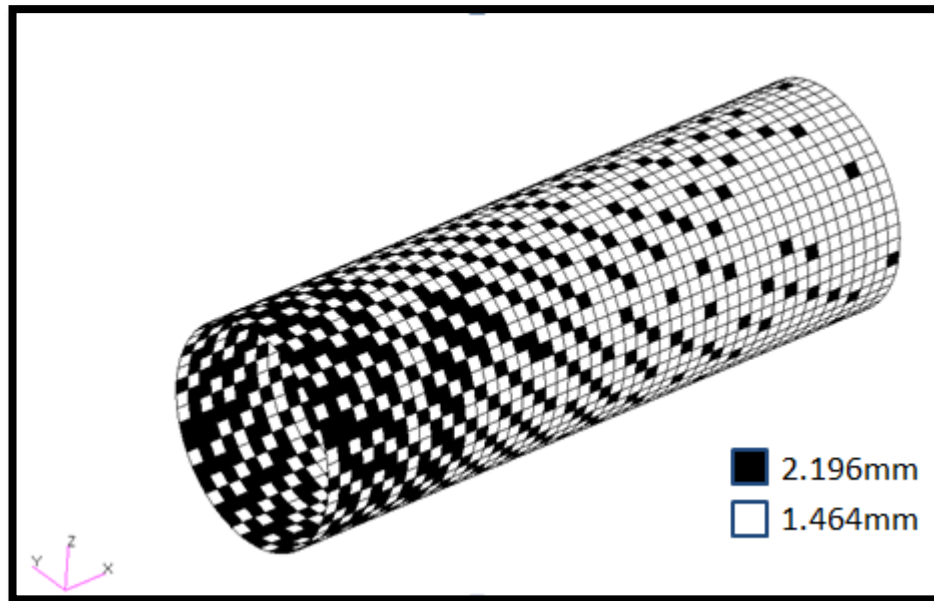


Figure 43 Thickness distribution for the VA-1 design under bending loading

To better understand the results presented, maximum Von Mises stress distribution of VA-1 is given in Figure 44 to compare with the stress distribution of CS-1 given in Figure 42. Also, the failure index distribution of VA-1 design is given in Figure 45.

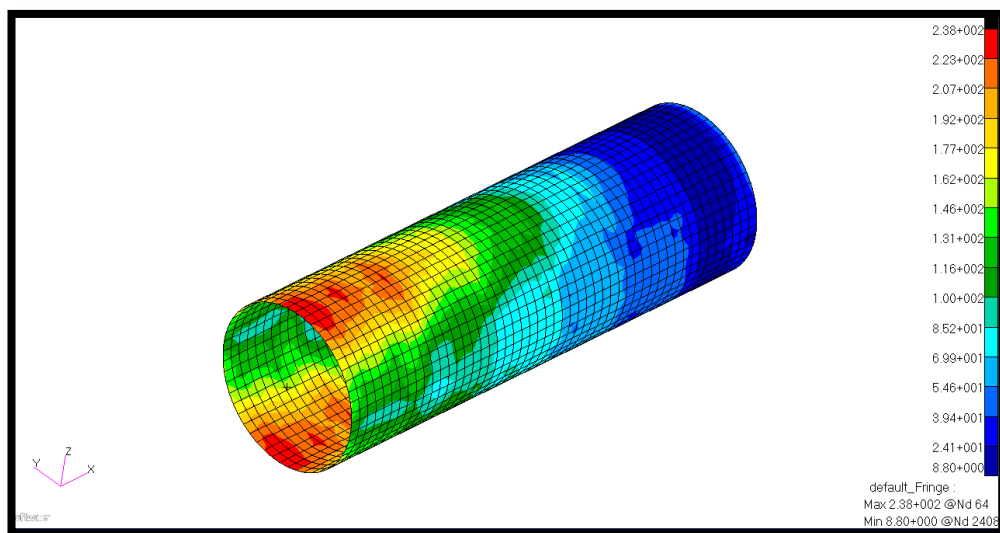


Figure 44 Maximum Von Mises stress distribution (MPa) of the VA-1 design under bending loading

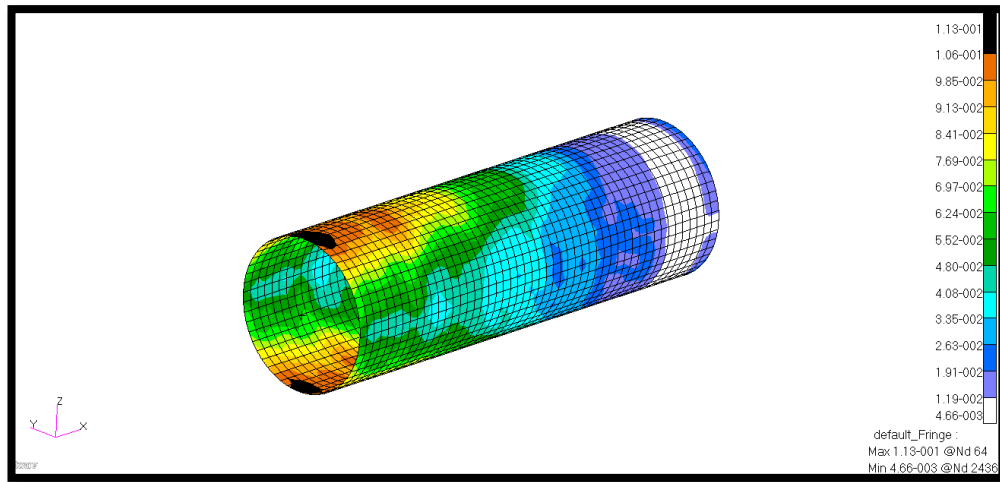


Figure 45 Maximum Failure Index distribution of the VA-1 design under bending loading

It is seen from the Figure 44 and Figure 45, the maximum Von Mises distribution and maximum failure index distribution spectrum are the same and the maximum values for failure index and Von Mises occurred at the same point.

It is noted that the thickness build-up on the compression side affected the buckling load carrying capability of the axially variable-stiffness cylinder. The stiffness variation resulted in the redistribution of the loads, such that the tension side was more effective in carrying loads. The maximum Von Mises stress is 238 MPa for the VA-1 design while the maximum Von Mises stress of the CS-1 design is 436 MPa. Actually, the maximum Von Mises values for CS-1 and VA-1 is not compared directly like buckling load factor because their thickness distribution is different. However, it is apparent that the maximum Von Mises value is decreased using variable stiffness approach. Moreover, it is not known which effect is more dominant in reducing the maximum stress; thickness distribution or fiber angle variation. In any case axially variable stiffness cylinder is seen to be more effective in reducing the maximum stress in the critical region of the cylinder.

The best result of the variable stiffness cylinders with circumferentially varying fiber orientation angle under bending loading is the VC-1 design. The result of VC-1 $[0/90/\pm<33/33>]_s$ is presented, at Table 12. However, it should be noted that VC-1 design is actually a constant stiffness laminate because parameters T_0 and T_1 which define the fiber orientation angle, are equal to each other, and in that case

orientation angle is straight. For this design, the specific buckling load factors is calculated as 3.29, and the mean thickness is 1.464 mm. As a result of optimization under bending loading, VC-1 and CS-1 turned to be the same laminate. Comparison of Table 11 and Table 12 Table 18 reveal that variable stiffness cylinders, with circumferentially varying fiber orientation, do not have superior results than the results of constant stiffness laminates. It is again stressed that in the present study, if the PSO algorithm determines the same solution 2 times, it is considered that there is no improvement in the optimum result and convergence is achieved. It should be noted that since only the fiber orientation angle is taken as the design variable, for the given loading, the optimization may not find a better solution for certain designs. However, it is considered that structural performances of the optimized cylinders are compared on equal terms, and utilizing the results presented, one can deduce which laminate design is better.

First buckling mode of the baseline design CS-1 and VA-1 design is given in Figure 46 and Figure 47 to see the change of buckling mode.

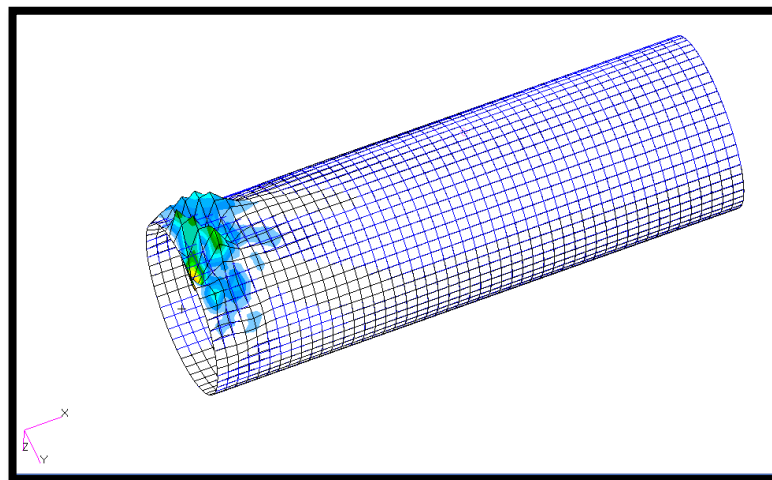


Figure 46 First buckling mode of CS-1 design under bending load

First buckling mode of CS-1 and VA-1 is different because of thickness and orientation angle variation as a result of variable stiffness approach.

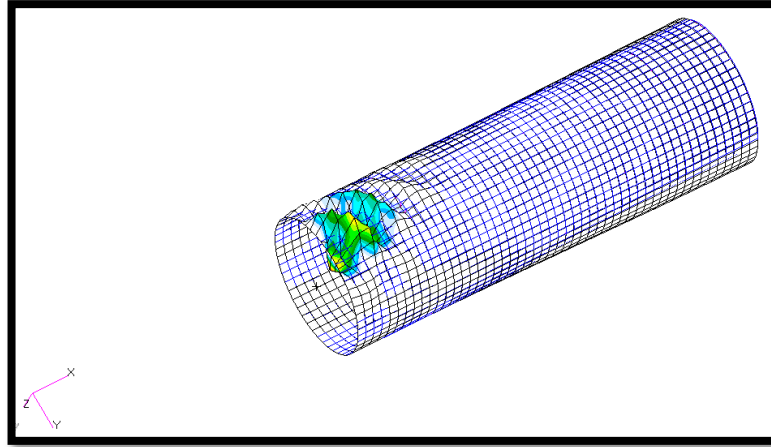


Figure 47 First buckling mode of the VA-1 design under bending loading

To conclude the optimization results under bending loading, the best results of constant, axial variable and circumferential variable stiffness cylinder designs are compared in Table 13. The improvements are given with respect to the baseline design CS-1.

Table 13 The best optimization results under bending load

| | CS-1 | VA-1 | VC-1 |
|---------------------------|-------------------|---------------------------|---------------------------|
| | $[0/90/\pm 33]_s$ | $[0/90/\pm < 57/21 >]_s$ | $[0/90/\pm < 33/33 >]_s$ |
| Mean Thickness(mm) | 1,464 | 1,67 | 1,46 |
| BLF | 3,29 | 5,02 | 3,29 |
| sBLF | 3,29 | 3,84 | 3,29 |
| Improvement | | 17% | 0% |

Based on the numerical results presented so far, it is seen that the performance of the laminated cylinder could be improved by using axially varying fiber orientation angle compared to the constant stiffness cylinder under bending loading. The improvement is 17 %. There is no improvement for the circumferential variable stiffness cylinder designs. It should be noted that since the comparison is based on the specific buckling load calculated utilizing the ratio of the mean thicknesses; the cylinders are compared on equal terms implying that weights of the cylinders are actually the same.

6.5.1. Design Sensitivity Analysis

In this study, to decrease the design space for optimization of fiber path, the fiber orientation angles are discretized by the *disc_val* parameter mentioned in Section 6.2. The value of discretization is 3 degrees. The design space of fiber orientation angle is defined from 3^0 to 90^0 and the discretization is performed. Therefore, design space becomes 1 to 30, and the fiber orientation angles can be taken as integer values ranging from 1 to 30. To study the effect of the discretization on the results of the optimization, the range design space of the fiber orientation angle is changed to 1^0 - 90^0 and the discretization value is made 1. Thus, fiber orientation angles can take integer values from 1 to 90.

For the bending load case, optimization is performed for the VA-1 design with the new design space to see the effect of the new discretization. For the 1 degree discretization, the optimum stacking sequence of VA-1 design is determined as $[0/90/\pm < 57/19 >]_s$. The result of optimization is given in Table 14 together with the results of the optimization for the 3 degree discretization case.

Table 14 The comparison of the optimization result under bending loading for different discretization value

| | VA-1 | VA-1* |
|--------------------|--------------------------|--------------------------|
| | $[0/90/\pm < 57/21 >]_s$ | $[0/90/\pm < 57/19 >]_s$ |
| <i>Disc_val</i> | 3 | 1 |
| Max. FI | 0,11 | 0,11 |
| BLF | 5,02 | 5,02 |
| Mean Thickness(mm) | 1,67 | 1,66 |
| sBLF | 3,84 | 3,89 |

*Disc_val is 1

From Table 14, it is seen that, for the discretization angle of 1 degree, as a result of the fiber orientation angle variation from 57^0 to 19^0 , the buckling load factor did not change. However, the mean thickness of the VA-1* becomes 1.66 mm so the specific BLF of VA-1* becomes 3.89. The specific BLF of VA-1 design is 3.84 and it is seen that there is a slight increase when the discretization angle is made 1 degree instead of 3 degrees. By increasing the resolution of the discretization, as expected slightly better improvement can be achieved. However, since the improvement in the specific buckling load factor is not significant, considering the time cost of the

optimization, discretization value of 3 degrees is considered to be a more proper value to conduct the studies in this thesis.

Therefore, the discretization value is taken again as 3 degrees for the rest of the optimization problems studied in this thesis.

6.6. Results of Torsional Load Case

This section investigates the optimization of buckling load factor of variable stiffness cylinder structures under torsional load. The simply supported cylindrical shell which is seen in Figure 48 is subjected to torsional loads which are distributed to the nodes around the circumference of the cylinder by the MPCs. As a result of the twisting deformation, torsional buckling may occur in the cylindrical structure. The aim of the optimization is again to get maximum buckling load factor under the constraints imposed. As specified before, the maximum failure index should be less than 1 to prevent failure.

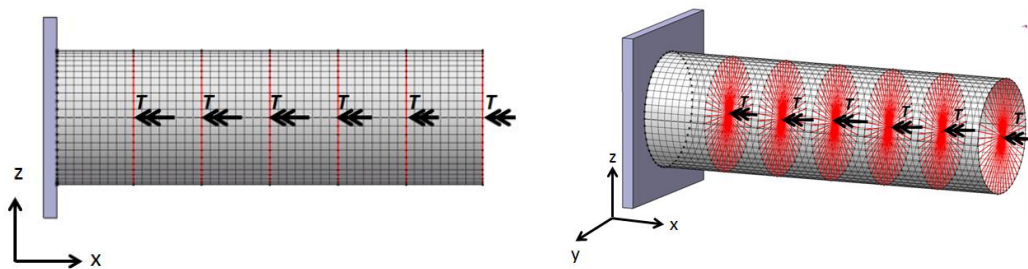


Figure 48 Torsional loads applied on the cylindrical structure

Optimization results of constant stiffness laminated shell designs with traditional fiber orientation angles of 0° , 90° and $\pm 45^\circ$, and optimization results of cylinders which also include of non-traditional ply angles different from 0° , 90° , and $\pm 45^\circ$ are presented in Tables 15 and 16, respectively.

Table 15 Buckling load factor results of constant stiffness laminated shell designs under torsional loading

| | TL-1 | TL-2 | TL-3 |
|----------------|-------------------|---------------------|-----------------|
| | $[0/90/\pm 45]_s$ | $[\pm 45/\pm 45]_s$ | $[0/90/0/90]_s$ |
| Max. FI | 0,25 | 0,26 | 0,88 |
| BLF | 1,5 | 0,8 | 1,18 |

Table 16 Optimization results of cylinders composed of non-traditional fiber orientation angles under torsional loading

| | CS-1 | CS-2 | CS-3 |
|----------------|-------------------|---------------------|---------------------|
| | $[0/90/\pm 45]_s$ | $[\pm 45/\pm 72]_s$ | $[\pm 21/\pm 63]_s$ |
| Max. FI | 0,25 | 0,31 | 0,24 |
| BLF | 1,5 | 1,07 | 1,50 |

As it is seen from Table 15 and Table 16, as a result of the fiber orientation angle optimization, TL-1 design is found to have the same stacking sequence as that of CS-1. From Table 16, it can be seen that optimization results of CS-1 and CS-3 are approximately equal. The maximum buckling load factor is obtained as 1.5 for both CS-1 and CS-3. Therefore, in the following CS-1 or CS-3 can be taken as the baseline design because they give the best values.

It is also noted that for the torsional load case, maximum failure index constraint are both satisfied in the optimized cylinder configurations. Also, curvature constraint is satisfied and all cylinder designs can be manufactured. First buckling mode of the baseline designs CS-3 is given in Figure 49.

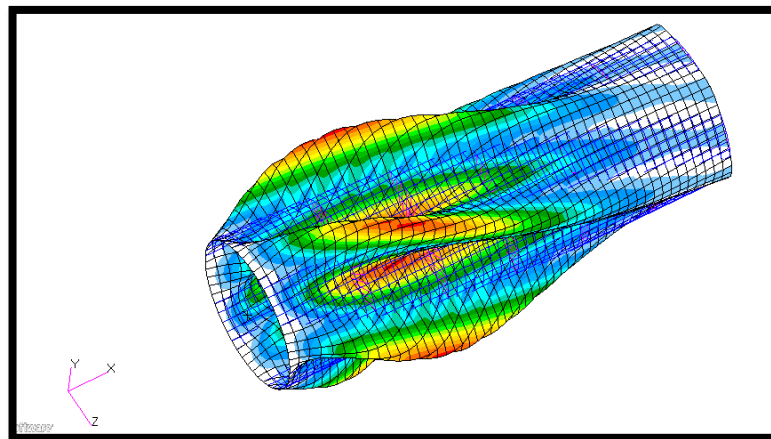


Figure 49 First buckling mode of the CS-3 design under torsional loading

Axially and circumferentially variable stiffness cylinders are optimized and the entire plies are covered by the optimum paths using the shifted path method, which is discussed in detail in Chapter 5. Table 17 and Table 18 present the results of the variable stiffness optimization under torsional load.

Table 17 Optimization results of variable stiffness cylinders with axially varying fiber orientation angle under torsional loading

| | VA-1 [0/90/±< 69/54 >] _s | VA-2 [±45/±< 90/90 >] _s | VA-3 [±< 3/3 > /±< 66/60 >] _s |
|---------------------------|---|--|--|
| Max. FI | 0,33 | 0,38 | 0,29 |
| BLF | 2,00 | 1,11 | 2,33 |
| Mean Thickness(mm) | 1,66 | 1,46 | 1,70 |
| sBLF | 1,56 | 1,11 | 1,72 |

Table 18 Optimization results of variable stiffness cylinders with circumferentially varying fiber orientation angle under torsional loading

| | VC-1 [0/90/±< 51/51 >] _s | VC-2 [±45/±< 90/90 >] _s | VC-3 [±< 3/3 > /±< 66/60 >] _s |
|---------------------------|---|--|--|
| Max. FI | 0,26 | 0,38 | 0,34 |
| BLF | 1,53 | 1,11 | 1,68 |
| Mean Thickness(mm) | 1,46 | 1,46 | 1,51 |
| sBLF | 1,53 | 1,11 | 1,58 |

Maximum failure indices and buckling load factor are obtained as a result of the optimization. After the evaluation of results for variable stiffness cylinders, it is seen that the specific buckling load factor of VA-3 and VC-3 are greater than the baseline design CS-3 given in Table 16.

In case of cylinder designs with axially and circumferential varying fiber orientation angle, VA-3 and VC-3 designs actually becomes hybrid laminated cylindrical shell having both constant and variable stiffness plies. Because in the VA-3 and VC-3 designs, parameters T_0 and T_1 defining the fiber orientation angle of the outer ply are equal to 3^0 and therefore lamina is actually a constant stiffness lamina. However, for the inner ply design, parameters T_0 and T_1 defining the fiber orientation angle are not equal and therefore fiber orientation angle varies in the axial direction from 66^0 to 60^0 .

From Table 17, it can be seen that VA-3 gives the best buckling load factor when compared to the circumferentially variable stiffness and constant stiffness cylinders. The specific buckling load factor of VA-3 is determined to be 15% greater than

buckling load factor of CS-3. The mean thickness of VA-3 design is 1.7 mm which is divided by the thickness of the baseline design CS-3 (1.464 mm) to determine the thickness ratio. The buckling load factor of VA-3, 2.33 is divided by the square of the thickness ratio to determine the specific buckling load factor. Thus, the constant stiffness and variable stiffness design can be compared in equal terms.

It should be noted that VC-3 design has the same stacking sequence as VA-3 design but the responses of VA-3 and VC-3 are different because of the different approaches used in creating the reference fiber paths and covering entire ply by shifting the reference path.

The thickness distribution of the cylinder VA-3 is given in Figure 50. Thickness distribution plot helps the evaluation of results of axially variable stiffness cylinder. Thickness distribution varies locally, because torsional load affects the sections of the cylinder, where the load is applied, locally due the transfer of the torsional load to the cylinder via MPCs. The buckling mode shape of VA-3 is shown in Figure 51. It is seen that in case of torsional loading maximum Von Mises stress is slightly higher than the maximum Von Mises stress of the baseline design CS-3.

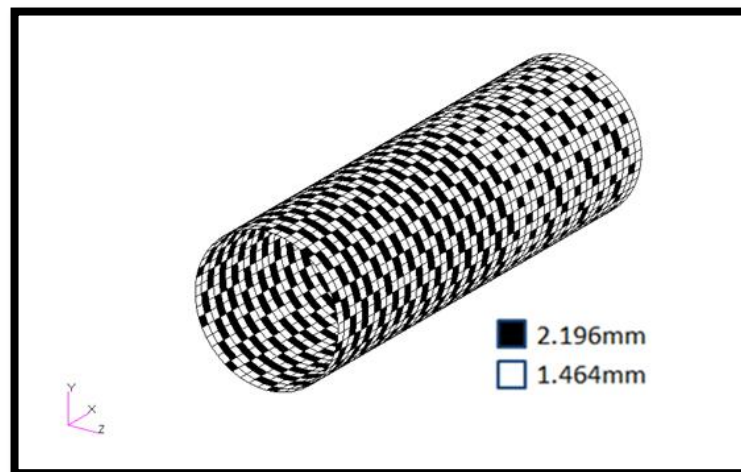


Figure 50 Thickness distribution of the VA-3 design under torsional loading

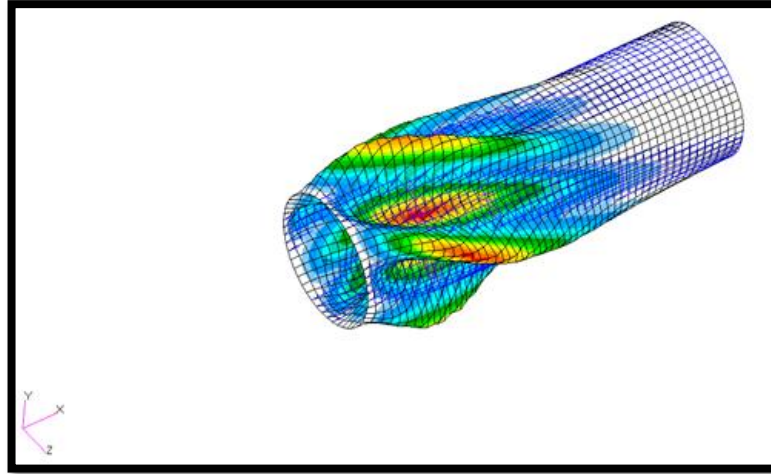


Figure 51 First buckling mode of the VA-3 design under torsional loading

The thickness distribution of the cylinder VC-3 is given in Figure 52. The mean thickness of VC-3 is 1.51 mm which is a bit higher than the thickness of the baseline design. The upper side of the VC-3 design is thicker, because the starting point of the courses and the ending point of the courses are overlaps while shifting the reference path. The specific buckling load factor of VC-3 design is 5 % higher than the BLF of the baseline design.

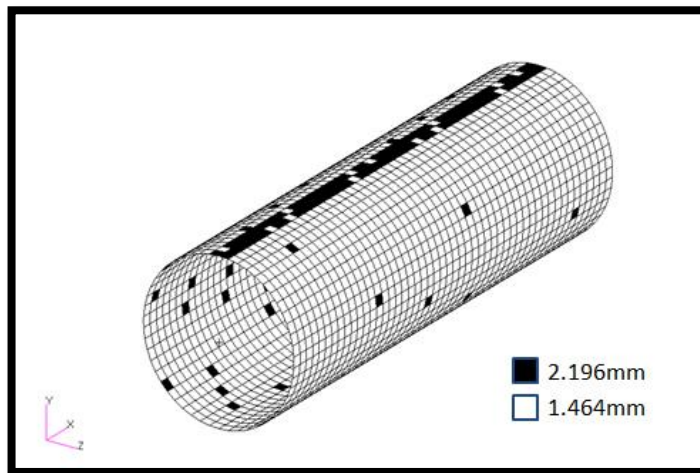


Figure 52 Thickness distribution of the VC-3 design under torsional loading

First buckling mode of VC-3 is also shown in Figure 53. From the comparison of the first buckling mode plots of the cylinders having plies with axially varying fiber orientation angle and circumferentially varying fiber orientation angle and non-

traditional constant stiffness baseline design, it is seen that first buckling mode is changing under the same load.

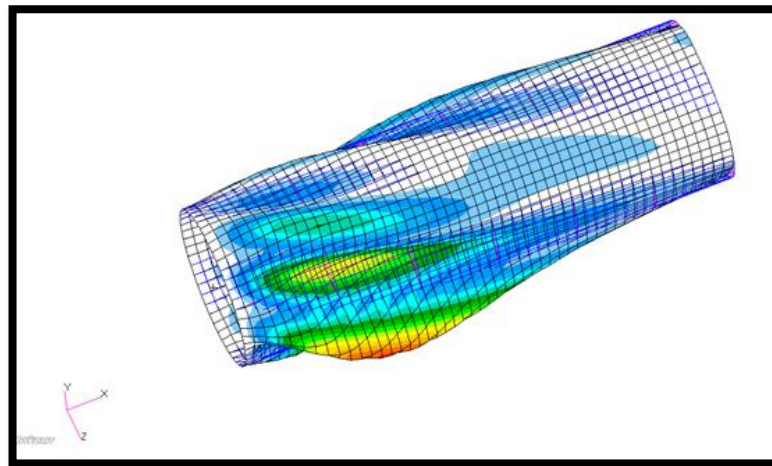


Figure 53 First buckling mode of the VC-3 design under torsional loading

Under the torsional load case, variable stiffness approach in the axial direction showed 15 % improvement when compared to constant stiffness cylinder results. There is also 5 % increased in the specific buckling load factor of the circumferentially variable stiffness cylinder design compared to the baseline constant stiffness cylinder design CS-3. The improvements relative to the baseline constant stiffness cylinder design CS-3 are summarized in Table 19. It is concluded that in terms of increasing the buckling load factor, fiber placement process presents advantages by the virtue variable thickness distribution and variable fiber orientation angle.

Table 19 The best optimization results under torsional load

| | CS-3 | VA-3 | VC-3 |
|---------------------------|---------------------|-----------------------------------|-----------------------------------|
| | $[\pm 21/\pm 63]_s$ | $[\pm < 3/3 > / \pm < 66/60 >]_s$ | $[\pm < 3/3 > / \pm < 66/60 >]_s$ |
| Mean Thickness(mm) | 1,464 | 1,7 | 1,51 |
| BLF | 1,50 | 2,32 | 1,68 |
| sBLF | 1,5 | 1,72 | 1,58 |
| Improvement | | 15% | 5% |

6.7. Results of the Combined Load Case

In the combined load case, torsional and bending loads are combined and applied the cylindrical structure again by using MPCs. The same laminate designs and optimization of 8 ply symmetric balanced laminate are performed and the results are presented. In this loading case, it is very hard for cylinder designs to maximize the buckling load factor because it is seen that for the bending and the torsional load cases have different structural response in terms of buckling characteristics. Failure index calculations are again performed for constraint.

Constant stiffness laminated cylindrical shell designs with traditional fiber orientation angles of 0° , 90° and $\pm 45^\circ$ are summarized in Table 20.

Table 20 Buckling load factor results of constant stiffness laminated shell designs under combined loading

| | TL-1 | TL-2 | TL-3 |
|----------------|-------------------|---------------------|-----------------|
| | $[0/90/\pm 45]_s$ | $[\pm 45/\pm 45]_s$ | $[0/90/0/90]_s$ |
| Max. FI | 0,38 | 0,56 | 1,59 |
| BLF | 1,17 | 0,64 | 0,88 |

The best design for traditional orientation is TL-1 and the buckling load factor is 1.17. For the combined load case, it is seen that designs TL-2 and TL-3 have buckling load factors less than 1, indicating that these cylinders actually buckle under the combined load case. In addition, maximum failure index of TL-3 is determined as 1.59 indicating that cylinder actually fails locally. It should be noted in the present study, although the failure index is given as a constraint, for the combined load case, since the overall load is high, optimization may end up with infeasible solution. Optimization terminates based on the convergence criterion, and after the termination of the optimization, it is possible that best solution may be in the infeasible region, as it is the case for TL-3 design. However, the straight fiber orientation angles which are different from 0° , 90° , and $\pm 45^\circ$ may result in better structural performance under combined loading in terms of buckling load factor. Optimization results of cylinders which also include of non-traditional ply angles different from 0° , 90° , and $\pm 45^\circ$ are presented in Table 21.

Table 21 Optimization results of cylinders composed of non-traditional fiber orientation angles under torsional loading

| | CS-1 | CS-2 | CS-3 |
|----------------|-------------------|---------------------|--------------------|
| | $[0/90/\pm 57]_s$ | $[\pm 45/\pm 81]_s$ | $[\pm 3/\pm 57]_s$ |
| Max. FI | 0,44 | 0,77 | 0,46 |
| BLF | 1,20 | 0,60 | 1,22 |

From Table 21, it is seen that maximum failure indices of all constant stiffness cylinders, with plies having non-traditional fiber orientation angles, are less than 1, therefore material failure is not predicted under the combined load case for the constant stiffness cylinders composed of non-traditional fiber orientation angles. The buckling load factor of the cylinders CS-2 design are less than 1, therefore cylinder CS-2 buckles under combined loading but other designs CS-1 and CS-3 do not buckle and they have close buckling load factors. Since CS-3 has slightly higher buckling load factor than CS-1, the constant stiffness cylinder design CS-3 is chosen as the baseline design for the combined load case. In the following, optimization results of variable stiffness cylinders are compared with the results of the baseline design CS-3. First buckling mode of CS-3 design is shown in Figure 54.

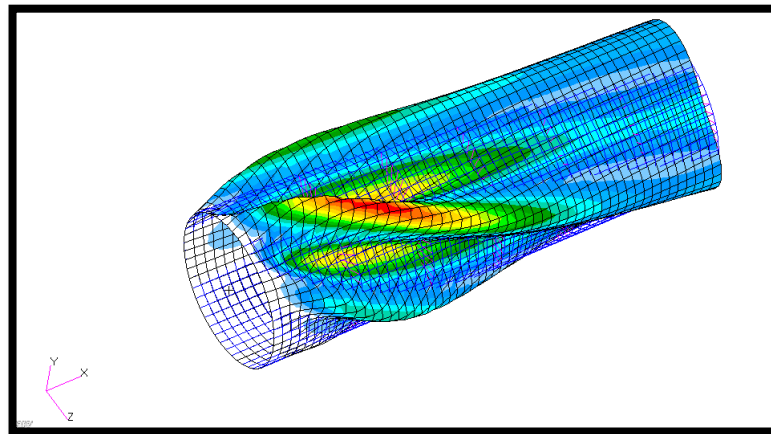


Figure 54 First buckling mode of the CS-3 design under combined loading

In the following, optimizations are performed for variable stiffness cylinders with the expectation that the variable stiffness cylinders may perform better than constant stiffness cylinders under combined loading. Optimization results of the axially variable stiffness cylinders are summarized in Table 22. The curvature constraint

check is also performed for all designs which are variable stiffness cylinders with axially and circumferentially varying fiber orientation angles.

As seen in Table 22, the maximum specific buckling load factor is obtained as 1.37 for the VA-3 design. For VA-3, failure constraint is also satisfied. The thickness buildup of the VA-3 design at the root region is shown in Figure 55.

Table 22 Optimization results of variable stiffness cylinders with axially varying fiber orientation angle under combined loading

| | VA-1 | VA-2 | VA-3 |
|--------------------|---------------------------|---------------------------|-------------------------------------|
| | $[0/90/\pm < 75/27 >]_s$ | $[\pm 45/\pm < 3/3 >]_s$ | $[\pm < 3/12 > / \pm < 72/48 >]_s$ |
| Max. FI | 0,38 | 0,57 | 0,51 |
| BLF | 1,71 | 0,73 | 2,28 |
| Mean Thickness(mm) | 1,73 | 1,46 | 1,89 |
| sBLF | 1,23 | 0,73 | 1,37 |

First buckling mode of VA-3 is given in Figure 56. Due to redistribution of the loads along the cylinder, first buckling mode of the VA-3 is very different than first buckling mode of the CS-3 design.

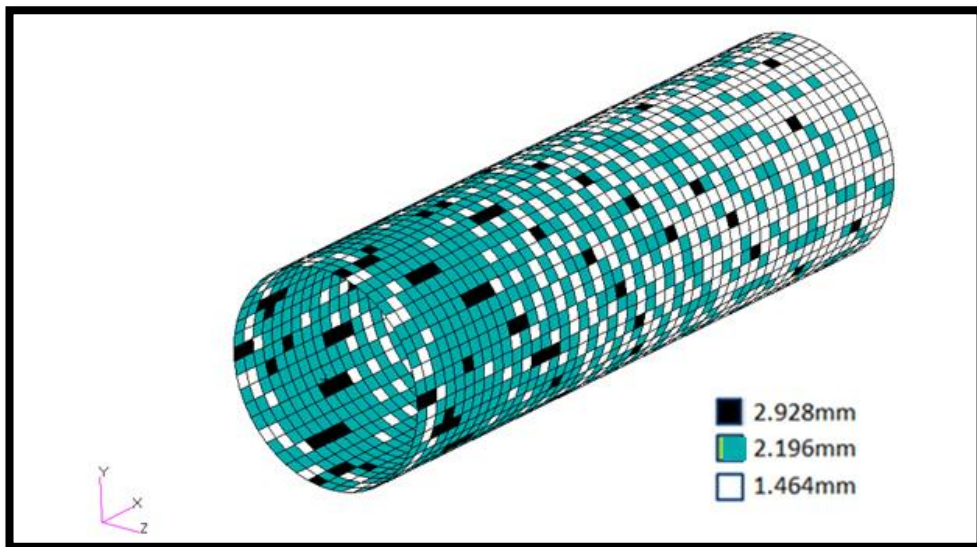


Figure 55 Thickness distribution of the VA-3 design under combined loading

For the combined load case, it is seen that there is 12 % increase in the buckling load carrying capability of the axially variable-stiffness cylinder VA-3 compared to the constant stiffness cylinder CS-3.

The optimization results for the circumferentially variable stiffness cylinders under combined loading are listed in Table 23. In Table 23, failure index, buckling load factor, mean thickness and specific buckling load are given for circumferentially variable stiffness cylinder designs under combined loading.

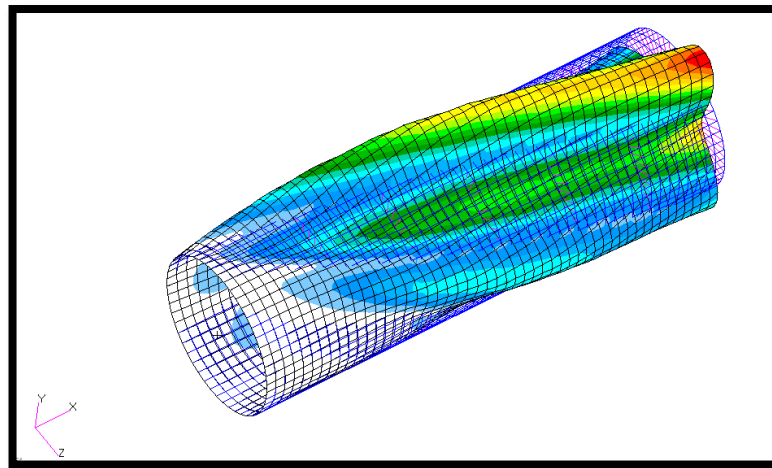


Figure 56 First buckling mode of the VA-3 design under combined loading

Table 23 Optimization results of variable stiffness cylinders with circumferentially varying fiber orientation angle under combined loading

| | VC-1 | VC-2 | VC-3 |
|---------------------------|---------------------------|-----------------------------|------------------------------------|
| | $[0/90/\pm < 45/57 >]_s$ | $[\pm 45/\pm < 81/75 >]_s$ | $[\pm < 3/3 > / \pm < 63/69 >]_s$ |
| Max. FI | 0,42 | 0,49 | 0,61 |
| BLF | 1,35 | 0,94 | 1,34 |
| Mean Thickness(mm) | 1,55 | 1,50 | 1,51 |
| sBLF | 1,21 | 0,90 | 1,26 |

Based on the results presented in Table 23, specific buckling load factor of one of the circumferentially variable stiffness cylinder is higher than the buckling load factor of the CS-3 design. Highest specific buckling load factor is obtained for the VC-3 design with a specific buckling load factor value of 1.26 which is slightly higher than the buckling load factor of the CS-3 design. The thickness distribution of the VC-3 design is shown in Figure 57. When the thickness distribution of the VC-3 design is

examined, it is seen that there is not too much thickness variation because the angle variation is small. The root region is not thicker like the VA-3 design, because as it is explained in Chapter 5, direction of variation and direction of shift are different for the axially and circumferentially variable stiffness laminates.

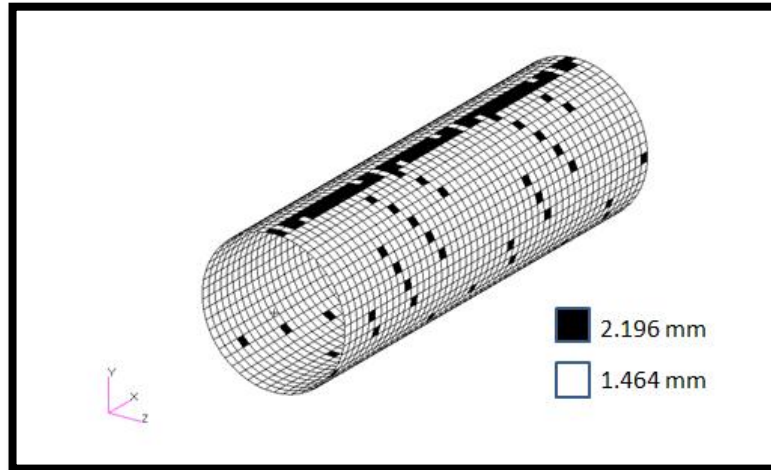


Figure 57 Thickness distribution of the VC-3 design under combined loading

In terms of specific buckling load factor, compared to the baseline design, 3 % improvement is seen in the VC-3 design under combined loading. First buckling mode of VC-3 design is given in Figure 58.

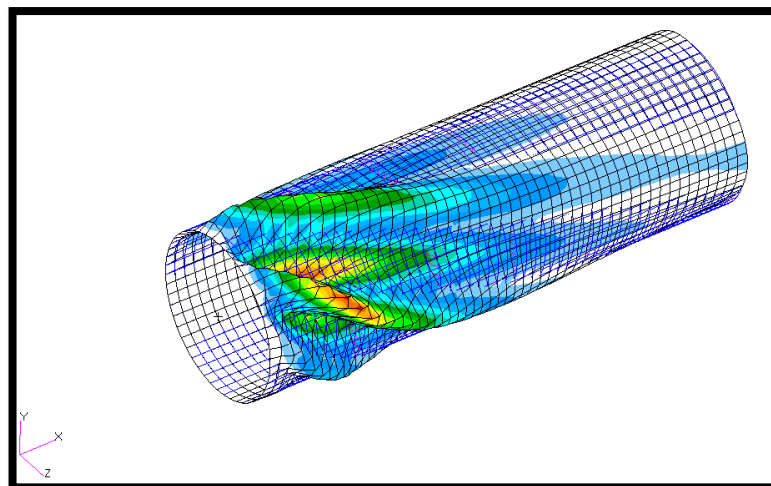


Figure 58 First buckling mode of the VC-3 design under combined loading

Based on the results presented, it is concluded that buckling performance of the variable stiffness cylinders improves for the combined load case. Best results are summarized in Table 24. It is noticed that axially variable stiffness approach gives better results than the circumferentially variable stiffness and constant stiffness cylinder designs.

Table 24 The best optimization results under combined load

| | CS-3 [±3/±57] _s | VA-3 [±< 3/12 >/±< 72/48 >] _s | VC-3 [±< 3/3 >/±< 63/69 >] _s |
|---------------------------|-------------------------------|---|--|
| Mean Thickness(mm) | 1,464 | 1,89 | 1,51 |
| BLF | 1,22 | 2,28 | 1,34 |
| sBLF | 1,22 | 1,37 | 1,26 |
| Improvement | | 12% | 3% |

It should be noted that in the literature, there are no researches performed like the optimization of variable stiffness cylinders under combined load case performed in this thesis. It is noted that either for the axially or the circumferentially variable stiffness cylinders, stiffness variation is only in one direction whereas for the combined load case, bending and torsional loads create more complex load distribution in the cylinder. If the fiber orientation angle is allowed to change both in the axial and in the circumferential direction, then it is possible that for the combined load case, higher improvements may be obtained in the structural performance of the variable stiffness cylinders compared to constant stiffness cylinders.

6.8. Results of Axial Load Case

The last load case that is studied is the axial load case and the variable stiffness concept for cylindrical structures under axial load is investigated. Axial load is applied to the tip of the cylinder in the axial direction and the root is fixed, as seen in Figure 59. The axial load F is 300 N/m for analysis and optimization.

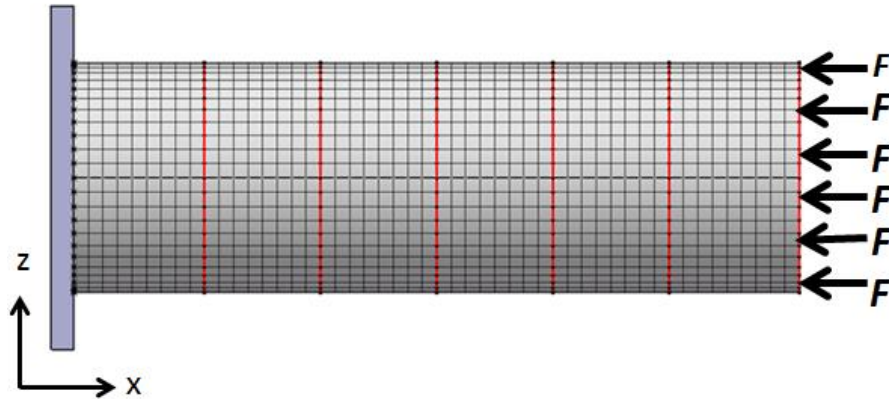


Figure 59 Axial loads applied to the cylindrical structure

To get a baseline design, constant stiffness cylinders having plies with traditional fiber orientation angles ($0^\circ, \pm 45^\circ, 90^\circ$) are analyzed under the axial load. Maximum failure index and the buckling load factor of the optimized laminated cylinders are given in Table 25.

Table 25 Buckling load factor results of constant stiffness laminated shell designs under axial loading

| | TL-1 | TL-2 | TL-3 |
|----------------|-------------------|---------------------|-----------------|
| | $[0/90/\pm 45]_s$ | $[\pm 45/\pm 45]_s$ | $[0/90/0/90]_s$ |
| Max. FI | 0,09 | 0,12 | 0,06 |
| BLF | 1,24 | 0,58 | 1,23 |

From Table 25, it can be seen that cylinders TL-1 and TL-3 do not buckle under the axial load and their buckling load factors are approximately same.

Optimization results of cylinders which also include of non-traditional ply angles different from $0^\circ, 90^\circ$, and $\pm 45^\circ$ are presented in Table 26.

Table 26 Optimization results of cylinders composed of non-traditional fiber orientation angles under axial loading

| | CS-1 | CS-2 | CS-3 |
|----------------|-------------------|-------------------|-------------------|
| | $[0/90/\pm 66]_s$ | $[\pm 45/0/90]_s$ | $[0/90/\pm 60]_s$ |
| Max. FI | 0,05 | 0,08 | 0,05 |
| BLF | 1,31 | 0,91 | 1,31 |

Based on the buckling load factor values given in Table 25 and Table 26 it is seen that 6 % increase in the BLF values are obtained for the cylinders composed of non-traditional fiber orientation angles under axial loading. Thus, it can be concluded that, non-traditional fiber orientation angles used in the plies improve the buckling capacity of the structures under the axial load. First buckling mode of the CS-1 design $[0/90/\pm 66]_s$ is given in Figure 60.

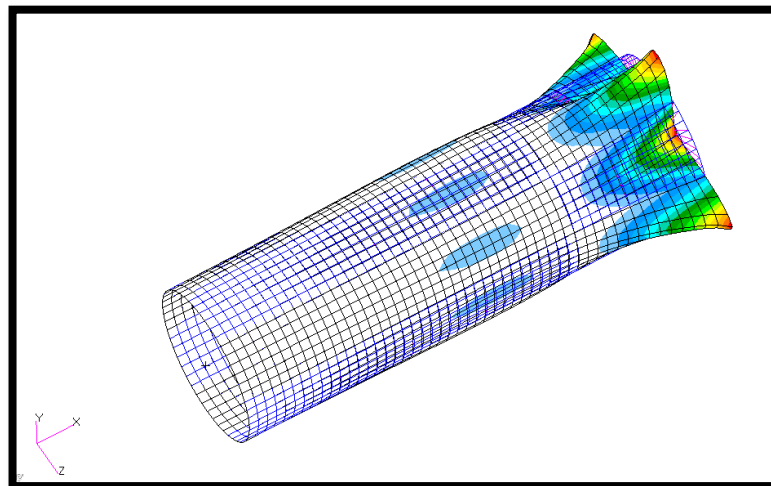


Figure 60 First buckling mode of the CS-1 design under axial loading

Axially variable stiffness cylinders are optimized to maximize the buckling load factor. In the optimization process, curvature and failure index constraints are also applied to maximize the buckling load factor. The results of the optimization for the axially variable stiffness cylinders are given in Table 27.

Table 27 Optimization results of variable stiffness cylinders with axially varying fiber orientation angle under axial loading

| | VA-1 | VA-2 | VA-3 |
|---------------------------|---------------------------|---------------------------|------------------------------------|
| | $[0/90/\pm < 18/75 >]_s$ | $[\pm 45/\pm < 3/3 >]_s$ | $[\pm < 3/9 > / \pm < 24/78 >]_s$ |
| Max. FI | 0,10 | 0,07 | 0,08 |
| BLF | 2,79 | 0,73 | 3,68 |
| Mean Thickness(mm) | 1,93 | 1,46 | 2,10 |
| sBLF | 1,61 | 0,73 | 1,79 |

Table 27 shows that specific buckling load factors of the optimum axially variable-stiffness cylinders VA-1 and VA-3 are higher than the buckling load factors of constant stiffness cylinders. For instance, specific buckling load factor of VA-3 design is 37 % higher than buckling load factor of the base line design CS-1. The improvement is satisfactory to show effectiveness of axially variable stiffness laminate approach. The thickness distribution of VA-3 is given in Figure 61.

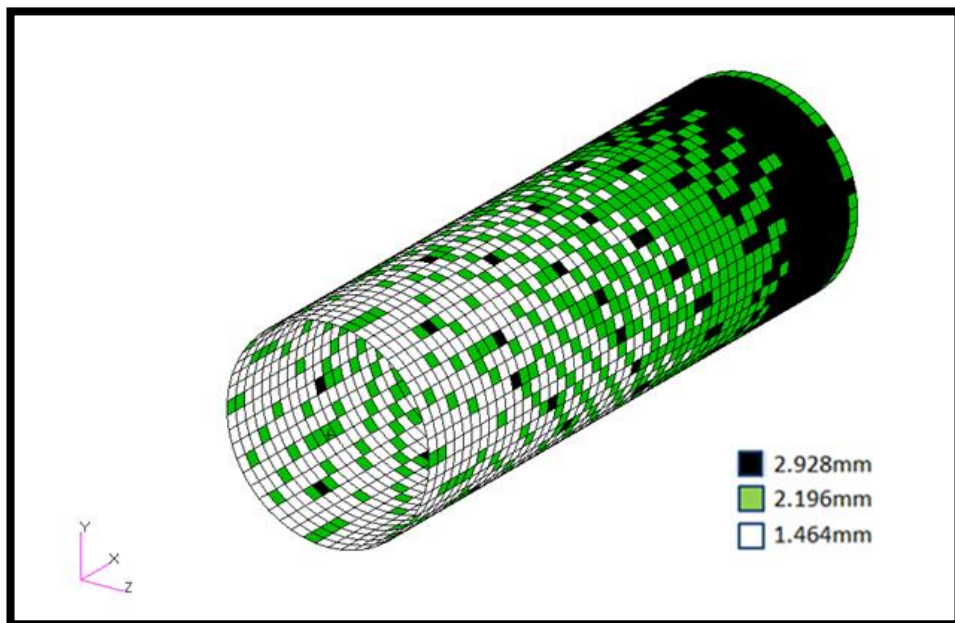


Figure 61 Thickness distribution of the VA-3 design, $[\pm < 3/9 > / \pm < 24/78 >]_s$

The thickness distribution of VA-3 design shows the thickness build up at the tip of the cylinder where the axial load is applied. Higher laminate thickness is achieved by the virtue of overlaps caused by the variation of the fiber orientation angle. The increased laminate thickness and fiber angle variation increases the specific buckling

load factor of the VA-3 design compared to the baseline constant stiffness cylinder CS-1.

First buckling mode of the VA-3 design is given in Figure 62.

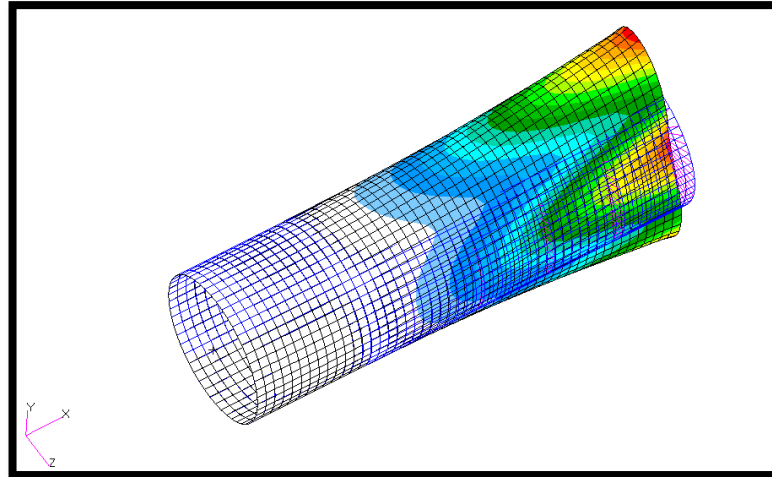


Figure 62 First buckling mode of the VA-3 design under axial loading

It is seen that first buckling mode of the axially variable stiffness cylinder VA-3 is different than first buckling mode of the baseline constant stiffness cylinder CS-1.

Another approach for variable stiffness laminate design is circumferential variation. The optimization results for the circumferentially variable stiffness cylinders under axial loading are listed in Table 28.

Table 28 Optimization results of variable stiffness cylinders with circumferentially varying fiber orientation angle under axial loading

| | VC-1 | VC-2 | VC-3 |
|---------------------------|---------------------------|-----------------------------|--------------------------------------|
| | $[0/90/\pm < 63/63 >]_s$ | $[\pm 45/\pm < 90/90 >]_s$ | $[\pm < 15/15 > / \pm < 90/78 >]_s$ |
| Max. FI | 0,06 | 0,07 | 0,06 |
| BLF | 1,31 | 0,81 | 1,42 |
| Mean Thickness(mm) | 1,46 | 1,46 | 1,47 |
| sBLF | 1,31 | 0,81 | 1,40 |

The best result among the circumferentially variable stiffness cylinder is the VC-3 design. Specific buckling load factor of the VC-3 design is higher than the buckling load factors of VC-1 and VC-2. However, compared to the baseline constant stiffness cylinder CS-1 design, circumferentially variable stiffness cylinder VC-3 showed a 7% improvement under the axial load. The thickness distribution of the VC-3 design is given in Figure 63.

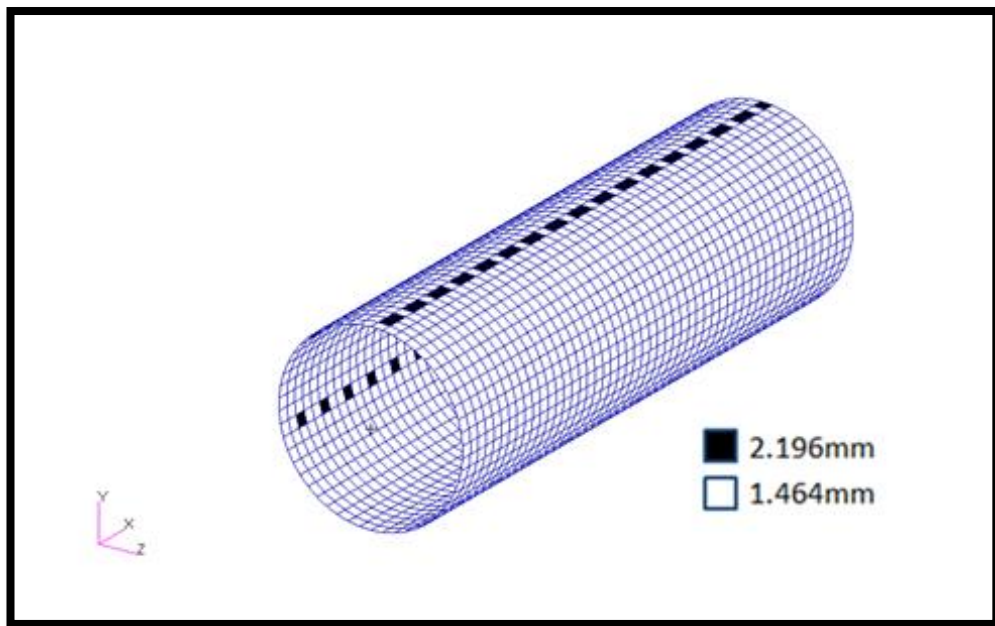


Figure 63 Thickness distribution of the VC-3 design under axial loading

It is noted that thickness of VC-3 is not too much, therefore the mean thickness is very close the thickness of the baseline constant stiffness cylinder which is 1.464mm. Therefore, 7 % increase in the specific buckling load factor of VC-3 only can be attributed to the fiber orientation angle variation.

First buckling mode of the VC-3 design is given in Figure 64. First buckling mode of CS-1 and VC-3 are approximately same, but the buckling load factors are different because of the variation of the fiber orientation angle.

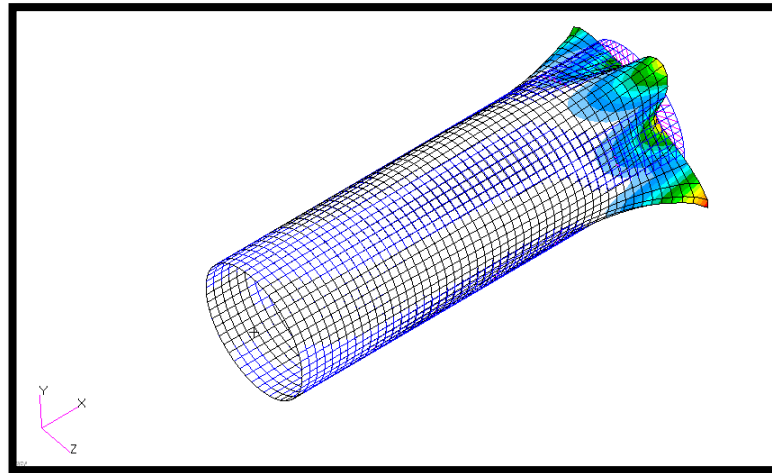


Figure 64 First buckling mode of the VC-3 design under axial loading

Based on the results of the optimization presented, it is concluded that axially variable stiffness cylinders are more effective in increasing the buckling load factor of fiber reinforced composite cylinders under axial loading. The best results are summarized in Table 29. The buckling load carrying capability of variable-stiffness designs is optimized by increasing the laminate thickness at critical region. For the axially variable-stiffness design, buckling load factor increased by up to 37% compared to the optimized baseline design, while for the circumferentially variable-stiffness design, buckling load factor increased by up to 7% compared to the optimized baseline design. This result shows that significant improvements in maximizing the buckling load factor of the cylindrical shell under axial loading can be achieved by using variable-stiffness cylinders. The overall results are listed in Table 29 and the improvements in the buckling load factor are given relative to the baseline design CS-1.

Table 29 The best optimization results under axial load.

| | CS-1 | VA-3 | VC-3 |
|---------------------------|-------------------|------------------------------------|--------------------------------------|
| | $[0/90/\pm 60]_s$ | $[\pm < 3/9 > / \pm < 24/78 >]_s$ | $[\pm < 15/15 > / \pm < 90/78 >]_s$ |
| Mean Thickness(mm) | 1,464 | 2,1 | 1,47 |
| BLF | 1,31 | 3,68 | 1,42 |
| sBLF | 1,31 | 1,79 | 1,4 |
| Improvement | | 37% | 7% |

The results presented in Table 29, gives the optimization results under axial loading with curvature and failure index constraints included. It is concluded that variable stiffness concept is can be applied successfully for the cylindrical structures under axial loading for increased buckling load capacity.

In general, when all the results of the optimization for the different load cases are evaluated, it is concluded that, compared to constant stiffness cylinders, axially variable stiffness cylinders show distinct improvement in the structural performance which is mainly measured by the specific buckling load factor. It should be noted that bending, torsional and axial load cases are the main loads that most of the structural components in aerospace structures are exposed to. Therefore, in terms of loading the study can be considered as general. In addition, in the present study, in the definition of the optimization problem maximum failure index, which is a measure of the strength, is considered as constraints besides the manufacturing constraint imposed. In most of the optimization studies performed in the literature regarding the variable stiffness concept, the main goal has been to optimize a specific structural performance metric, such as the buckling load, without applying any constraints. The effort has always been to come up with fiber paths resulting in variable stiffness with the ultimate goal of improving a structural performance metric such as the buckling load. However, in this thesis optimization of constant and variables stiffness cylinders are performed by applying manufacturing and strength constraints. Therefore, improvements achieved in the buckling load factor, with the use of variable stiffness concept, are the real improvements, not the ideal improvements that one could have obtained without imposing any constraint on the optimization problem.

CHAPTER 7

CONCLUSION

This thesis presents the analysis and optimization of fiber-placed, variable-stiffness composite cylindrical shells, and comparison with the baseline constant stiffness cylinders. The lessons learned and the future aspects are discussed in this chapter.

Tow-placement machines have made it possible to manufacture varying fiber orientation and thickness in the plies. Fiber-orientation angle depends on the position in a specific tow path and gaps and overlaps between courses cause a change in the thickness of ply. With the curvilinear fiber paths more favorable stress distributions and improved laminate performance can be obtained. The work performed in this thesis presents a fundamental study on the fiber path optimization of composite cylindrical structures. Fiber orientation is defined to vary in either the axial direction or in the circumferential direction of the cylindrical shell. A limited number of design variables are used to define a reference path to cover the entire surface of the cylinder with the automated fiber placement technique. [4] Complete ply is then constructed by shifting the reference course, in the perpendicular direction to the stiffness variation.

For the analysis and optimization of fiber placed cylindrical shells, specialized a finite element model modeling methodology is developed. The thickness variation, due to overlaps and the orientation angle variation within each tow path is calculated to get an accurate finite element model by using this tool. In the developed method, thickness variation due to gaps and overlaps and the fiber orientation angle variation within each tow path are calculated to get an accurate finite element representation of

the fiber placed cylindrical shell. Golden Section search is used to determine the distance between the center of each element and the centerline of the reference tow path. Based on the distance calculated, a decision is made whether gap or overlap occurs in the position of the element. The variable-stiffness properties are implemented using a subroutine in Matlab environment. The subroutine writes the stacking sequence of the laminate comprising each element to the Nastran input file because each element has a unique stacking sequence. The variable-stiffness cylinders are analyzed using the commercially available finite element program MSC.Nastran. Output of the Nastran finite element analysis is used to determine the response of various variable stiffness cylinder configurations. The buckling load factor is used as the objective function to be maximized in the design optimization problems that are set up. In the optimization process, maximum failure index and manufacturing constraints are also implemented so that optimized configurations satisfy the strength constraint and also cylinders can actually be manufactured. It should be noted that curvature constraint must be imposed in order to prevent the wrinkling of the fiber. Therefore, in the case studies performed manufacturing constraint is also applied in the optimization process.

Optimization of the reference fiber path is performed by using Particle Swarm Optimization. PSO is a simple optimization algorithm, and it is suited for problems that are not easily differentiable. The PSO code is specialized for fiber path optimization and is written in the MATLAB environment. Nastran finite element solver and PSO code are coupled for optimization. In PSO, every design cycle needs function evaluations equal to the total number of individuals in the population. Every function evaluation means a finite element analysis in Nastran. For the specified population numbers, it is observed that PSO gives satisfactory results, but the optimization lasts long. Therefore, to decrease the time cost, if curvature constraint is violated, Nastran solution cycle is by-passed, and objective function is heavily penalized so that optimization lasts shorter. Moreover, the range of the fiber orientation angle is discretized to decrease the design space so that it is possible to obtain the optimum solution in a short time compared to the continuous optimization. The optimization routine is applied to a problem with 2 design variables that define the reference fiber path on the cylindrical shell.

The variable-stiffness cylinders are compared on the basis of the specific buckling load factor, i.e. the buckling load factor normalized with the square of the mean thickness of the shell. It should be noted that the resultant buckling load factor is scaled by the square of the mean thickness to obtain a cylinder with equal thickness that is equal to the thickness of the baseline cylinder to provide a better measure of comparison. If the buckling load factor is not scaled, it might have caused misleading representation of the improvements achieved by the variable stiffness design compared to constant stiffness design.

The application of the variable-stiffness concept is expanded from flat panels to cylindrical shells. Mathematical expressions are derived to define the fiber paths with varying fiber orientation angle and stacking sequence of the laminate is determined as a function of the location [4, 6].

8-ply symmetric balanced variable-stiffness composite cylinder, having a radius of 101 mm and length of 635 mm, subjected to different loads is optimized to increase the buckling load factor. Four load cases are investigated to optimize the cylindrical structure subject to two constraints. Before the optimization of variable stiffness cylinders, the baseline design is determined for each load case by using the constant stiffness laminates with traditional and non-traditional orientation angles. The first investigated load case is the bending load case, which is applied to the cylinder center by using MPCs. Manufacturing and maximum failure index constraints are also included in the optimization. For the bending load case, with the axially variable stiffness cylinder, 17% improvement in the buckling load carrying capability is achieved compared to the optimized baseline laminate with equal mass. On the other hand, for the bending load case, circumferentially variable stiffness cylinders did not show significant improvement in the buckling load factor.

For the torsional load case, as a result of continuous fiber path optimization, nearly 15% increase is obtained in the specific buckling load factor of the axially variable stiffness cylinder with respect to the optimized constant-stiffness cylinder. If the loading varies along the length, then each region possesses a particular stiffness configuration while changing thicknesses and orientations. Circumferentially variable stiffness cylindrical shells showed small improvement

under the torsional loading when compared to the axially variable stiffness cylindrical shells, because thickness and fiber orientation variation did not support the critical region sufficiently to enhance the buckling load factor for the torsional load case. It should be noted that the variable parameters are the fiber orientation angles so that it is only controlled the fiber orientation angle in the optimization process and the thickness variation results of the fiber orientation angle.

As the third load case, torsional and bending loads are combined and applied to the cylindrical shell. In this case study, axially and circumferentially variable stiffness laminates showed improvement in the buckling load factor. Again, for the axially variable stiffness cylindrical design improvement is higher than the circumferentially variable stiffness cylindrical shell. The difference between specific buckling load factors for these two approaches is explained using the thickness and maximum Von Mises stress distribution of the cylindrical shell. When bending and torsional loads are applied separately, the buckling load factor of the axially variable stiffness cylinder increased by 17 %. Under combined loading, the increase is 12 %. In the combined bending and torsional load case, the loading does not change only in one direction, but the direction of variation of fiber paths are only in one direction. Therefore, for the combined load case, the increase in the buckling load factor is slightly less than the increase in the buckling load factor of the bending load case. For the combined load case, in the optimized cylinder configurations, the material failure criterion is also satisfied for all designs. When the stress distributions of the best axially variable stiffness cylinder and the baseline constant stiffness cylinder are compared, it is seen that the maximum Von Mises stress reduced significantly for the axially variable stiffness cylindrical shell.

A significant improvement for the specific buckling load factor of the axially variable-stiffness cylinder is obtained for the pure axial load case. When compared to the baseline cylinder, 37 % in the buckling load factor is calculated for the axially variable stiffness cylinder compared to the baseline constant stiffness cylinder. % 7 improvement is also seen for the circumferentially variable stiffness cylinder under axial compressive loading. It is concluded that stiffness variation proved to be beneficial for the structural performance of variable stiffness composite cylinders

loaded in the axial direction. The improvements in buckling load carrying capability of variable-stiffness composite cylinders with overlaps are due to the increased laminate thickness of the cylinder as well as the resulting stiffness variation in favor of the buckling load factor.

In general, the present study showed that the improvements in buckling load factors could be realized for cylindrical shells utilizing the variable stiffness concept achieved by the fiber placement technology. Variable-stiffness cylinders with variable thickness and variable fiber orientation angle improved the buckling load carrying capability by the redistribution of the loads. The higher buckling load carrying capability shows that there is potential for weight reduction using variable-stiffness cylinders and the introduction of the variable stiffness concept obviously promises advantages for the reasons just discussed.

A full scale laminate optimization including the ply numbers as the design variables in the optimization problem was beyond the scope of this thesis. With constant ply number, it is shown that increased structural performance can be obtained when variable stiffness concept is used under different load cases. The research on variable-stiffness cylinders discussed in this thesis covers only a small part of the work that needs to be done before variable-stiffness composite cylinders can be applied to real aerospace structures.

The finite element modeling analysis and optimization tool presented, allows for a wide range of designs to be quickly and accurately generated. Case studies on the maximization of the buckling load by optimizing the fiber paths showed the great potential that the variable stiffness concept presents. In addition, results presented in this thesis provide a resource to compare against the results of future research of fiber-placed variable-stiffness cylinders. Most of the previous research of variable stiffness laminates has acknowledged their potential in raising the buckling load of laminated shells. In this respect present study contributes to the studies performed in the variable stiffness concept. Comparative study of axially and circumferentially variable stiffness cylinders has not been performed before. In the literature studies on the cylindrical shells focuses on the circumferentially variable stiffness cylinders, and in most of these studies thickness variation due to gaps and

overlaps is not taken into consideration. [4, 6, 20] In the present study, in all of the optimization studies performed, manufacturing constraint is considered and penalty is applied whenever the manufacturing constraint is violated. The mesh size of the element is fixed for all optimization problems and the finite element analysis can be performed for different mesh size to see the effect of the mesh size.

It is considered that in the future fiber placement technology will be the major production method of composite structures due to the automation that they offer. However more importantly, with the fiber placement machines it is possible to optimize responses of a composite structure much more effectively compared to the straight fiber case by merely using stacking sequence optimization. Future work might be aimed at developing a different design method for variable-stiffness plies. The reference fiber path definition can be made such that more variables can be added to the reference fiber path equation resulting in nonlinear change of the fiber orientation along axis of the composite laminate. This would increase the efficiency of the continuous fiber paths for meeting the load paths within the composite structure.

A two-dimensional stiffness variation on a cylindrical shell could also be obtained by combining axial stiffness variation with circumferential stiffness variation within the laminate. The curvature constraint and the thickness variation are easily evaluated for plies constructed using the shifted course method, while it is more complicated to evaluate the manufacturing constraints if all fiber paths are unique. In the present study shifted fiber paths are used in the continuous fiber path optimization.

REFERENCES

1. Gürdal, Z. and Tatting, B. F. *Design and Manufacture of Tow-Placed Variable Stiffness Composite Laminates with Manufacturing Considerations*. s.l.: 13th U.S. National Congress of Applied Mechanics, June 25th 1998.
2. J.A. Mondo, M.J. Pasanen, R.J. Langone, and J.P. Martin. *Advances in automated fiber placement of aircraft structures*, 1997
3. M.W. Hyer, R.J. Rust, and W.A. Waters. *Innovative design of composite structures: Design, manufacturing, and testing of plates utilizing curvilinear fiber trajectories*. Technical Report NASA-CR-197045, NASA, Nov 1994
4. A.W. Bloom. *Structural Performance of Fiber-Placed, Variable-Stiffness Composite Conical and Cylindrical Shells*. PhD thesis, Delft University of Technology, Nov 2010.
5. W. G. Roeseler, B. Sarh, and M. U. Kismarton. *Composite structures: The first 100 years*. In *Proceedings of the 16th International Conference on Composite Materials*, Kyoto, Japan, July 2007.
6. Z. Gürdal and R. Olmedo. *In-plane response of laminates with spatially varying fiber orientations: Variable stiffness concept*. *AIAA Journal*, 31(4):751–758, 1993
7. B. F. Tatting and Z. Gürdal. *Design and manufacture of tow-placed variable stiffness composite laminates with manufacturing considerations*. In *Proceedings of the 13th U.S. National Congress of Applied Mechanics*, 1998.
8. B. Morey. *Automating composites fabrication*. *Manufacturing Engineering*, 140(4), 2008.
9. Muser, C., Hoff, N. J., “*Stress Concentrations in Cylindrically Orthotropic Plates with Radial Variation of the Compliances*,” *Progress in Science and Engineering of Composites*, Eds. T.Hayashi, K. Kawata, and S. Umekawa, ICCM-IV, Tokyo, Vol. 2, 1982, pp. 389-396.

10. R.A. Kisch. *Automated fiber placement historical perspective*. In *Proceedings of the SAMPE 2006 Conference*, Long Beach, CA, USA, 2006
11. M. W. Hyer and R. F. Charette. *Use of curvilinear fiber format in composite structure design*. *AIAA Journal*, 29(6):1011–1015, 1991.
12. M. W. Hyer and H.H. Lee, "The Use of Curvilinear-fiber Format to Improve Buckling Resistance of Composite Plates with Central Circular Holes." *Composite Structures*, Vol. 18, No. 3, 1991, pp. 239-261.
13. Olmedo and Z. Gürdal. *Buckling response of laminates with spatially varying fiber ori-entations*. In *Proceedings of the 34th AIAA/ASME/ASCE/AHS/ASC Structures, Structural Dynamics and Materials (SDM) Conference*. AIAA, 1993.
14. Waldhart, C. *Analysis of Tow-Placed, Variable-Stiffness Laminates*. s.l. : Thesis Submitted to the Faculty of the Virginia Polytechnic Institute and State University, June 5th 1996.
15. Langley , P. T., *Finite Element Modeling of Tow-Placed Variable-Stiffness Composite Laminates*. s.l. : Thesis Submitted to the Faculty of the Virginia Polytechnic Institute and State University, June 5th 1996.
16. B. F. Tatting and Z. Gürdal. *Automated finite element analysis of elastically-tailored plates*. Technical report, Dec 2003. NASA/CR-2003-212679.
17. Z. Gürdal, B. F. Tatting, and K. C. Wu. *Variable stiffness composite panels; effects of stiffness variation on the in-plane buckling response*. *Composites Part A: Applied Science and Manufacturing*, 39(5):911–922, 2008.
18. K. C. Wu, Z. Gürdal, and J.H. Starnes. *Structural response of compression-loaded, towplaced, variable stiffness panels*. In *Proceedings of the 43rd AIAA/ASME/AHS/ASC Structures, Structural Dynamics and Materials (SDM) Conference*, Denver, CO, USA, Apr2002. AIAA.
19. Jegley, Dawn C., Tatting, Brian F. and Gürdal, Zafer *Optimization of Elastically Tailored Tow-Placed Plates With Holes..* s.l. : AIAA.
20. Inci, H., *Discrete Fiber Angle and Continuous Fiber Path Optimization in Composite Structures*. MS. Thesis, Middle East Technical University, February 2012

21. Brandmaier, H. E. (1970), '*Optimum filament orientation criteria*', *Journal of Composite Materials* 4(3), 422–425.
22. Ostrander O., Roberts A. , Hauber D., *Extending the Range of Applications for Automated Fiber Placement, the First International Symposium on Automated Composites Manufacturing*, CA, April 2013
23. S. Nagendra, S. Kodiyalam, J.E. Davis and V.N. Parthasarathy, "*Optimization of Tow Fiber Paths for Composite Design*," *Proceedings of the AIAA/ASME/ASCE/AHS/ASC 36th SDM Conference*, April 10-13, 1995, New Orleans, LA, pp. 1031-1041.
24. A. Khani, M. M. Abdalla, and Z. Gürdal. *Circumferential stiffness tailoring of long composite non-circular cylinders. In 8th World Congress on Structural and Multidisciplinary Optimization*, Lisbon, Portugal, 2009b.
25. B. F. Tatting. *Analysis and Design of Variable Stiffness Composite Cylinders. PhD thesis, Virginia Polytechnic Institute and State University*, Oct 1998.
26. K.C. Wu. *Design and manufacturing of tow-steered composite shells using fiber placement. In 50th AIAA/ASME/ASCE/AHS/ASC Structures, Structural Dynamics and Materials (SDM) Conference*, Palm Springs, CA, USA, 2009. AIAA.
27. R. M. Jones. *Mechanics of Composite Materials. Taylor and Francis*, 2nd edition, 1999.
28. Kennedy, J., Eberhart, R.C.: *Particle Swarm Optimization. Proc. IEEE Int. Conf. Neural Networks. Piscataway, NJ* (1995) 1942{1948
29. Kennedy, J. (1997). "*The particle swarm: social adaptation of knowledge*". *Proceedings of IEEE International Conference on Evolutionary Computation*. pp. 303–308.
30. Hasançebi, Oğuzhan. *CE 587 Structural Optimization - Lecture notes*. 2011
31. Poli, R. (2008). "*Analysis of the publications on the applications of particle swarm optimisation*". *Journal of Artificial Evolution and Applications* 2008: 1–10. doi:10.1155/2008/685175.

32. Poli, R. "An analysis of publications on particle swarm optimisation applications". *Technical Report CSM-469*, Department of Computer Science, University of Essex, UK, 2007
33. X6. Hu, X., and R.C. Eberhart, *Solving Constrained Nonlinear Optimization Problems with Particle Swarm Optimization*, *Proceedings of the Sixth World Multiconference on Systemics, Cybernetics and Informatics* Orlando, USA. 2002
34. "NASA Technology", www.nasa.gov, October 21, 2008
35. Homaifar, A., Lai, A.H.-Y., Qi, X.: *Constrained Optimization via Genetic Algorithms*. *Simulation* 2 (4) (1994) 242-254
36. Coello, C.A.C., "Theoretical and Numerical Constraint Handling Techniques used with Evolutionary Algorithms: A Survey of the State of the Art", *Computer Methods in Applied Mechanics and Engineering*, Vol. 191, No. 11-12, (2002), 1245-1287.
37. "Airbus Gets OK to Compete with Boeing 787". *Chicago Sun-Times via Aircraft Maintenance Technology*. 21 December 2006.
38. C. S. Lopes, P. P. Camanho, Z. Gürdal, and B. F. Tatting. *Progressive failure analysis of tow-placed, variable-stiffness composite panels*. *International Journal of Solids and Structures*, 44(25-26):8493–8516, 2007.
39. "German Airbus A350 XWB Production commences" (Press release). Airbus S.A.S. 31 August 2010. Retrieved 23 May 2011.

Appendix A : Nastran Input File

Description of the Nastran input file .bdf is given.

```

SOL 101      CEND      % MSC.Nastran Linear Static Solver 101
TITLE = MSC.Nastran job created on combined load case
ECHO = NONE
SUBCASE 1
$ Subcase name : Default
  SUBTITLE=Default
  SPC = 2
  LOAD = 2
  DISPLACEMENT (SORT1, REAL)=ALL
  SPCFORCES (SORT1, REAL)=ALL
  STRESS (SORT1, REAL, VONMISES, BILIN)=ALL
  ESE = ALL
BEGIN BULK
$ Direct Text Input for Bulk Data
PARAM      POST      0
PARAM      PRTMAXIM YES
$ Elements and Element Properties for region : laminate_prop
$ Composite Property Record created from P3/PATRAN composite material
$ record : laminate
$ Composite Material Description :
$ Pset: "laminate_prop" will be imported as: "pcomp.1"

```

| MAT8 | 1 | 129000. | 9100. | .32 | 5300. | 5300. | 5300. | 1.59-9 |
|--------|---|---------|-------|-----|-------|-------|-------|--------|
| CQUAD4 | 1 | 1 | 1 | 2 | 53 | 52 | | |
| CQUAD4 | 2 | 2 | 52 | 53 | 104 | 103 | | |
| CQUAD4 | 3 | 3 | 103 | 104 | 155 | 154 | | |
| CQUAD4 | 4 | 4 | 154 | 155 | 206 | 205 | | |
| CQUAD4 | 5 | 5 | 205 | 206 | 257 | 256 | | |

| 1 | 2 | 3 | 4 | 5 | 6 | 7 |
|--------|-----|-----|-------|-------|-------|-------|
| CQUAD4 | EID | PID | GRID1 | GRID2 | GRID3 | GRID4 |

Output request,
Displacement
Stresses

Material Information

EID is the element identification number (integer>0)

PID is identification number of a PSHELL or PCOMP property entry which is created for each element.

GRID is the grid point identification numbers of connection points.

```

...
...
CQUAD4 2495 2495 2294 2245 2296 2345
CQUAD4 2496 2496 2345 2296 2347 2396
CQUAD4 2497 2497 2396 2347 2398 2447
CQUAD4 2498 2498 2447 2398 2449 2498
CQUAD4 2499 2499 2498 2449 2500 2549
CQUAD4 2500 2500 2549 2500 2551 2600
} 2500 CQUAD4 Elements

$ Nodes of the Entire Model
GRID 1 0. 101. 0.
GRID 2 0. 100.204 12.6526
GRID 3 0. 97.8301 25.1053
GRID 4 0. 93.9148 37.1619
GRID 5 0. 88.5203 48.6329
} GRID information X, Y, Z location

...
...

PCOMP 1 0. 0.
1 0.18300 0. YES
1 0.18300 90. YES
1 0.549 74.5 YES
1 0.549 -74.5 YES
1 0.549 -74.5 YES
1 0.549 74.5 YES
1 0.18300 90. YES
1 0.18300 0. YES
PCOMP 2 0. 0.
1 0.18300 0. YES
1 0.18300 90. YES
1 0.732 73.6 YES
1 0.732 -73.6 YES
1 0.732 -73.6 YES
1 0.732 73.6 YES
1 0.18300 90. YES
1 0.18300 0. YES
} PCOMP 1 [0/90/± <T0/T1>]s 8 plies with mid-plane symmetric and balanced

...
...
Element Thickness Orientation Angles

```

The PCOMP property entry may be used when the element is a composite consisting of layers of unidirectional fibers. The information on the PCOMP entry includes the thickness, orientation, and material identification of each layer. The detail explanation of PCOMP card is given below.

| 1 | 2 | 3 | 4 | 5 | 6 | 7 | 8 | 9 | 10 |
|-------|------|--------|--------|--------|------|--------|--------|-------|----|
| PCOMP | PID | Z0 | NSM | SB | FT | TREF | GE | LAM | |
| PCOMP | 1 | | | 5000.0 | HILL | 0.0 | | | |
| | MID1 | T1 | THETA1 | SOUT1 | MID2 | T2 | THETA2 | SOUT2 | |
| | 1 | 0.0054 | 0.0 | YES | 1 | 0.0054 | 45.0 | YES | |
| | MID3 | T3 | THETA3 | SOUT3 | etc. | | | | |
| | 1 | 0.0054 | 90.0 | | | | | | |

- Z0 is composite offset.
 - Use default = -(composite thickness)/2
- NSM is nonstructural mass
- SB is allowable interlaminar shear stress
 - Put as Bonding Shear Stress in Patran 2D Orthotropic Material
 - Required for failure indices
- FT is the ply failure theorem
 - Required for failure indices
- TREF is reference temperature
 - Overrides TREFs on ply MAT8s
- GE is element damping
 - Overrides GE on ply MAT8s
- LAM is layup options
- MIDi is ply material ID
 - MAT8 ID
- Ti is ply thickness
- THETAi is ply angle
- SOUTi is data recovery option

```

...
...
PCOMP      2499                0.      0.
  1      0.18300      0.      YES
  1      0.18300      90.      YES
  1      0.366      28.4      YES
  1      0.366     -28.4      YES
  1      0.366     -28.4      YES
  1      0.366      28.4      YES
  1      0.18300      90.      YES
  1      0.18300      0.      YES
PCOMP      2500                0.      0.
  1      0.18300      0.      YES
  1      0.18300      90.      YES
  1      0.183      27.5      YES
  1      0.183     -27.5      YES
  1      0.183     -27.5      YES
  1      0.183      27.5      YES
  1      0.18300      90.      YES
  1      0.18300      0.      YES
ENDDATA 46ab91b7

```

PCOMP 2500
 $[0/90/\pm <T_0/T_1>]_s$
 8 plies with mid-plane symmetric and balanced

2500 PCOMP cards created for 2500 CQUAD4 elements

The basic illustration is seen below. CQUAD4 card has information about, PCOMP card number. PCOMP card has information about the material, thickness and orientation angle. MAT8 card is defined for the used material.

| | | | | | | | | |
|--------|------|---------|-------|-----|-------|-------|-------|--------|
| CQUAD4 | 2369 | 2369 | 966 | 967 | 1018 | 1017 | | |
| PCOMP | 2369 | | | | | | 0. | 0. |
| | 1 | 0.18300 | 0. | YES | | | | |
| | 1 | 0.18300 | 90. | YES | | | | |
| | 1 | 0.549 | 71.6 | YES | | | | |
| | 1 | 0.549 | -71.6 | YES | | | | |
| | 1 | 0.549 | -71.6 | YES | | | | |
| | 1 | 0.549 | 71.6 | YES | | | | |
| | 1 | 0.18300 | 90. | YES | | | | |
| | 1 | 0.18300 | 0. | YES | | | | |
| MAT8 | 1 | 129000. | 9100. | .32 | 5300. | 5300. | 5300. | 1.59-9 |

Appendix B : Golden Section Method

Following is the algorithm for Golden Section Method;

Step 1 *Choose x^{lower} and x^{upper}*

$\tau = 0.618$

$\varepsilon = error = \Delta x_{final} / (x^{upper} - x^{lower})$

Iterate up to ε is less than 0.0001

Step 2 $x_1 = (1 - \tau)x^{lower} + \tau x^{upper} \quad f_1 = f(x_1)$

$x_2 = \tau x^{lower} + (1 - \tau)x^{upper} \quad f_2 = f(x_2)$

Step 3 *while $\varepsilon > 0.0001$*

if $f_1 > f_2$

$x^{lower} = x_1, x_1 = x_2, f_1 = f_2$

$x_2 = \tau x^{lower} + (1 - \tau)x^{upper} \quad f_2 = f(x_2)$

else

$x^{upper} = x_2, x_2 = x_1, f_1 = f_2$

$x_1 = (1 - \tau)x^{lower} + \tau x^{upper} \quad f_1 = f(x_1)$

end

end

Appendix C : Example for the Optimization Variable Stiffness Cylinder

In this part, the optimization procedure is explained step by step. The optimization code and MSC. Nastran coupling is demonstrated. How the PSO and optimization parameters are used is also shown.

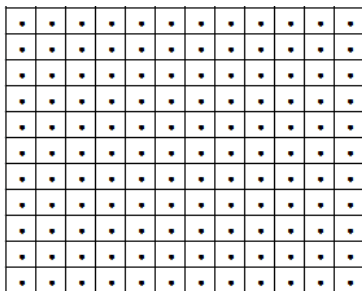
Firstly, we start with the example of Main Matlab code input parameters

| | |
|-----------------|--------------------------|
| <i>n_swarm</i> | 8 |
| <i>n_ite</i> | 4 |
| <i>lam_con</i> | $[\pm 45 < T_0/T_1 >]_s$ |
| <i>var_dir</i> | Axial Direction |
| <i>load_c</i> | Bending Load |
| <i>disc_val</i> | 3 |

Other input parameters are the PSO parameters.

| | PSO Parameters |
|-----------|-----------------------|
| c_1 | 2 |
| c_2 | 2 |
| w_{max} | 1 |
| w_{min} | 0,4 |
| α | 0,99 |
| σ | 0,4 |
| r_g | 10^4 |

Before the optimization, the element center of each quad element is calculated as shown in the figure given below for the cylinder.



The design space of T_0 and T_1 is defined between 3^0 and 90^0 .

Because the design space is discretized by 3 degrees, the range of design space for each design variable becomes 1 to 30.

The maximum velocity of T_0 and T_1 is defined at the beginning of the PSO.

$$T_0, v_{max} = \sigma * (T_{0max} - T_{0min})$$

$$T_1, v_{max} = \sigma * (T_{1max} - T_{1min})$$

$$T_{0max} = 30 \text{ and } T_{0min} = 1$$

$$T_{1max} = 30 \text{ and } T_{1min} = 1$$

$$T_0, v_{max} = 11,6$$

$$T_1, v_{max} = 11,6$$

For each particle $i=1:8$;

1. Create and initialize a population of T_0 and T_1 with random positions and velocities on 8 dimensions in the defined problem space.

Eight random (T_0, T_1) particles;

(5,8) , (12,20), (17,3) , (6,1) , (29,19), (15,8) , (11,13), (26,21)

The design space is discrete so MATLAB creates the population in a discrete manner to reduce the design space for the fiber path optimization problems studied. The created “discrete” values are multiplied with a coefficient *disc_val*. For instance, *disc_val* is equal to 3 and , T_0 and T_1 can take the values between 3^0 and 90^0 . The design space is discretized by 3 degrees, therefore range of the design space becomes 1 to 30. Therefore, T_0 and T_1 can take 30 different values to create a variable stiffness lamina. The initial population is created with random positions and velocities, T_0 and T_1 can take values between 1 and 30.

Eight random (T_0, T_1) particles becomes;

(15,24) , (36,60), (51,9) , (18,3) , (87,57), (45,24) , (33,39), (78,63)

2. Evaluate each (T_0, T_1) according to the objective function, fx_BLF.m

Before the evaluation, the curvature constrained is checked.

Then, GSO.m is called to calculate the distance between the paths and element center, and the distance information is performed to fx_BLF.m. According to the distance information, the thickness of each element for each ply is determined. After the orientation angle and the thickness values are determined, the PCOMP cards are created for each element. File fx_BLF.m creates the input file for MSC.Nastran. After this step, fx_BLF.m calls for a Nastran execution.

The first evaluation is performed for $[\pm 45/\pm < 15/24 >]_s$ laminate design.

The input file of Nastran, which is prepared, is used in the Nastran run to produce the output file which has all the results. For the case studies, linear static and buckling analysis are performed for the composite cylindrical shells. The output .f06 files are read by fx_BLF.m to target Von Mises stress of each element of each layer and the buckling load factor. The stress information is used to calculate failure indices by using Tsai-Wu failure criteria. By using the unconstrained problem formulation, the buckling load factor is calculated again and returned the PSO.m.

This step is repeated for 8 (T_0, T_1) particles.

3. PSO operations are performed. If a particle's current position is better than its previous best position, it is updated.

For example, during the iteration, if the new particle is iterated as (6,16) for the first particle, and if the new first particle (6,16) gives better result than the previous first particle (5,8), then the first particle's best position is updated to (6,16)

4. PSO operations, determine the best particle (T_0, T_1)

For 8 particles, the best particle is determined by comparing the results of the particles. The one which gives the best result is the best particle.

5. PSO operations, update particles' velocities

$$vT_{0i}^{k+1} = w * T_{0i}^k + c_1 * r_1(\dots) * (T_{0pbest}^k - T_{0i}^k) + c_2 * r_2(\dots) * (T_{0gbest} - T_{0i}^k)$$

$$vT_{1i}^{k+1} = w * T_{1i}^k + c_1 * r_1(\dots) * (T_{1pbest}^k - T_{1i}^k) + c_2 * r_2(\dots) * (T_{1gbest} - T_{1i}^k)$$

Velocity vT_{0i}^{k+1} (which denotes the amount of change) is a function of the difference between the individual's personal best T_{0pbest}^k and its current position, and the differences between the neighborhood's best T_{0gbest} and its current position. c_1 and c_2 are the cognitive (individual), and social (group) learning rates. r_1 and r_2 are uniformly distributed random numbers in the range 0 and 1. The values of c_1 and c_2 are usually assumed to be 2 so that $c_1 * r_1$ and $c_2 * r_2$ ensure that the particles would overfly the target.

The weighting function is usually utilized, w is the inertia factor and α is the decreasing factor of the inertia that is formulated as:

$$w = \begin{cases} 0.4 & \text{if } w < w_{min} \\ w * 0.99 & \end{cases}$$

6. PSO operations update particles position (T_0, T_1)

$$T_{0i}^{k+1} = T_{0i}^k + vT_{0i}^{k+1}$$

$$T_{1i}^{k+1} = T_{1i}^k + vT_{1i}^{k+1}$$

7. Loop to step 2 until the stopping criterion is met.

4 iteration loops are performed to find optimum solution. After the first cycle of the optimization, the optimum particle is sent to first step as a random particle and optimization cycle starts again. If the same optimum particle is found as a result of the second optimization cycle, the optimization program is terminated, else the program continues to the optimization until the same optimum solution is found twice.